

Folding DNA to create nanoscale shapes and patterns

Supplementary Notes 1–11

Paul W. K. Rothemund

Computation and Neural Systems, and Computer Science, California Institute of Technology, Pasadena, California, United States of America

Supplementary Note S1: Design of DNA origami

The program used for designing DNA origami, `multishapes.m`, may be downloaded from:

<http://www.dna.caltech.edu/SupplementaryMaterial/>

Below is a description of how design proceeds using this program. It is not meant to be a manual but rather to show the level of abstraction at which the origami are designed, and to show the various types of diagrams that the program can draw to aid in design. If scaffolded DNA origami becomes widely used, a better CAD design tool will have to be written. Given a desired shape (for example the red outline in Fig. 1a) design of a DNA origami to approximate it proceeds in five phases (two manual design steps and three passes of the program):

1. **Generation of a block diagram.** By hand, a rough geometric model is generated. It is comprised of rectangular blocks in which each block is taken to be one turn of DNA wide and one DNA helix plus the inter-helix gap in height. (Such a block diagram sloppily overestimates the height of a structure by one inter-helix gap.) An example block diagram is in Supplementary Fig. S1 step 1.

This step is performed with an eye towards the next step (generation of a folding path), in some cases the block diagram is conceived almost simultaneously with the folding path. The phase of the underlying periodic crossover lattice is chosen as well; generally this phasing is chosen so that seams and long edges of the shape align with columns of periodic crossovers. For blocks on the edge of the diagram, it is useful to keep track of the relationship of such blocks to the underlying crossover lattice. For an origami with 1.5-turn spacing between crossovers there are 3 possible offsets that an edge may have with respect to the underlying lattice—call them 0, +1 and -1 (Origami with 2.5 turn spacing have 5 possible offsets). For designs with a central seam, blocks on edges of offset 0 are colored red and blocks on edges of offset +1 and -1 are colored yellow and orange, depending on whether they occur to the left or right of the central seam. At this point the placement of seams may already be apparent; if so, half-blocks are used along seams. Adjacent half-blocks involved in the same scaffold crossover are colored the same (one of either green or purple) but adjacent half-blocks that participate in different crossovers are given different colors.

2. **Generation of a folding path,** by raster fill, through the block diagram. For a given shape there are many compatible raster fill patterns; currently the raster fill pattern must be hand-designed. For any helical domain in which the scaffold is to start and end on the same side of the helix (top or bottom), an integral number of turns (blocks) is traversed. For any helical domain in which the scaffold starts and ends on opposite sides of the helix, the scaffold traverses an odd number of half-turns (half-blocks). An example folding path is in Supplementary Fig. S1 step 2.
3. **Generation of a first pass design** based on the block diagram and folding path. The lengths of various helical domains, in units of DNA turns, are implied by the block diagram and folding paths; these are what is input to the computer program. For every design with seams presented here *except* the 3-hole disk, a single vertical seam was used in the design and so a simple matrix representation of the domain lengths could be used. Supplementary Fig. S1 step 3 shows a matrix (`design_turns`) of these domain lengths that is input to the program. (The equilateral and sharp triangle have a single seam *in each domain* that could be similarly specified by a single matrix. For the 3-hole disk, the position of seams was entered as a separate matrix and the routing of the scaffold between these seams as a matrix slightly more complicated than the `design_turns` matrix.) Column C0 gives the total number of turns in a particular row of the design. Column C1 and C4 give the total number of turns to the left and right of the seam, respectively. (Column C0, the sum of C1 and C4, was thus redundant and was used for checking the design.) Columns C2 and C3, unused for this design, give the offset (in number of turns) from the seam of the left and right helical domains, respectively; this feature is not used for the house design here, but is used for the bottom “legs” of the star design. The program converts lengths given (by the user) in turns to numbers of bases (matrix `design_lengths`) and outputs a first-pass design.

The first pass design can be output either as a line diagram (as in Supplementary Fig. S1 step 3) or as a detailed diagram showing the sequence of the scaffold layed out along the folding path, and the sequence of the staples where they appear in the final folded structure (Supplementary Fig. S2). In the detailed design diagram staple strands are indexed by xy position of the adjacent crossover and the designation ‘a’ or ‘b’ depending on whether the staple falls to the left or right of the crossover, respectively. Here names are of the form $sXtYP$ where X is the x position, Y is the y position, and P the position with respect to the adjacent crossover.

- Refinement of the helical domain lengths** to minimize strain in the design. In a third sort of diagram (Supplementary Fig. S3), the computer program displays the predicted twist at each base position as a color (assuming the spacing of crossovers represents an exact number of half turns). Red indicates that the base at a particular position is pointing up, blue that it is pointing down. At crossover points, strand backbone positions should fall at the tangent point between helices; thus bases from the helix above a crossover should be blue and those from the helix below a crossover should be red. (More specifically, the color of bases at the crossover should be spaced equally clockwise and counterclockwise of the colors blue and red, that themselves should occur exactly at the tangent point.) All of the crossovers internal to the design are spaced 16 bases apart and related by a glide symmetry that should balance strain. This can be observed for the two types of crossovers (‘+’, major-groove up and ‘-’ major-groove down) that occur internally in a shape, shown in both the boxed regions and at the lower left of Supplementary Fig. S3. (A naive view is that the bases of the crossover will actually be centered around the tangent point between helices. In reality, twist strain might be relieved by distortion of the crossover but the idea is that if so, such a distortion will be balanced by that of neighboring symmetrically-placed crossovers.)

Ideally, at all other crossovers in the design, the orientation of bases would be similar to that desired for the balanced internal crossovers. However, because of the non-integral number of bases in a single turn, and the major-minor groove angle, it is not possible to put all crossovers in this optimal orientation. Crossovers along the edges of the shape, in particular, must be adjusted to minimize strain. The program computes a “strain energy” along the edges of the design, and so positions of predicted high strain can be identified. (For a given strand passing through a crossover, the computed strain energy is just the sum of the squared angular deviation from the tangent point for the base before and the base after the crossover.)

By hand, helical domain lengths are changed by single bases until the strain energy is minimized. The map of twists aids in this process. For example, high twist strain occurs in a couple scaffold crossovers in the first pass design (marked by ‘s’ labels inside ovals in Supplementary Fig. S3). These crossovers were initially designed to be 5 bases away from the nearest internal crossover (a ‘-’ crossover). At bottom right, the situation for one such crossover may be compared to that which would occur if the distance to the nearest internal crossover were changed to 6 bases, as well as the ‘ideal’ situation for this type of crossover, that of a ‘+’ type crossover. The 6-base distance creates the least strain.

Once the appropriate adjustments are decided, a matrix of adjustments is input to the design program, with the original design (Supplementary Fig. S4, `design{ADJUSTMENTS}`, top). The matrix gives adjustments for the left and right edges of each helical domain in the design, columns C1 and C2 for domains to the left of the seam and columns C3 and C4 for columns to the right of the seam. The program updates `design_lengths` (Supplementary Fig. S4, bottom) accordingly and a second pass diagram is generated (Supplementary Fig. S5).

- Breaking and merging of strands.** The merging of strands is specified by giving a pairwise list of the names to be merged (i.e. `s-2t9b` and `s-1t8a`) along with the name of the new strand (i.e. `s-1t8e`). The program checks to see that all strands to be merged have adjacent 3’ and 5’ bases. The position of strands to be broken is specified by the name of a strand and the position along its length at which it is to be broken. The pattern of merges is not unique. Supplementary Fig. S6, Supplementary Fig. S8, and Supplementary Fig. S10 show three different diagrams (full sequence, line drawing, and crossover map) of a design that features bridging staple strands across the seam. Supplementary Fig. S7, Supplementary Fig. S9, and Supplementary Fig. S11 show three different diagrams (full sequence, line drawing, and crossover map) of a design that has no bridging staples. Diagrams are interleaved to allow comparison of the differences between these two designs. Using a PDF viewer, flip back and forth between two diagrams of the same type to see the effect of different merge patterns. Particularly interesting are the crossover maps, Supplementary Fig. S10 and Supplementary Fig. S11. The addition of bridging staples creates a characteristic pattern of “bars” down the center of the design which is observed in experiments that using bridging staples (and not observed in experiments that don’t use bridging staples.) Supplementary Fig. S12 highlights the the basic type of grid underlying each merge pattern and the implications for applying pixels to the pattern.

The design method given here is a generalization of that developed by Nadrian Seeman for creating rigid molecules out of parallel helical domains (here helices are technically ‘antiparallel’ in the standard terminology), which was first elaborated for the creation of double-crossover molecules (molecules with two parallel helices, ref. 16) and later extended to triple crossover molecules (molecules with three parallel helices,²⁴). The main principle used in these works is that **crossovers may be used to hold helices rigidly in a parallel orientation**. More specifically, **wherever the twist of two parallel helices bring the backbones of the two helices sufficiently close, reciprocal strand exchange can be used to incorporate a crossover**. Further, an amazing aspect of the principle is that such a crossover does not disturb base pairing in either helix; the crossover appears to contain only single phosphate from each strand. The basic principle can be extended to many general schemes with a variety of crossover spacings and crossover types (parallel or antiparallel), as was mentioned in ref. 16. Here I explore a scheme that uses a regular grid of antiparallel crossovers (spaced an odd number of half-turns apart) in the bulk of a shape but on the edges and seams of a shape admits the placement of a crossovers with arbitrary offsets (in integral numbers of turns) from the underlying crossover grid.

The composition of double crossovers into periodic two dimensional crystals²⁵ showed that, through the use of sticky-end interactions, arbitrary numbers of helices could be held in a parallel arrangement by crossovers. Because the natural equilibrium length for a single turn of DNA appears to be close to 10.5 base pairs^{26, 27}, and because DNA backbones are not symmetrically spaced around the helix (there is a major and minor groove), designs of such two dimensional DNA nanostructures (which must use integral numbers of DNA bases) invariably incorporate features that should cause strain. That is, the design assumes a DNA geometry slightly different than that of a single isolated helix with 10.5 bases per turn with ‘normal’ major/minor groove angles. This difficulty appears to have manifested itself experimentally. A number of 2D DNA nanostructures form tubes rather than sheets^{15,22}.

The solution to this problem was first articulated to me by Erik Winfree, and was implicit in the design of DAO-E double crossover lattices²⁵: **crossovers (and nicks) in extended structures of parallel helices should be placed so that they have symmetries which balance strain**. This principle is described at length in ref. 15 and its supplemental materials; it is also often described as ‘corrugation’²². The principle has demonstrably inhibited tube formation in at least one system²².

For DNA origami this criterion was used in the placement of crossovers; after merging it does not hold true for nicks in some designs. The use of 16 bases to represent 1.5 turns of DNA (in the 1.5-turn crossover spacing structures) or 26 bases to represent 2.5 turns of DNA (in the 2.5-turn crossover spacing structures) means that the helical domains between crossovers are slightly overtwisted or undertwisted, respectively. To balance this strain, alternating columns of staple crossovers are related by a glide symmetry—the local configuration of crossovers in one column is identical to that of crossovers in the next column over after a translation and a ‘flip’ (a rotation about one of the crossovers in-plane axes). Cross-section 1 of Fig. 1d shows the presumed orientation of backbones through one column of crossovers in the lattice, and the top two helices of cross-section 2, the presumed orientation of crossovers in an adjacent column 1.5 turns away (alternatively the diagrams for ‘+’ and ‘-’ crossovers in Supplementary Fig. S3). This symmetry should tend to balance strain in the origami and cause them to be, on average, flat. (So far, no experimental evidence has demonstrated that the origami are flat, however).

The use of a glide symmetry means that large regions of a DNA origami should have balanced strain. However, at seams and edges this is not necessarily true, even where a seam or edge lines up with the underlying crossover lattice. At seams or edges, because DNA has a major and minor groove, a crossover involving staple strands is in tension with an adjacent crossover involving the scaffold strand. Such a configuration of crossovers in tension has never before been used in DNA nanostructures. For example, in Fig. 1d the cross-section through a seam (cross-section 2) has been drawn so that the staple crossover is relaxed (top two helices of three) and the scaffold crossover (bottom two helices of three) is highly strained. Perhaps both crossovers assume some intermediate conformation.

How the strain is actually relieved is unknown, the final base pairs of each helix may be distorted. Strain at seams or edges does not appear to cause any gross defects in the origami; bases at the end of the helices are highly available for stacking against other DNA origami which suggests that the last base pair does form and assumes a planar configuration. If, in the future, strain associated defects should be detected at edges, then one or two scaffold bases could be left unpaired and allowed to form a hairpin that should relax the crossover.

Another place that the design of scaffolded DNA origami currently breaks with normal DNA nanotechnology is in its use of a wide range of sequences for its antiparallel crossovers. Customarily, crossover sequences are drawn from one of a few sequences that both form an immobile branched junction²⁸ and have well-characterized geometry. Such junctions have been designed with minimal symmetry so that the junction cannot branch migrate back and forth. Because the crossover sequences in the DNA origami demonstrated here are determined by the M13mp18 DNA sequence, and hundreds of them are used, a few probably have symmetries that would allow them to branch migrate a few bases; the crossover sequences have not been inspected for such properties. Further, different crossover sequences show a varying tendency to assume one of two different stacked-X conformers^{29, 30}, one of which is incompatible with

the DNA origami's intended structure at every crossover.

It is hoped that the juxtaposition of multiple crossovers in DNA origami inhibits both branch migrations and conformer isomerizations; isomerization or migration to an undesired form at one junction would tend to increase strain between adjacent junctions. A study of a pair of symmetric antiparallel junctions juxtaposed with an asymmetric antiparallel junction has shown that the asymmetric junction can prevent the adjacent symmetric junctions from branch migrating³¹. But the same study showed that two symmetric antiparallel junctions juxtaposed next to each other *can* branch migrate. Thus it seems possible that several symmetric junctions near each other might conspire and migrate. Indeed it seems likely that some local rearrangements of junctions in origami happen; since they are likely to be smaller than a few nanometers, they cannot be observed by AFM. Eventually higher resolution structural information on DNA origami will determine if such isomerizations occur. Importantly, I note that there is no reason why better characterized, well-behaved junction sequences should not be incorporated into DNA origami designs if it helps to create more precise structure. The incorporation of specific crossover sequences will require the use of a synthetic scaffold rather than a natural one, a practical inconvenience for very long scaffolds.

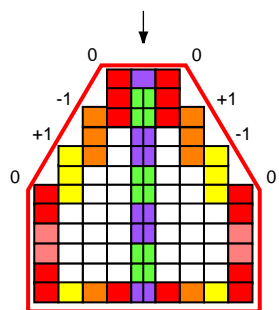
A note on seams: while most seams presented here are vertically aligned (for simplicity and convenience in design), and this necessitates the use of bridges to strengthen seams, it is possible to create staggered seams (as E. Winfree has suggested) so that staple strands naturally cross and bridge the seam vertically (between two adjacent helices) and no creation of horizontal bridges would be required. In these cases the addition of horizontal bridges across some parts of the seam might still add additional strength. A small instance of staggered seams occurs in the smiley face design. Above the right hand eye a small 2-helix seam appears that, because it is not aligned with other seams would not necessarily need bridges. An experiment in which the staples at this position were rearranged to remove horizontal bridging gave smileys of (not surprisingly) similar quality.

A note on folding paths and arbitrary shapes: there may be additional constraints on DNA origami that limit the family of shapes that can be approximated a little. In particular, shapes with lots of long thin projections or thin "waists" connecting two different parts of the shape may not form very well. As presented here, the minimum allowable width of a vertically oriented structure (such as a tall thin rectangle), if the scaffold rasters progresses in one direction vertically, is 1.5 turns, or about 5.4 nm wide. I have not tested the formation of such a narrow structure. The narrowest equivalent structure occurs at the jaw hinge of the smiley, 4.5 turns wide, about 16 nm wide. While most smileys are well formed, a significant number have dislocations along these 4.5 turn waists and it appears to be a weak spot.

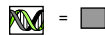
In some shapes it is desired that a strand pass both back and forth through a narrow waist so that it may access different portions of the shape. For example, consider a vertically oriented hourglass shape. If it is desired that a circular scaffold be used, then the scaffold must pass both up and down the narrow waist of the hourglass. As presented here, the minimal allowable width of the waist, which would accommodate the scaffold going up and down, would be 3 turns or about 11 nm. This width is the width of the top 4 helices of the star and because they do not image well, it seems that such a narrow waist may be floppy (in isolation). Clearly the analogous waist down the center of the smiley, which is 6 turns or 22 nm wide forms well and is mechanically stable in the context of the larger structure. Note that it is asymmetric and is composed of 1.5 turn and 4.5 turn wide vertical rasters.

Similarly, consider a horizontally oriented hourglass. For a circular scaffold to pass both left and right through the waist of the hourglass would require two helices, and so in principle the waist could be about 5 nm wide. However, I am unsure how well such a skinny waist would form. Again the smiley gives the best example of the smallest such waist so far. Below each eye is a four helix waist, about 11 nm wide which forms well and is stable.

1. Block diagram

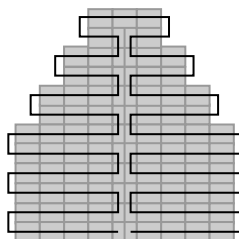


Block includes inter-helix gap.



10.6 bases, 3.63 nm
32 bases \approx 3 turns

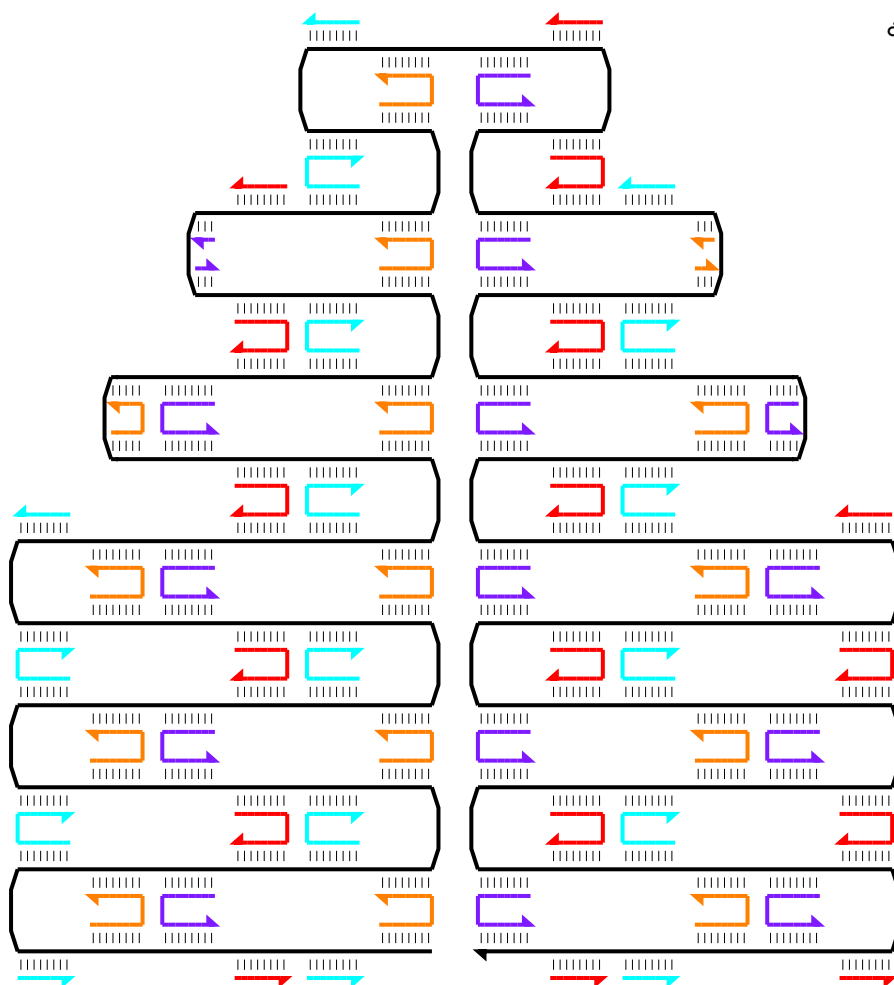
2. Folding path



3. First pass design

```
% C0 C1 C2 C3 C4
design_turns = [
[3 1.5 0 0 1.5]; %H1
[3 1.5 0 0 1.5]; %H2
[5 2.5 0 0 2.5]; %H3
[5 2.5 0 0 2.5]; %H4
[7 3.5 0 0 3.5]; %H5
[7 3.5 0 0 3.5]; %H6
[9 4.5 0 0 4.5]; %H7
[9 4.5 0 0 4.5]; %H8
[9 4.5 0 0 4.5]; %H9
[9 4.5 0 0 4.5]; %H10
[9 4.5 0 0 4.5]; %H11
[9 4.5 0 0 4.5]; %H12
];
```

Program outputs first pass design:



```
design_lengths =
C0 C1 C2 C3 C4
32 16 0 0 16 %H1
32 16 0 0 16 %H2
54 27 0 0 27 %H3
54 27 0 0 27 %H4
74 37 0 0 37 %H5
74 37 0 0 37 %H6
96 48 0 0 48 %H7
96 48 0 0 48 %H8
96 48 0 0 48 %H9
96 48 0 0 48 %H10
96 48 0 0 48 %H11
96 48 0 0 48 %H12
```

Supplementary Figure S1: First three steps of origami design.

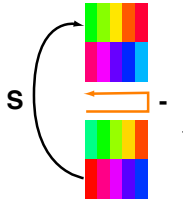
```

3          2          1          0          1          2          3
s-3t0b          s-1t0a  s-1t0b          s1t0a  s1t0b          s3t0a
< < < < ---GGAGAGGG< <GTAATTAC--- < < <
> --- --- --- --- CCTCTCCC---CGCGCGTT-----GGCCGATT---CATTAAATG--- --- --- >
/ < < < < <GCGCGCAA-----CCGGCTAA< < < < \
| s-2t1a ) ( s-2t1b s0t1a s0t1b s2t1a ) ( s2t1b |
\ > > > > >GTATTGGG-----CCTGTCGT> > > > /
< --- --- --- --- GCCAAACG---CATAACCC< <GGACAGCA---CGGTCGAC--- --- --- <
> > > > >CGTTTGC> \ / >GCCAGCTG > > >
( s-3t2b s-1t2a ) ( s-1t2b | | s1t2a ) ( s1t2b s3t2a )
< < < < <CACTTTTC TTTTGGT< / \ <GACCTTTC GCCCGTCA< < <
> --- --- CTG---GTGAAAAG---AAAACCA---CCCTGGCG> >TTTCCCGA---CTGGAAG---CGGCAGT---GAG --- --- >
/ < < < < <GAC< <GGGACCCG-----AAAGGGCT< <CTC < < \
| s-2t3a ) ( s-2t3B s0t3a s0t3b s2t3A ) ( s2t3b |
\ > > > > >TGA> >TTGCCCTT-----GAGCTAAC> >GCG > > /
< --- --- ACT---CTGCCCGT---TGTCGACT---AACGGAA< <CTCGATTG---AGTGTAAT---TAACGCAA---CGC --- --- <
> > > > >GACGGGCA ACAGCTGA> \ / >TCACATTA ATTGCGTT> > > >
( s-3t4b s-1t4a ) ( s-1t4b | | s1t4a ) ( s1t4b s3t4a )
< < < < <GTTGAGAG AGTCCCGG< / \ <CCGTGGGG TCCGAAAT< < <
> --- GGACC---GCTTGCTG---CAACTCTC---TCAGGGCC---AGGCGGTG> >ACTCATT---GGCACCCC---AGGCTTTA---CACTTTAT---GCTTC --- >
/ < < < < <CTGG CGAACGAC< <TCCGCCAC-----TGAGTAAT< <GTGAAATA CGAAG < < \
| s-2t5a ) ( s-2t5b s0t5a s0t5b s2t5a ) ( s2t5b |
\ > > > > >ACGCT GGTTTGCC> >CTGTTTGA-----TGTTATCC> >AACATACG AGCCG > > /
< --- TGCGA---CCAACGCG---GGTCGTCC---GCTTTTAG---GACAAACT< <ACAATAGG---CGAGTGTT---AAGGIGTG---TTGTATGC---TCGGC --- <
> > > > >CCAGCAGG CGAAAATC> \ / >GCTCACAA TTCCACAC> > > >
( s-3t6b s-1t6a ) ( s-1t6b | | s1t6a ) ( s1t6b s3t6a )
CCGATAAG< <TAAACGG CTAAAGCC< / \ <GTCCTTTG TCGATACT< <CTCAGACC <CTCAGACC
>GGCTATTC---TTTTGATT---TATAAGGG---ATTTTGGC---GATTTCGG---AACCACCA> >ATTTACAA---CAGGAAAC---AGCTATGA---CCATGATT---ACGAATTC---GAGCTCGG>
/ < < < < <AAAATAA ATATTCCC< <TTGGTGGT-----TAAAGTGT< <GGTACTAA TGCTTAAG< < \
| s-2t7a ) ( s-2t7b s0t7a s0t7b s2t7a ) ( s2t7b |
\ > > > > >GGTTGAGT GTTGTTC> >CCACTATT-----GTGCCAAG> >TCGACTCT AGAGGATC> > > /
<GCTCTATC---CCAACTCA---CAACAAGG---TCAAACCT---TGTTCTCA---GGTGATAA< <CACGGTTC---GAACGTAC---GGACGTCC---AGCTGAGA---TCTCCTAG---GGGCCCAT<
CGAGATAG> >AGTTTGA ACAAGAGT> \ / >CTTGCATG CTTGCAGG> >CCCGGGTA
( s-3t8b s-1t8a ) ( s-1t8b | | s1t8a ) ( s1t8b s3t8a )
GGGACTAT< <AACTGCAA CCTCAGGT< / \ <CAAAATGT TGCAGCAC< <GCAATGGG
>CCCTGATA---GACGGTTT---TTCGCCCT---TTGACGTT---GGAGTCCA---CGTTCCTT> >TGGCCGTC---GTTTTACA---ACGTCGTG---ACTGGGAA---AACCTGG---CGTTACCC>
/ < < < < <CTGCCAAA AAGCGGGA< <GCAAGAAA-----ACCGGCAG< <TGACCCCTT TTGGGACC< < \
| s-2t9a ) ( s-2t9b s0t9a s0t9b s2t9a ) ( s2t9b |
\ > > > > >CACTACGT GAACATC> >TTGGGGTC-----TATTACGC> >GATGTGCT GCAAGCGC> > > /
<GCTACCGG---GTGATGCA---CTTGGTAG---TGGGTTTA---GTTCAAAA---AACCCAG< <ATAATGCG---GTGACCG---CTTTCCCC---CTACACGA---CGTCCGC---TAATTCAA<
CGATGGCC> >ACCCAAAT CAAGTTTT> \ / >CAGCTGGC GAAAGGGG> >ATTAAGTT
( s-3t10b s-1t10a ) ( s-1t10b | | s1t10a ) ( s1t10b s3t10a )
TTAGCCCC< <GCTAAATC ACGAAATG< / \ <CGGGCGTG GCTAGCGG< <GTCGGACT
>AATCGGGG---GCTCCCTT---TAGGGTTC---CGATTTAG---TGCTTTAC---GGCACCTC> >GCGAAGAG---GCCCGCAC---CGATCGCC---CTTCCCAA---CAGTTGCG---CAGCCTGA>
/ < < < < <CGAGGGAA ATCCAAG< <CCGTGGAG-----CGTTCTC< <GAAGGGTT GTCAACGC< < \
| s-2t11a ) ( s-2t11b s0t11a s0t11b s2t11a ) ( s2t11b |
\ > > > > >GACGGGA AAGCCGGC> >GAAGGGAA-----CCGGCACC> >ACCAGGCA AAGCGCCA> > > /
<ATCTCGAA---CTGCCCTT---TTCGGCCG---CTTGCACC---GCTCTTTC---CTTCCCTT< <GGCCGTGG---CGAAGACC---ACGGCCTT---TGGTCCGT---TTCGGGT---AAGCGGTA<
>TAGAGCTT> >GAACGTGG---CGAGAAAG> >GCTTCTGG---TGCCGGAA> >TTCGCCAT<
s-3t12b s-1t12a s-1t12b s1t12a s1t12b s3t12a

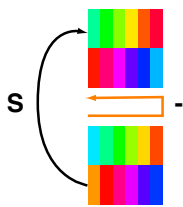
```

Supplementary Figure S2: First pass diagram, staple strands with xy labels and explicit bases.

first pass,
5 bases from crossover,
program reports high strain
in scaffold crossovers
(s, ovals). Consider left side.

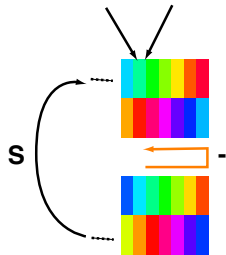


second pass,
switch to 6 bases,
Is strain lowered?

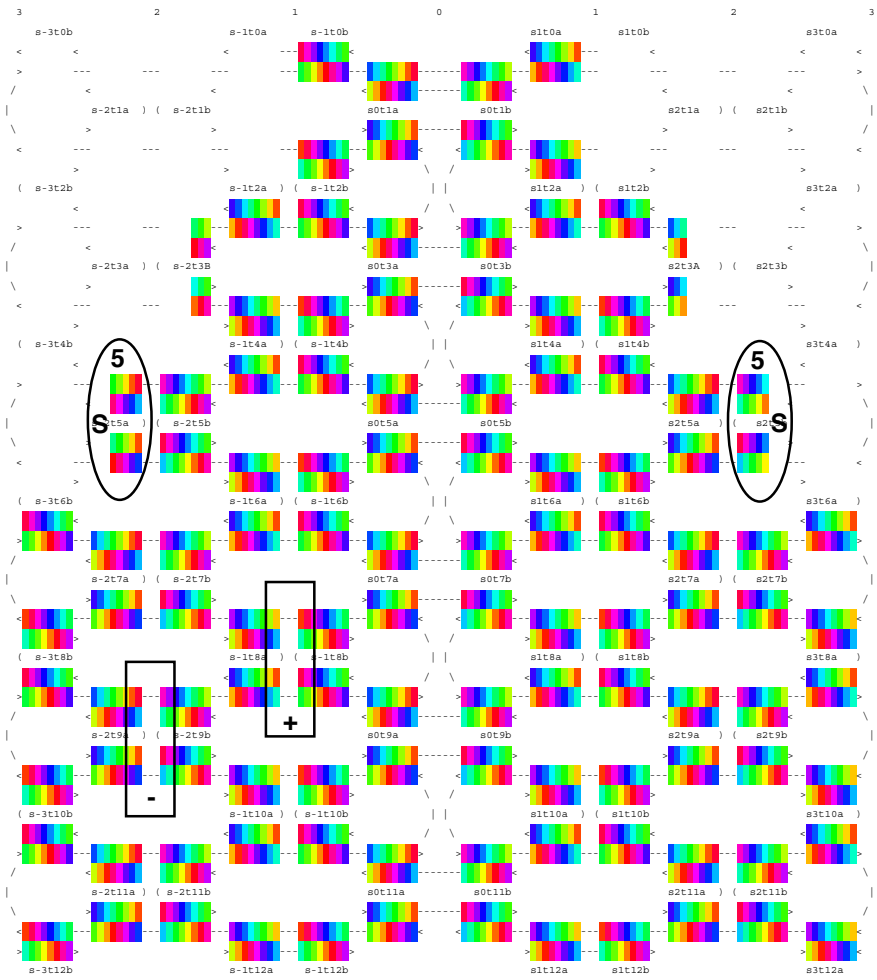


Inspect crossovers for
situation with N+1 bases, and
compare calculated strain.

6-7 boundary 5-6 boundary



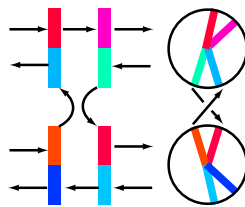
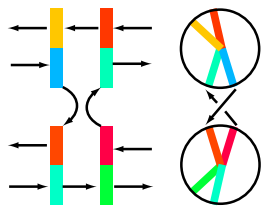
Map of twist at every base in origami.
Cross sections viewed from left.
Color indicates twist of each base.



Compare with balanced crossovers,
placed every 1.5 turns

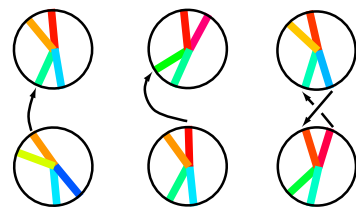
major groove up (+)

minor groove up (-)



6 bases minimize strain.
here, only scaffold crosses.

6 bases 5 bases + is ideal



Colors (and hence twists) of exchanging strands are
the same but colors of non-exchanging strands indicate
positions of major and minor grooves.

Supplementary Figure S3: First pass diagram, twists displayed as colors for examination of strain.

In the second pass a matrix of adjustments (in nucleotides) is defined:

```

%      C1  C2  C3  C4
design{ADJUSTMENTS} = [
      [0  0  0  0];    % H1
      [0  0  0  0];    % H2
      [0  0  0  0];    % H3
      [0  0  0  0];    % H4
      [1  0  0  1];    % H5
      [1  0  0  1];    % H6
      [0  0  0  0];    % H7
      [0  0  0  0];    % H8
      [0  0  0  0];    % H9
      [0  0  0  0];    % H10
      [0  0  0  0];    % H11
      [0  0  0  0];    % H12
];

```

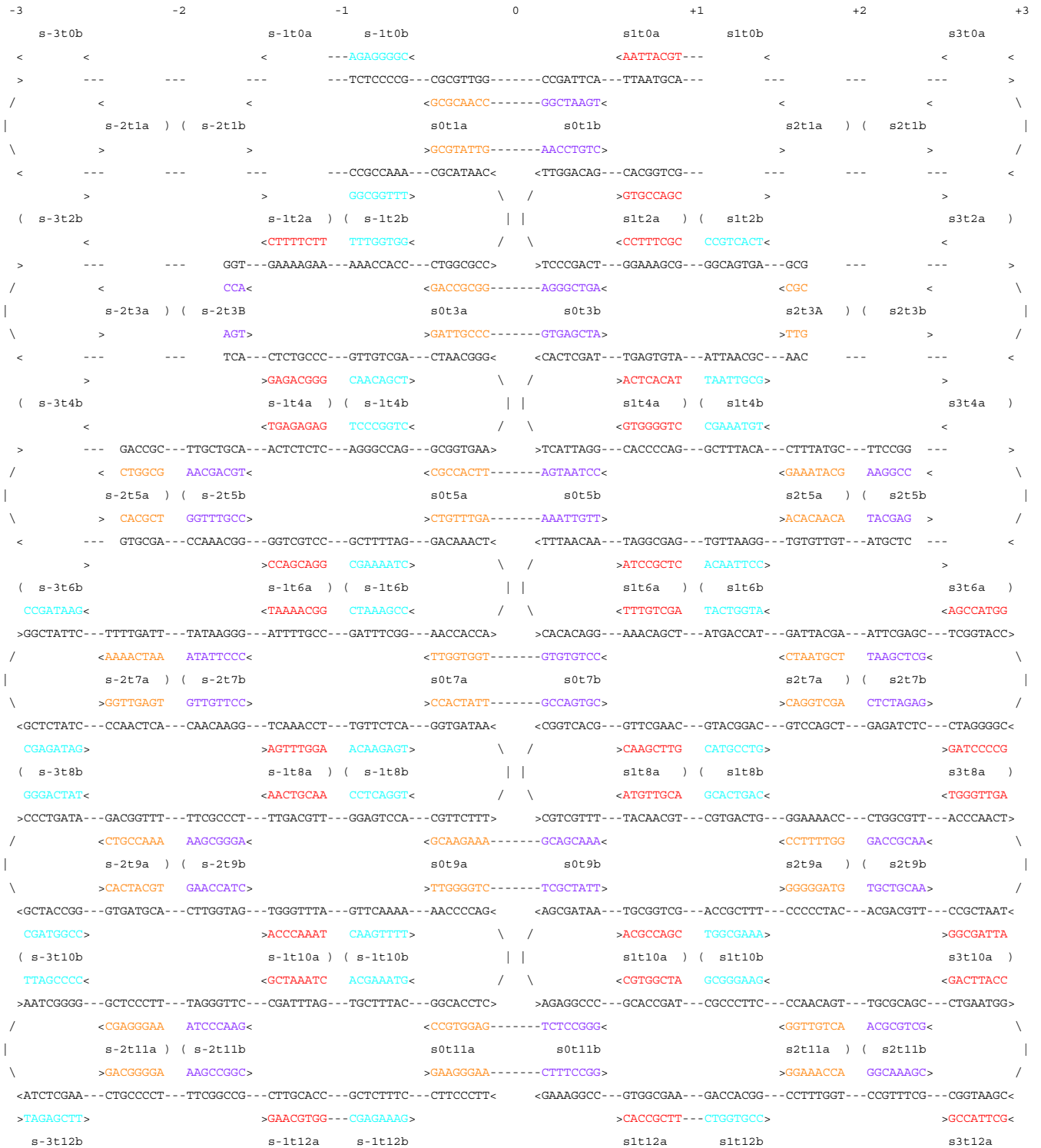
And the design lengths are updated accordingly.

```

design_lengths =
      C0      C1      C2      C3      C4
      32      16       0       0      16
      32      16       0       0      16
      54      27       0       0      27
      54      27       0       0      27
      76      38       0       0      38
      76      38       0       0      38
      96      48       0       0      48
      96      48       0       0      48
      96      48       0       0      48
      96      48       0       0      48
      96      48       0       0      48
      96      48       0       0      48

```

Supplementary Figure S4: Adjustments to applied during the second pass.



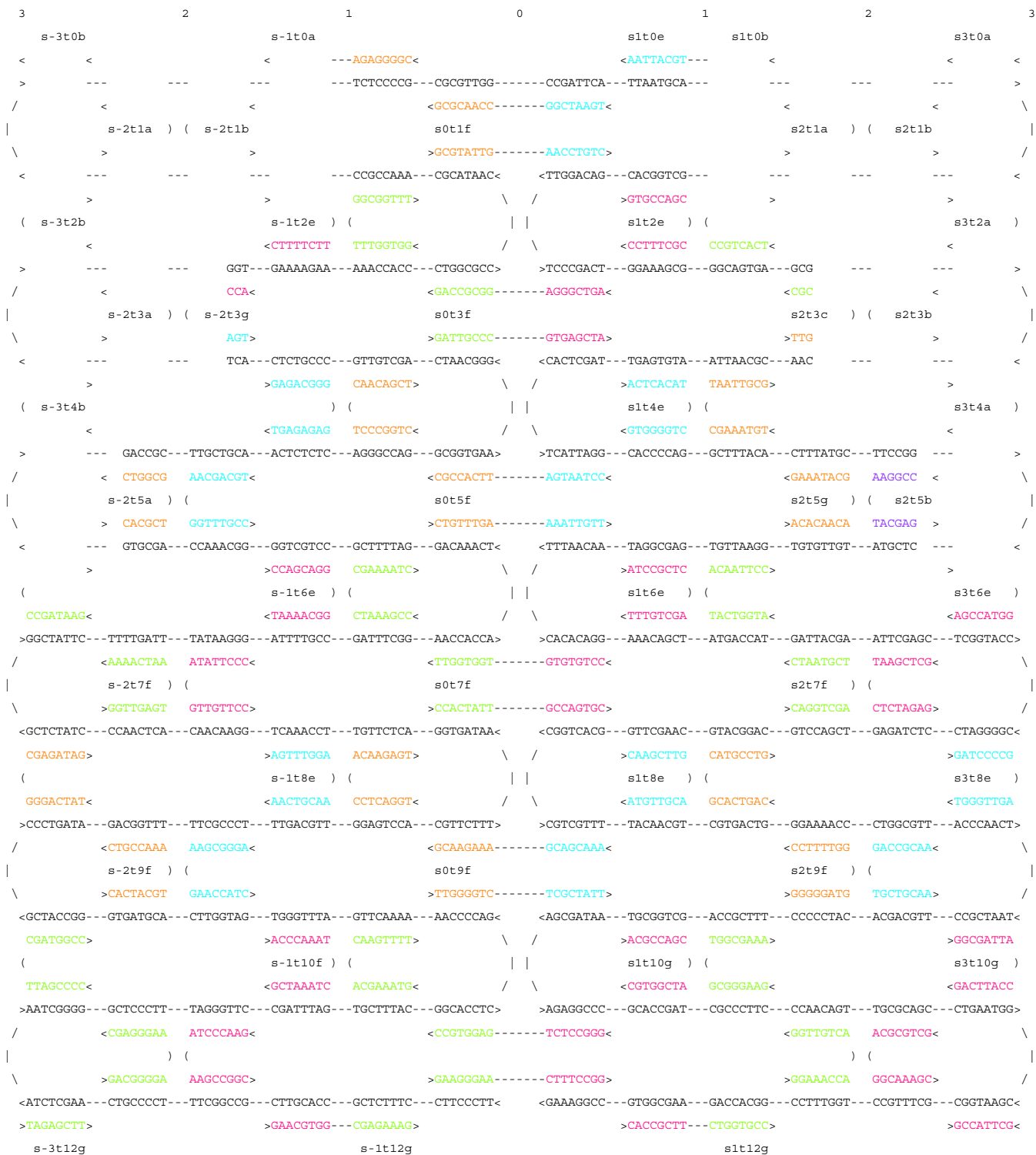
Supplementary Figure S5: Second pass diagram with staple strands before merge.

```

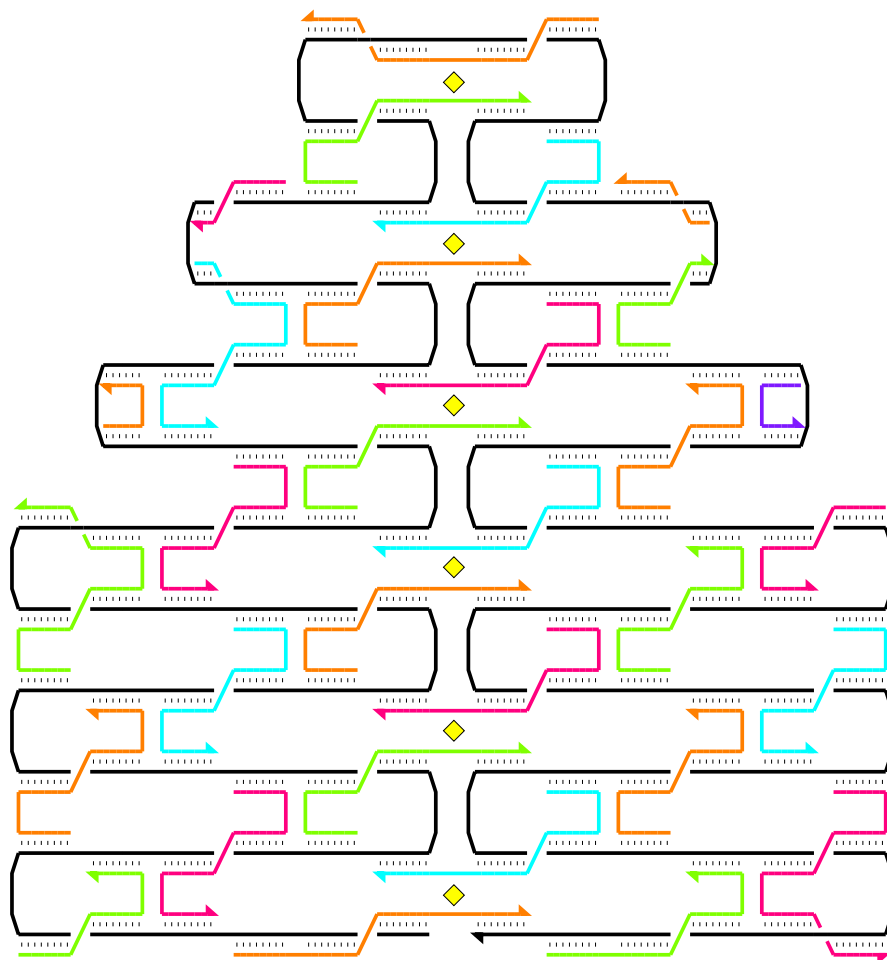
-3          -2          -1          0          +1          +2          +3
s-3t0b          s-1t0a          s1t0g          s1t0b          s3t0a
< < < < ---AGAGGGGC< <AATTACGT--- < < < <
> --- --- --- --- ---TCTCCCGC---CGCGTTGG-----CCGATTCA---TTAATGCA--- --- --- --- >
/ < < < < <GCGCAACC-----GGCTAAGT< < < < < \
| s-2t1a ) ( s-2t1b          s2t1a ) ( s2t1b |
\ > > > > >GCGTATTG-----AACCTGTC> > > > > /
< --- --- --- --- ---CCGCCAAA---CGCATAAC< <TTGGACAG---CACGGTCG--- --- --- --- <
> > > > >GGCGGTTI> \ / >GTGCCAGC > > > >
( s-3t2b          s-1t2e ) ( s-1t2i | |          s1t2i ) (          s3t2a )
< < < < <CTTTTCTT TTTGGTGG< / \ <CCTTTTCG CCGTCACT< < < < <
> --- --- GGT---GAAAAGAA---AAACCACC---CTGGCGCC> >TCCCAGCT---GGAAAGCG---GGCAGTGA---GCG --- --- >
/ < < < < <CCA< <GACCGCGG-----AGGGCTGA< <CGC < < < \
| s-2t3a ) ( s-2t3g          s2t3c ) ( s2t3b |
\ > > > > >AGT> >GATTGCC-----GTGAGCTA> >TTG > > > /
< --- --- --- --- ---TCA---CTCTGCC---GTGTGCGA---CTAACGGG< <ACTCGAT---TGAGTGTA---ATTAACGC---AAC --- --- <
> > > > >GAGACGGG CAACAGCT> \ / >ACTCACAT TAATTGCG> > > > >
( s-3t4b          ) ( s-1t4i | |          s1t4i ) ( s1t4f          s3t4a )
< < < < <TGAGAGAG TCCCGGTC< / \ <GTGGGGTC CGAAATGT< < < < <
> --- GACCGC---TTGCTGCA---ACTCTCTC---AGGGCCAG---GCGGTGAA> >TCATTAGG---CACCCAG---GCTTTACA---CTTTATGC---TTCCGG --- >
/ < CTGGCG AACGACGT< <CGCCACTT-----AGTAATCC< <GAAATACG AAGGCC < < \
| s-2t5a ) (          ) ( s2t5b ) (          |
\ > CACGCT GGTTTGCC> >CTGTTTGA-----AAATGTGT> >ACACAACA TACGAG > > > /
< --- GTGCGA---CCAAACGG---GGTCGTCC---GCTTTTAG---GACAAACT< <TTTAACAA---TAGGCGAG---TGTTAAGG---TGTGTTGT---ATGCTC --- <
> > > > >CCAGCAGG CGAAAATC> \ / >ATCCGCTC ACAATTCC> > > > >
(          s-1t6e ) ( s-1t6i | |          s1t6i ) ( s1t6f          s3t6e )
CGGATAAG< <TAAACGG CTAAAGCC< / \ <TTTGTGCA TACTGGTA< <AGCCATGG < < < <
>GGCTATTC---TTTTGATT---TATAAGGG---ATTTTGCC---GATTTTCGG---AAACCACA> >CACACAGG---AAACAGCT---ATGACCAT---GATTACGA---ATTCGAGC---TCGGTACC>
/ < AAAACTAA ATATTCCC< <TTGGTGGT-----GTGTGTCC< <CTAATGCT TAAGCTCG< < < < \
|          ) (          ) (          |
\ >GGTTGAGT GTTGTTC> >CCACTATT-----GCCAGTGC> >CAGGTGCA CTCTAGAG> > > > /
<GCTCTATC---CCAACTCA---CAACAAGG---TCAAACCT---TGTTCCTA---GGTGATAA< <CGGTCAGC---GTTCGAAC---GTACGGAC---GTCCAGCT---GAGATCTC---CTAGGGGC<
CGAGATAG> >AGTTTGA ACAAGAGT> \ / >CAAGCTTG CATGCCTG> >GATCCCCG
( s-3t8g          s-1t8e ) ( s-1t8i | |          s1t8i ) ( s1t8f          s3t8e )
GGGACTAT< <AACTGCAA CCTCAGGT< / \ <ATGTTGCA GCACTGAC< <TGGGTTGA < < < <
>CCCIGATA---GACGGTTI---TTCGCCCT---TTGACGTT---GGAGTCCA---CGTTCCTT> >CGTCGTTT---TACAACGT---CGTGACTG---GGAAAACC---CTGGCGTT---ACCCAAC>
/ < CTGCCAAA AAGCGGGA< <GCAAGAAA-----GCAGCAAA< <CCTTTTGG GACCGCAA< < < \
|          ) (          ) (          |
\ >CACTACGT GAACCATC> >TTGGGGTC-----TCGCTATT> >GGGGGATG TGCTGCAA> > > > /
<GCTACCGG---GTGATGCA---CTTGGTAG---TGGTTTA---GTTCAAAA---AACCCAG< <AGCGATAA---TGCGGTCG---ACCGCTTI---CCCCCTAC---ACGACGTT---CCGCTAAT<
CGATGGCC> >ACCCAAAT CAAGTTTI> \ / >ACGCCAGC TGGCGAAA> >GGCGATTA
( s-3t10f          s-1t10e ) ( s-1t10i | |          s1t10i ) ( s1t10f          s3t10g )
TTAGCCCC< <GCTAAATC ACGAAATG< / \ <CGTGGCTA GCGGGAAG< <GACTTACC < < < <
>AATCGGGG---GCTCCCTT---TAGGGTTC---CGATTTAG---TGCTTTAC---GGCACCTC> >AGAGGCC---GCACCGAT---CGCCCTTC---CCAACAGT---TGCGCAGC---CTGAATGG>
/ < CGAGGGAA ATCCCAAG< <CCGTGGAG-----TCTCCGG< <GGTTGTCA ACGCGTCG< < < \
|          ) (          ) (          |
\ >GACGGGA AAGCCGGC> >GAAGGGAA-----CTTTCCGG> >GGAACCA GGCAAAGC> > > > /
<ATCTCGAA---CTGCCCTT---TTCGCCCG---CTTGACC---GCTCTTTC---CTTCCCTT< <GAAAGGCC---GTGGCGAA---GACCACGG---CCTTTGGT---CCGTTTCG---CGTAAGC<
>TAGAGCTT> >GAACGTGG---CGAGAAAG> >CACCGCTT---CTGGTGCC> >GCCATTGC<
s-3t12f          s-1t12j          s1t12g

```

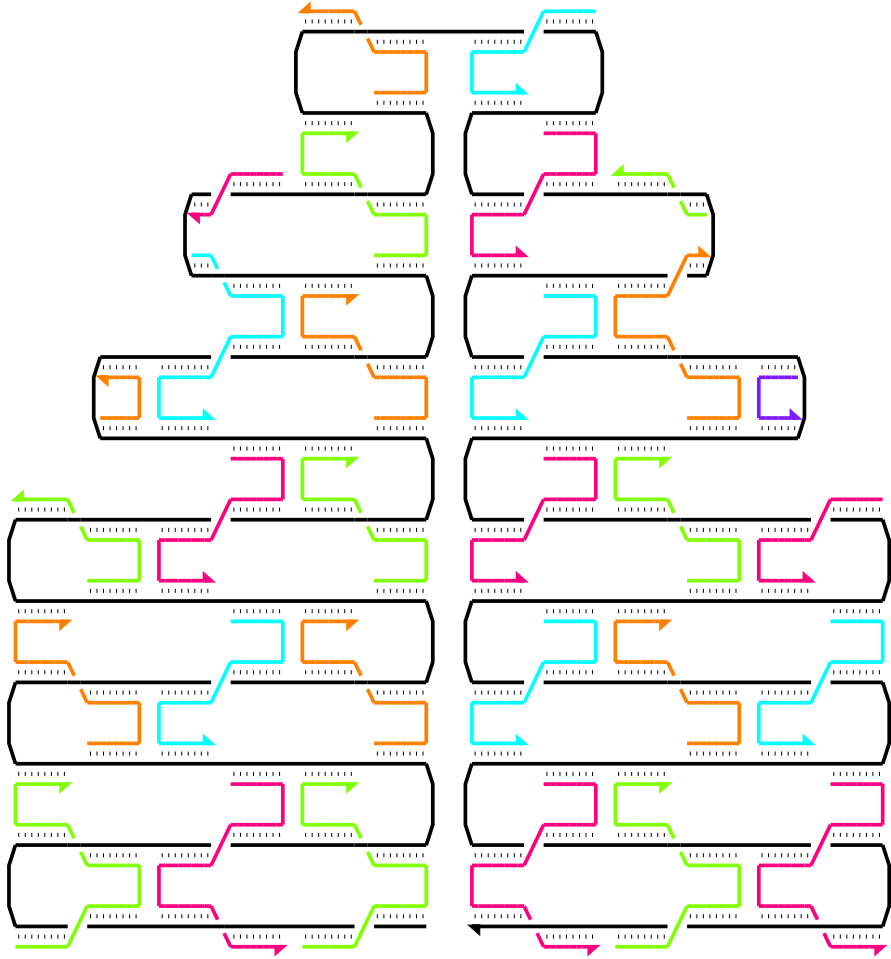
Supplementary Figure S6: Third pass diagram with staple strands after merge (bridged seam).



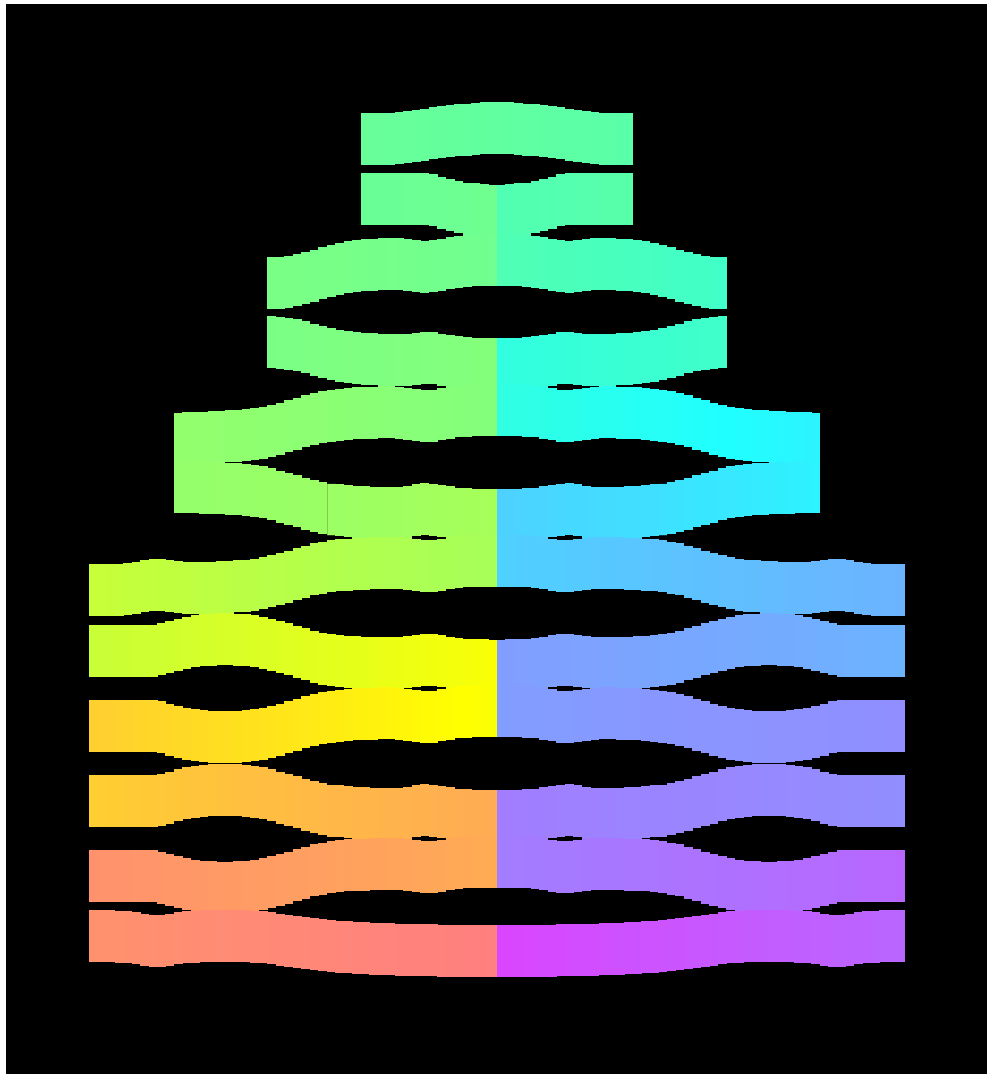
Supplementary Figure S7: Third pass diagram with staple strands after merge (unbridged seam).



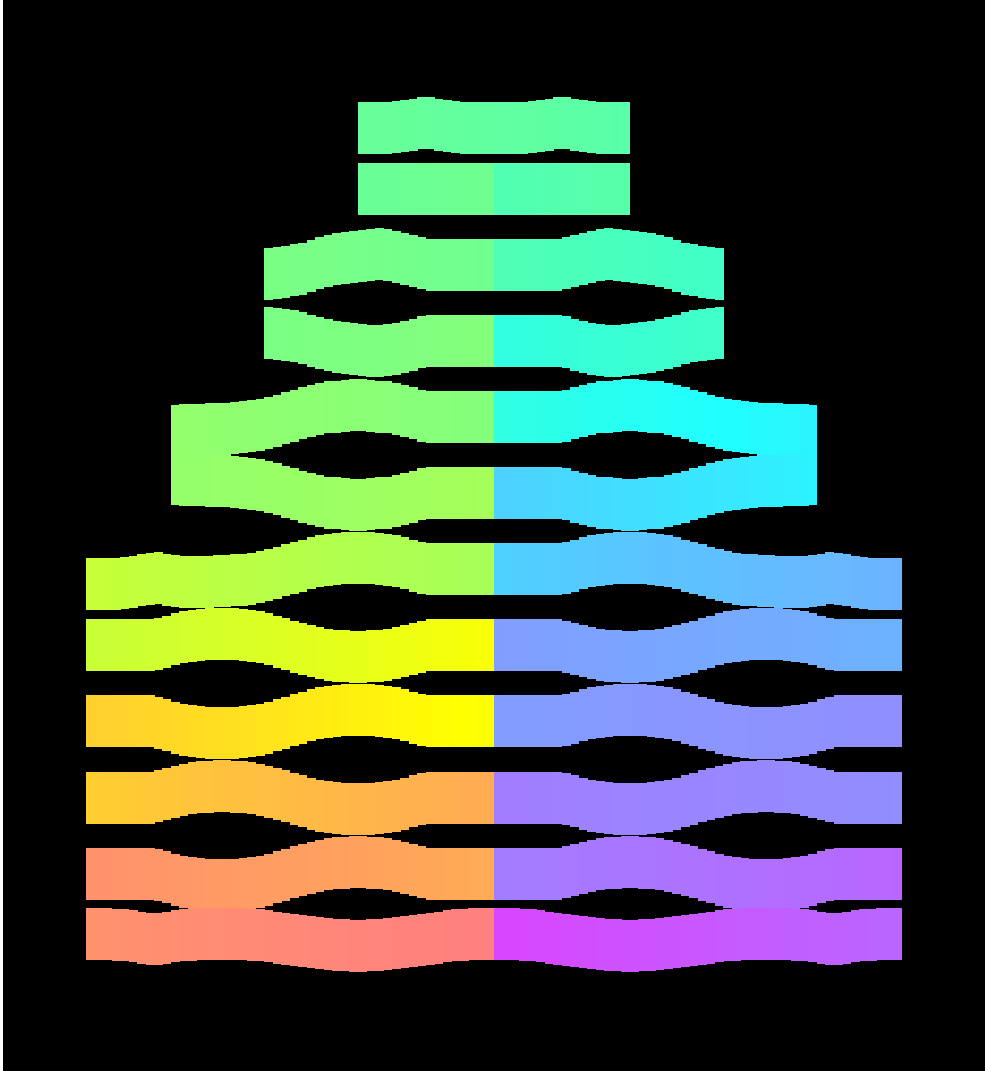
Supplementary Figure S8: Third pass diagram with staple strands after staggered merge.



Supplementary Figure S9: Third pass diagram with staple strands after rectilinear merge.



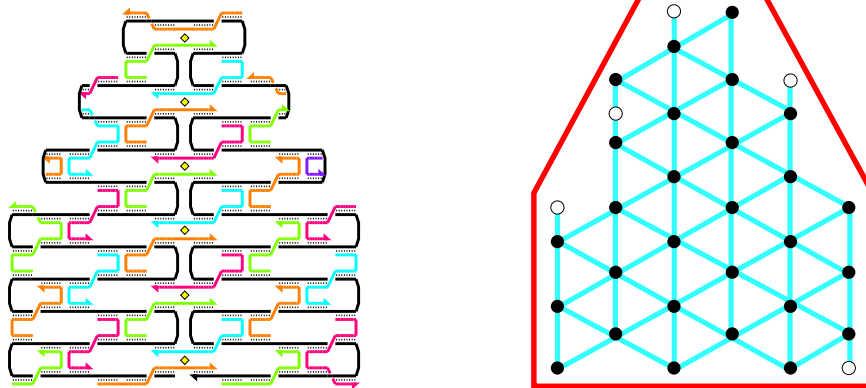
Supplementary Figure S10: Crossover diagram of bridged design.



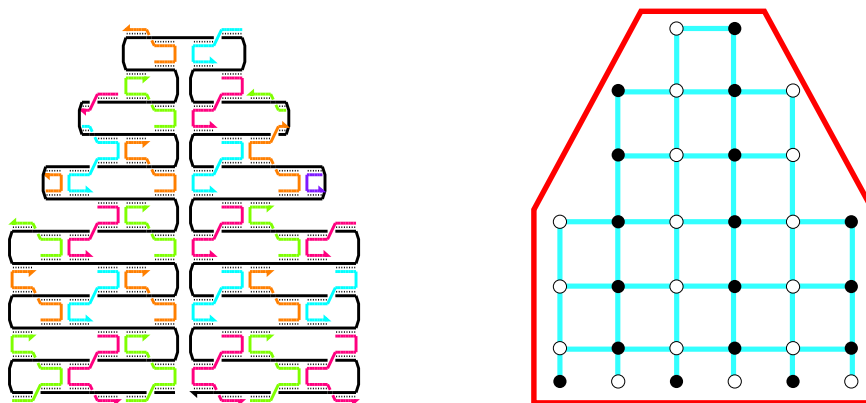
Supplementary Figure S11: Crossover diagram of unbridged design.

a

Staggered merge pattern

**b**

Rectilinear merge pattern



Supplementary Figure S12: Different patterns of merges yield different types of grids for any pixel pattern. Black dots indicate merges made on the top face of the structure, white dots indicate merges made on the bottom face. To create a ‘1’ pixel a hairpin is added at the position of one of the merges. Special cases on the edge of the shape are not normally used for pixels. **a** A staggered pattern of merges. In this case all modifications made to the middle of a staple strand fall on the same face of the lattice. **b** A rectilinear pattern of merges. In this case a modifications made to the middle of a staple strand fall on alternating faces of the lattice, depending on the column in which they occur. While the structure in **a** has a bridged seam, and the structure in **b** has an unbridged seam, the basic pattern of merges is independent of whether or not the seam is bridged.

Supplementary Note S2: Effects of inter-helix gaps and DNA bending on the length and width of DNA nanostructures

When the first planar DNA nanostructures based on parallel double helical domains were made (DNA tile lattices based on double-crossover molecules²⁵) a few assumptions were made about their structure. It was assumed (1) that the helices would be lie close-packed and (2) that the helices would be without bends. Implicit in these assumptions were two more: (3) the length of DNA nanostructures with parallel helices (measured perpendicular to the helices) was assumed to be given by $2h$ nanometers where h is the number of helices and (4) the width was assumed to be $.34n$ nanometers where n was the number of nucleotides in the structure. Here I review what has been learned about these assumptions. (1) turns out to be incorrect, at least for structures imaged by AFM on mica under buffer. Because of this, (2) appears to be incorrect and (3) is not a good approximation for the length (top to bottom) of a DNA nanostructure. While (4) is probably inexact it turns out to remain a useful approximation for the width of a DNA nanostructure.

When a DNA nanostructure with parallel helices bound by together crossovers is imaged by AFM, the result does not model a series of close-packed cylinders. Instead, AFM seems to reveal gaps between helices, typically 1-2 nm wide, whose position and length follow the pattern of crossovers in the underlying structure. Wherever two helices have a crossover, no gap is observed; a few nanometers away from a crossover, an inter-helix gap is observed.

The source of the inter-helix gap is unknown, it may be electrostatic repulsion between helices (as first, to my knowledge, suggested by Rizal Hariadi), or detailed geometry of the crossovers (free crossovers, when not constrained by adjacent crossovers in a multi-crossover molecule, assume an angle of approximately 60 degrees^{32, 33}). It remains for the gap to be measured on different substrates, or in solution, or by a different imaging technique such as TEM, or for it to be measured as a function of salt concentration which might be expected to change the gap by changing the screening of electrostatic interactions.

Whatever the source, the width of the gap appears to depend on the spacing of crossovers: here origami with 16 nt spacing (about 1.5 turns) between crossovers have a ~ 1 nm gap, origami with 26 nt spacing (about 2.5 turns) appear to have a ~ 1.5 nm gap. I note that the relationship between crossover spacing and gap width is not yet proven. Here, all structures with 2.5-turn spacing have one pattern of nicks—that of Fig. 1c—that yields staples that connect only 2 helical domains; on the other hand, all structures with 1.5 turn spacing have a pattern of nicks—that of Fig. 1e that connect 3 helical domains. Thus it is possible that 2.5-turn spacing structure with a nick pattern like that of Fig. 1e might have a different spacing than the 2.5-turn structures explored here. To test whether the pattern of nicks has an effect one could re-render the 2.5-turn spacing square with 3-helix spanning staple strands as in Fig. 1e.

Because the interhelix gap appears to set the aspect ratio of DNA nanostructures constructed from parallel helices, we can use it to attempt to engineer the length and width of DNA origami. With an estimate of the gap in hand, it is simple to design DNA origami with a desired *length* (if a roughly periodic pattern of crossovers is used): the length of the structure should be $2h + (h - 1)g$ nm where h is the number of 2 nm wide helices and g is the inter-helix gap. Lengths measured by AFM are typically within 5% of the predicted length by this formula; it assumed that this error is caused by AFM drift or miscalibration. Note that the formula predicts lengths roughly 50% and 75% greater than those that would be predicted assuming close-packed helices.

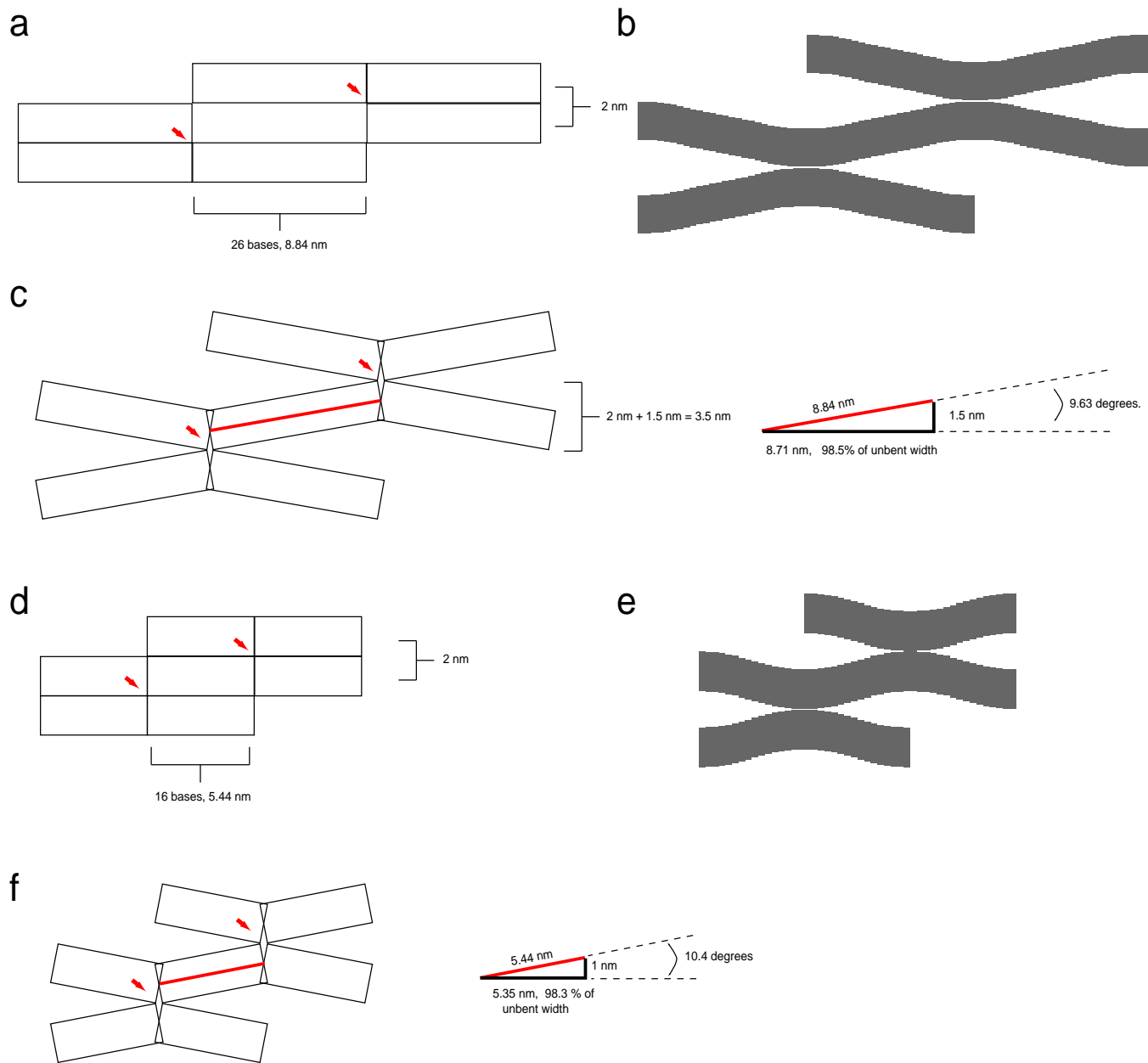
Given an estimate of the inter-helix gap, it would seem *a priori* more difficult to estimate or design the *width* of a DNA origami. To create the inter-helix gap it appears the DNA helices must bend back and forth between the crossovers in which they participate. If one assumes that the contour length of a helix of DNA does not change as it bends and follows a curve, then the end to end distance of a DNA helix following such a curve must be shorter than the end to end distance of a straight helix of the same number of nucleotides. That is, to get a correct estimate for the width of an origami, one must take the bend into account.

However, very little is known about the nature of the bending. So far, few AFM images of DNA have a resolution high enough for the contour of the helix to be traced explicitly and so it seems there is not enough data to model it accurately. Exactly what curve is followed by the helix is probably affected by electrostatic repulsion between the DNA backbones, mechanics of DNA bending, the amount of supercoiling between crossovers, and detailed geometry of the junctions. In the schematic drawing of DNA origami (row 2, Fig. 2) I give a cartoon version of the bending that seeks to reproduce structures seen in AFM images based on the pattern of crossovers in the design. Zooms of the curve used, (based on the sums of exponentials that decay away from crossovers) are giving in Supplementary Fig. S13b and e. There is no reason to believe that these curves are physically accurate.

As a very rough estimate of the change in width due to helix bending, close-packed versions of the 2.5 turn spacing and 1.5 turn spacing lattices (Supplementary Fig. S13 a and d) were deformed by bending the helical domains between crossovers an amount appropriate to create the inter-helix gap (≈ 10 degrees). The projection of these bent domains on the x-axis was then calculated and taken as the new width between crossover. The width between crossovers

changed less than -2% in both cases (Supplementary Fig. S13 c and f), because of the small angles involved. I note that because I use 32 nt to cover 3 helical turns in the 1.5 turn spacing designs, the DNA in most designs is overtwisted (relative to 10.5 bases/turn) by 1.5%. Thus it is possible that relaxation of supercoiling might have a compensatory effect (relative to the effect of bending) on the width of DNA origami. (On the other hand, 52 bases are used to cover 5 turns in the 2.5 turn spacing designs and they are 1% undertwisted with respect to 10.5 bases/turn.)

Finally, the experimental widths of DNA origami are typically within 10% of that predicted using the $.34n$ nanometers approximation. Thus while helix bending appears to happen to accommodate the inter-helix gap, the width of structures is predicted by the formula $.34n$ nanometers to within AFM error.



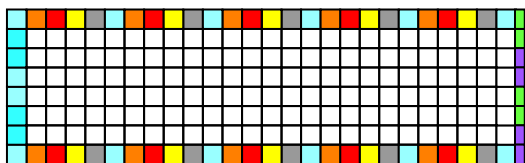
Supplementary Figure S13: A figure that suggests that the effect of helix bending between crossovers contributes little to the width of a DNA origami.

Supplementary Note S3: Designs and sequences

In this note, for all large designs I include: (1) a block diagram and reproduction of the folding path (2) an enlargement of the schematics used to diagram the effects of crossover position on helix bending as in Fig. 2, row 2 and (3) the list of sequences used. A few comments:

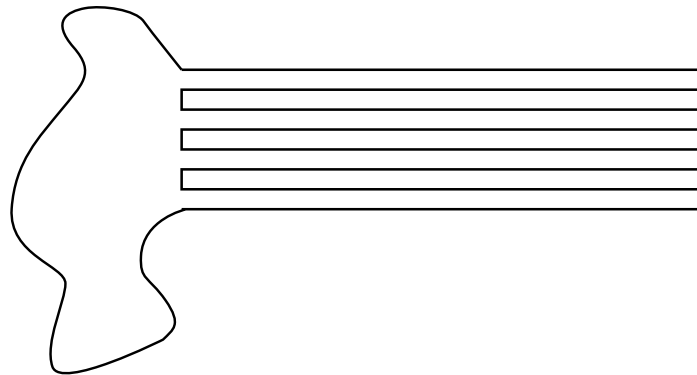
1. **Because they are very large and do not print well, the full designs with staple and scaffold sequences explicitly written out appear in a separate file as Supplementary Note 12, not here.**
2. For the 1/3 square, the crossover diagram is not included but is similar to that for the full square.
3. For the smiley and star I include high-resolution AFM that corresponds well to the crossover models for comparison. For the smiley I include a model of how smileys can maximize stacking interactions.
4. For the tall rectangle, two different crossover diagrams are given, one for a bridged seam, and one for the unbridged seam (as used in Fig. 3e-i).
5. At the end of this note the full sequence of the New England Biolabs clone of M13mp18 used in this paper is included (Supplementary Fig. S39). The sequence is unpublished and appears to be available only from the NEB web site.

a



26.5 turns wide at 10.4 bases/turn -> 276 bases
8 helices tall

b



Supplementary Figure S14: Schematics for $\sim 1/3$ of the square (8 helices) in Fig. 2a used in the first origami experiments (Supplemental Note S5.3). **a** Block diagram. Designed for 2.5-turn spacing blocks have 5 different offsets with respect to the underlying lattice of crossovers, hence the 5 different hues of blocks in different columns. As in other block diagrams, orange block/red block boundaries have an offset of 0 turns with respect to the underlying lattice of crossovers. **b** Folding path. A circular scaffold is used.

1y_1C; GAGCCCCGATTAGAGCTTGACGGG
x3y_1C; CAAGTTTTTGGGGTCGAGGTGCCGT
x5y_1C; CGAAAAACCGTCTATCAGGGCGATGG
x7y_1C; AGTTGGAAACAAGAGTCCACTATTTAA
x9y_1C; AATCGGCAAAATCCCTTATAAATCAAAGAATAG

x0y0A; CTGGGTGCCTAATGAGTGCCTGGCGAGAAAGGAAGGAA
x0y0B; GAAAGCCGGCAACTAAGTACACATTA
x2y0A; CCAGTCGGGAAACGGAAACCCATAAAGG
x2y0B; AAAGCACTAAATCCTGTCGTGCCAGC
x4y0A; GGGAGAGCGGTTCCATCACCCAAAT
x4y0B; CCCACTACGTGAATGCGTATTGGGCG
x6y0A; GAGACGGGCAACACACGTCAAAAGGG
x6y0B; AGAACGTGGACTCGCTGATTGCCCTT
x8y0A; GCAAGCGTCCACTGAGTGTGTTC
x8y0B; CCCGAGATAGGGTGTGGTTGCCCC

x1y1A; ATTGCGTTGCGCTCTCACAATCCAC
x1y1B; AAATTGTTATCCGCACTGCCCGCTT
x3y1A; TGCATTAATGAATCTCGAATTCGTAA
x3y1B; CCCGGTACCAGCGGCCAACCGCGG
x5y1A; CCAGGTGTTTTTGCACAGCTTGCA
x5y1B; AAACGACGGCCAGTCTTTTACCAGT
x7y1A; CACCGCTGGCCGTTGGGTAAACGCC
x7y1B; GCAAGCGATTAAAGAGAGATTGCA
x9y1A; AGCAGGCAAAATCTTCGCTATTAC
x9y1B; GAAGGCGATCGGTGCGGCCCTGTTGATGGTGTCCGA

x0y2A; CGCGTCTGGCCTTCCCTGTAGCCGAAGCATAAAGTGTAAAGC
x0y2B; ACAACATACGAGCCAGCTTTCATCAA
x2y2A; GTCGGATTCCTCGGTTCCTGTGTG
x2y2B; TCATGGTCATAGCTGGGAACAACGG
x4y2A; CGTTGGTGTAGATACTCTAGAGGATC
x4y2B; TGCCTGCAGTCCGGGCGCATCGTAA
x6y2A; GACGACAGTATCGTCACGACGTTGTA
x6y2B; AGGGTTTTCCAGGCCCTCAGGAAGAT
x8y2A; GCTTCTGGTCCGAGGGGATGTCT
x8y2B; GCCAGCTGGCAAGAACCCAGGCAAA

x1y3A; CATTAAATGTGAGTAAATCAGCTCAT
x1y3B; ATTAATTTTTGTGAGTAAACAAACC
x3y3A; CGGATTGACCGTATATTTAAATTTGTA
x3y3B; TTGTATAAGCAAAATGGGATAGGTCA
x5y3A; CCGTGCATCTGCCCCCGGTTGATAA
x5y3B; TCAATCATATGTAAGTTTGGGGGAC
x7y3A; CGCACTCCAGCCAACAAGGAATCGA
x7y3B; GAGTCTGGAGCAAGCTTTCGGCACC
x9y3A; GCGCCATTCGCATTTTGGAGATCT
x9y3B; AATGCCGAGAGGGTAGCTATTTCCAGGCTCCCAACTGTTGG

x0y4A; CAATAAATCATACAGGCAAGGGAAACGCCATAAAAAAAT
x0y4B; TTTTAAACCAATACAAAGAATTAGCA
x2y4A; TAAAGCTAAATCGGTAAAAATTCGC
x2y4B; AACGTTAATATTTGTTGTACAAAAA
x4y4A; GGGAAGCCCTTAAAAAACAGGAAGA
x4y4B; TCAGAAAAGCCCTTTCACGCAAGG
x6y4A; TTTTAAATGCAATTAATAAGTATGATG
x6y4B; TGAACGTAATCGGCCTGAGTAAATG
x8y4A; AAGCCGGAGACAGGTCATTGCCTGA
x8y4B; ACAAAGCTATCAGTCAATCACCAT

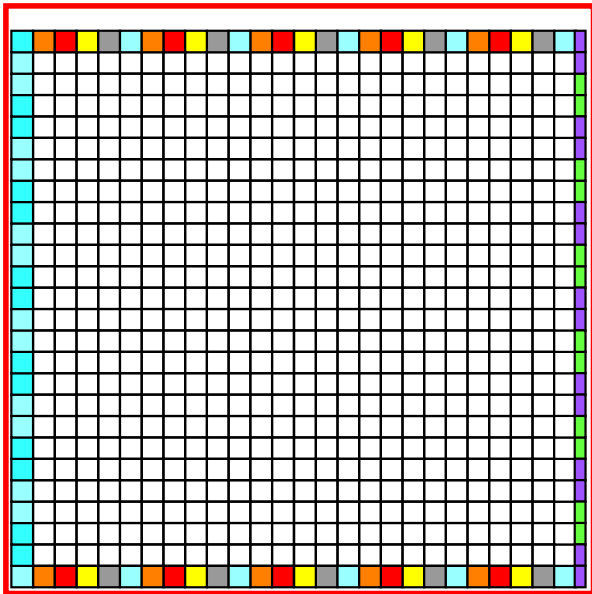
x1y5A; AAATTAAGCAATAGCTGAAAAGGTGG
x1y5B; ATTTGGGCGCGAAAGCCTCAGAGCA
x3y5A; CATTATGACCCGTATTTCGCAATGG
x3y5B; GACCATTAGATACTAATACTTTTGGC
x5y5A; ATAAAAATTTTACAGTGTATCCCA
x5y5B; TCATTCCATATAAGAACCCTCATATA
x7y5A; GTAGTAAAGATTTGTTTAAATATG
x7y5B; CTGTAGCTCAACACAAAAGGGTGAGA
x9y5A; CAATATGATATCTTTTCCGGATGCG
x9y5B; CTCCTTTTGATAAGAGTCAATAACCGTTCTAGCTGATAAAT

x0y6A; ATGTTTAGACTGGATAGCGTCAATAGTAGCATTAAACATC
x0y6B; CATCAATCTACTCAATACTGCGGAA
x2y6A; CTCAAATGCTTTATAGCTATATTTTC
x2y6B; TCAATAACCTGTTAACAGTTTACAGAAA
x4y6A; AGGTCTTTACCTGTAGATTAGTTT
x4y6B; ATTTCTGCGAAGCAGACTATTATAGTC
x6y6A; GATTAGAGGAAGGTGTGGAAGTT
x6y6B; CAACTAAAGTACCCCGAAGACTTC
x8y6A; AAAGCAACCAAGCTGAATATAATG
x8y6B; TTAGAGCTTAATTCGGAAAGCAAACT

x1y7C; TCGTCATAAATATTCAATGAATCCCC
x3y7C; ACGAGAATGACCATAAATCAAATAATC
x5y7C; AGAAGCAAAAGCGGATTGCTCAAAAAA
x7y7C; AAATATCGCGTTTTAATTCGAGCTTC
x9y7C; CCAACAGTCCAGGATTAGAGAGTACCTTTAATG

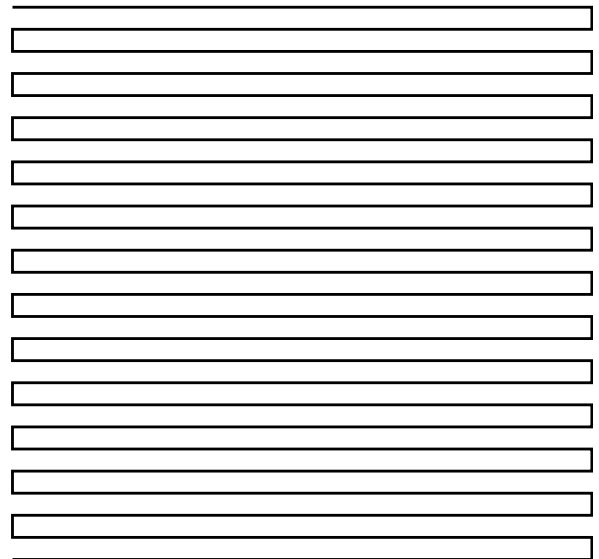
Supplementary Figure S15: Strands used to create $\sim 1/3$ of a square.

a

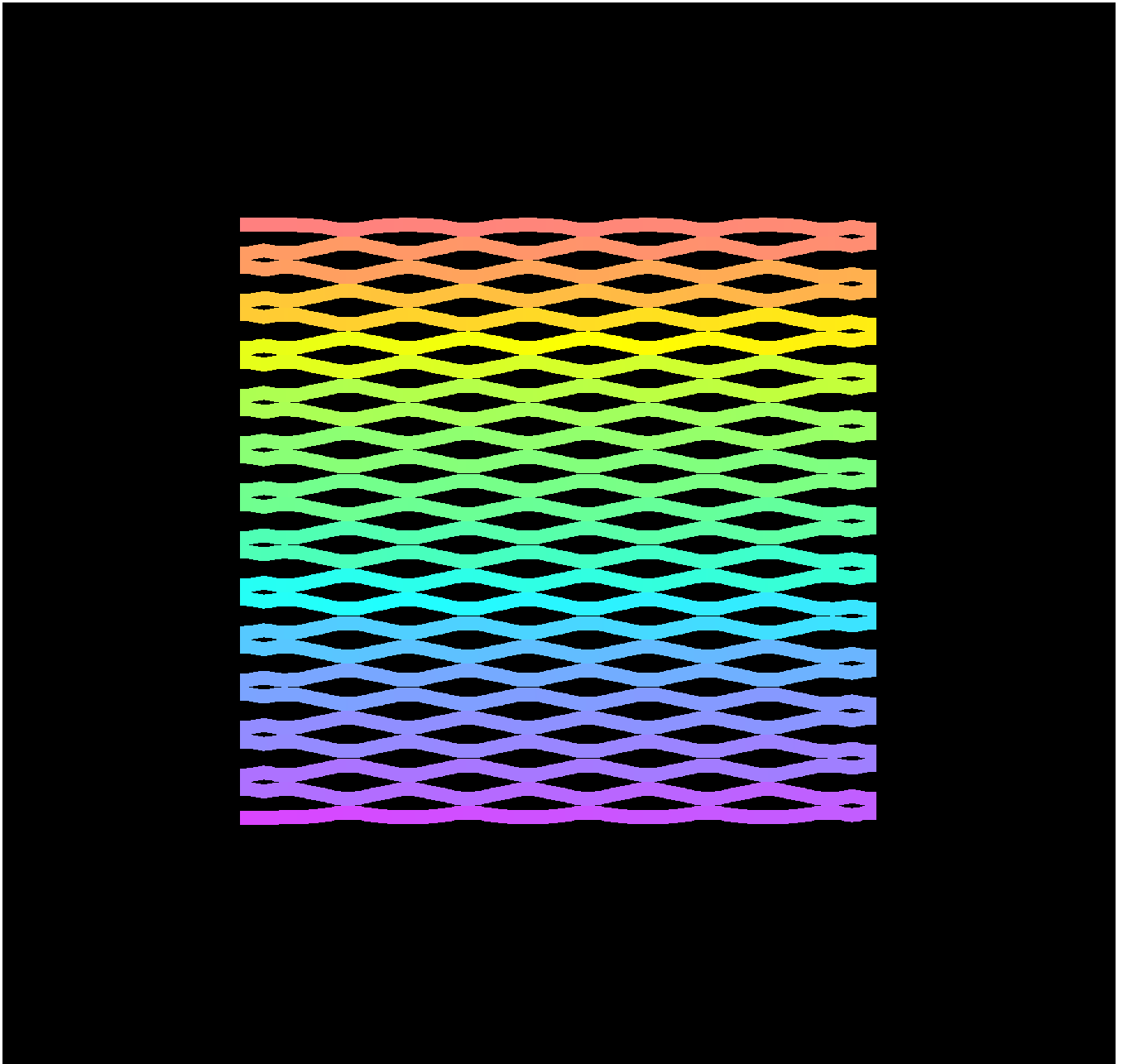


26.5 turns wide at 10.4 bases/turn -> 276 bases
26 helices tall

b

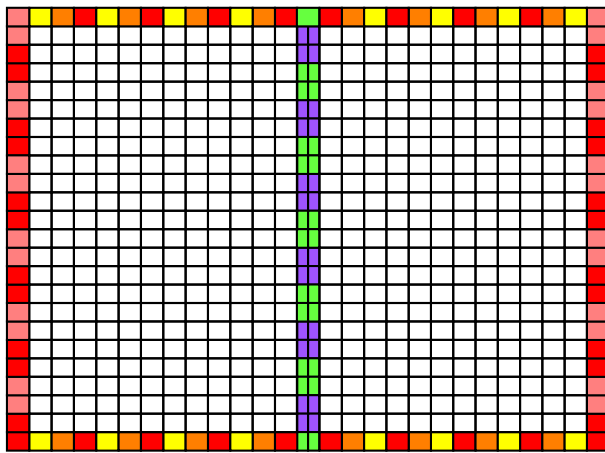


Supplementary Figure S16: Schematics for the square in Fig. 2a. **a** Block diagram. Designed for 2.5-turn spacing, blocks have 5 different offsets with respect to the underlying lattice of crossovers, hence the five different hues of blocks in different columns. As in other block diagrams, orange block/red block boundaries have an offset of 0 turns with respect to the underlying lattice of crossovers. The red square highlights our prediction for how well the design is expected to approximate a square. **b** Folding path.



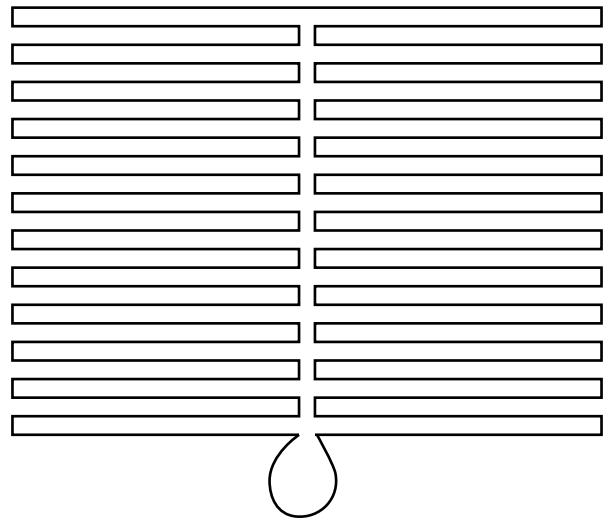
Supplementary Figure S17: Crossover induced structure of square.

a

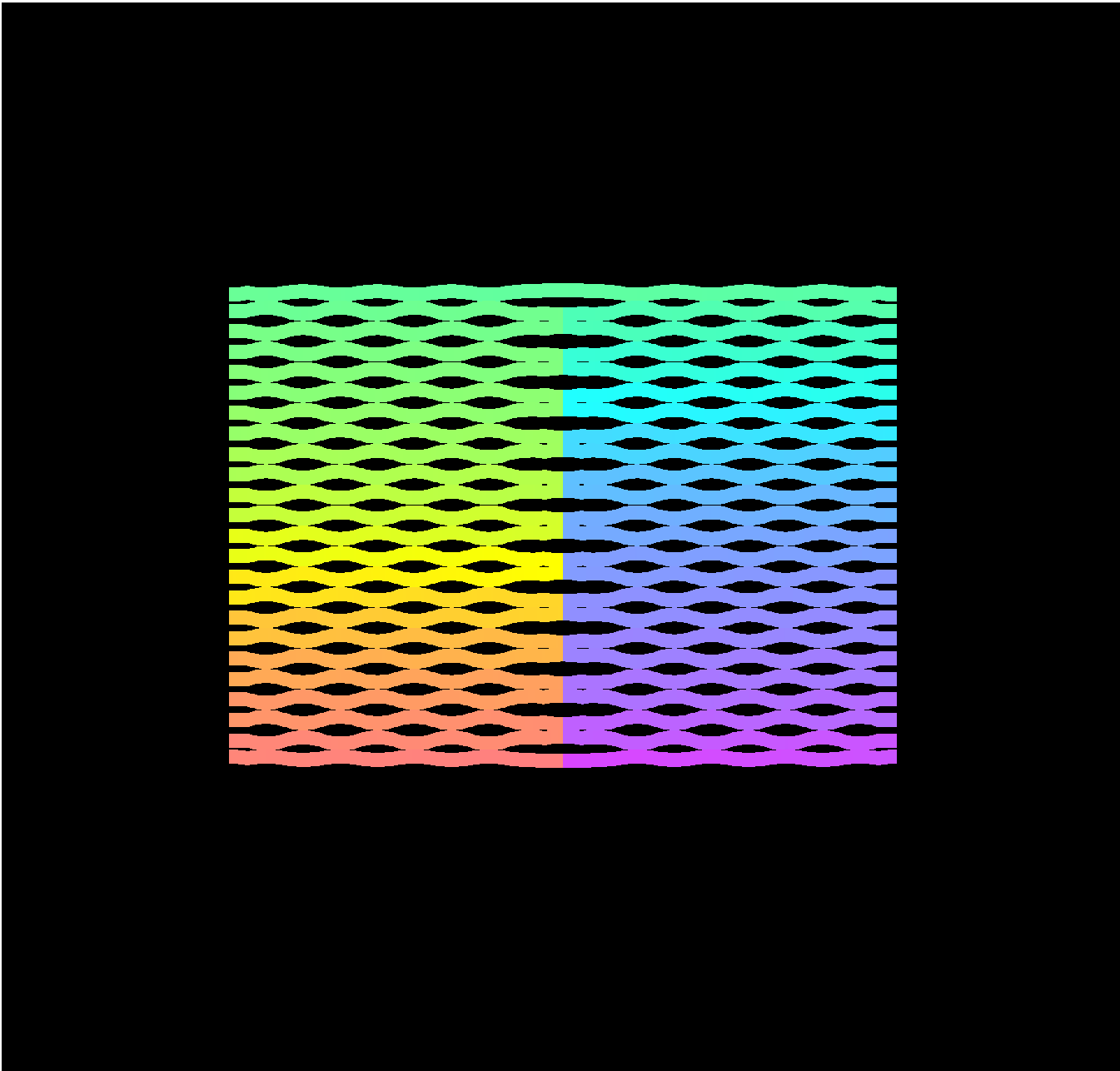


27 turns wide at 10.666 bases / turn -> 288 nt
24 helices tall

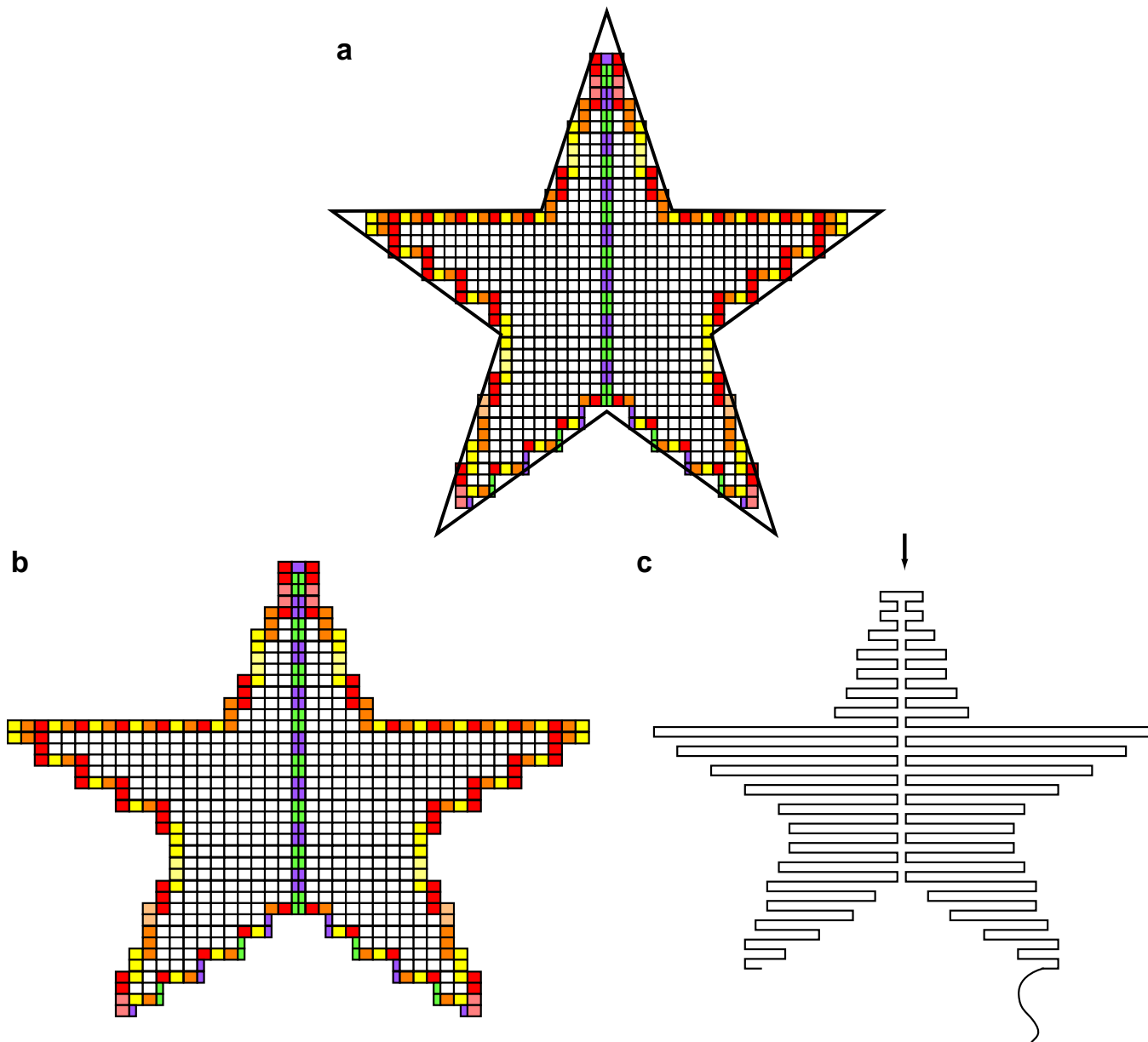
b



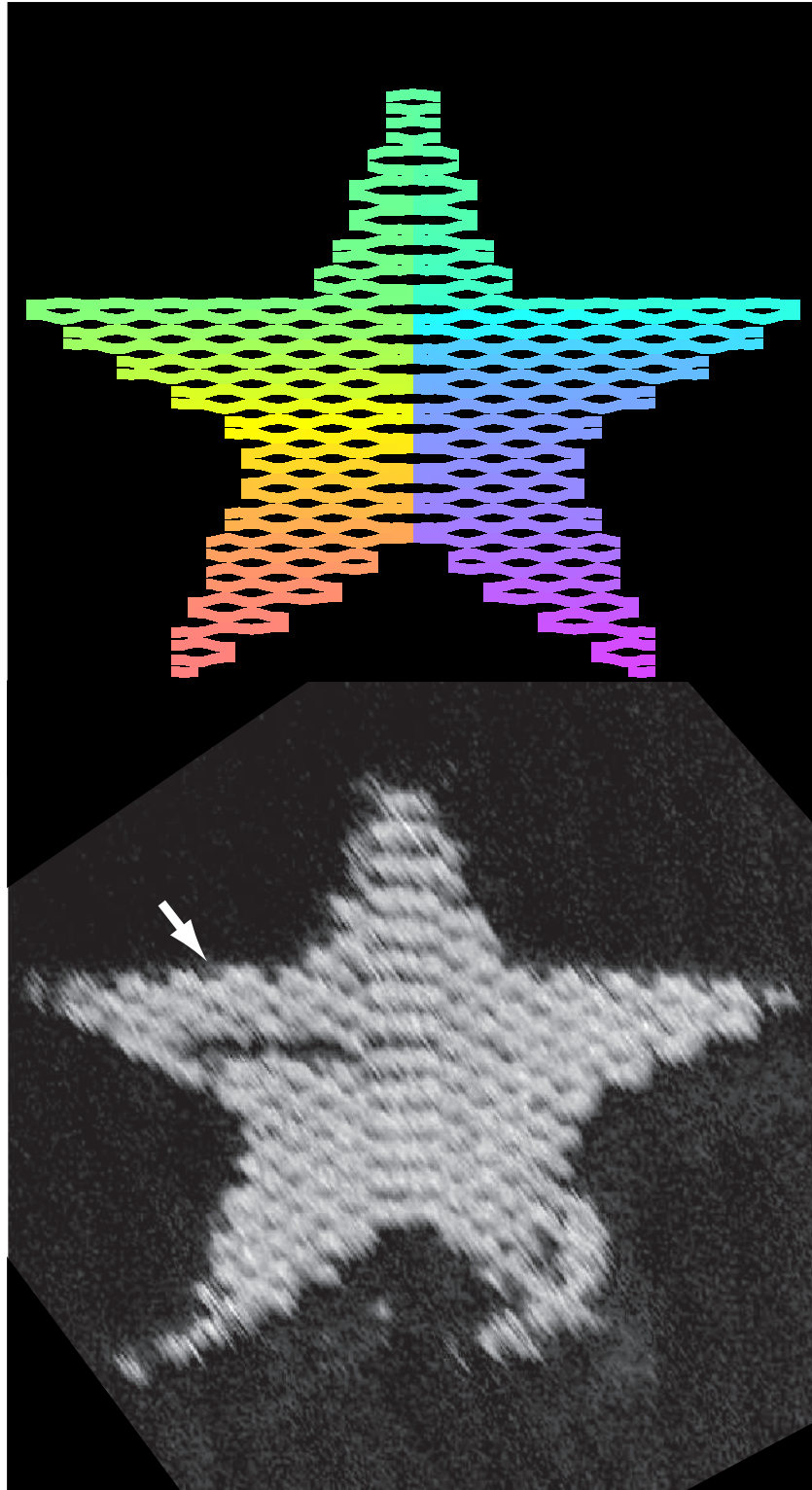
Supplementary Figure S19: Schematics for the rectangle Fig. 2b. **a** Block diagram. **b** Folding path.



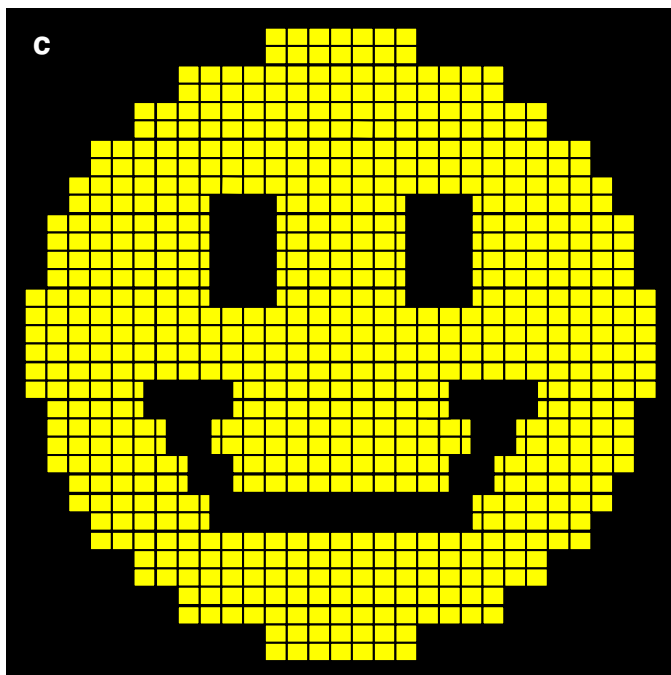
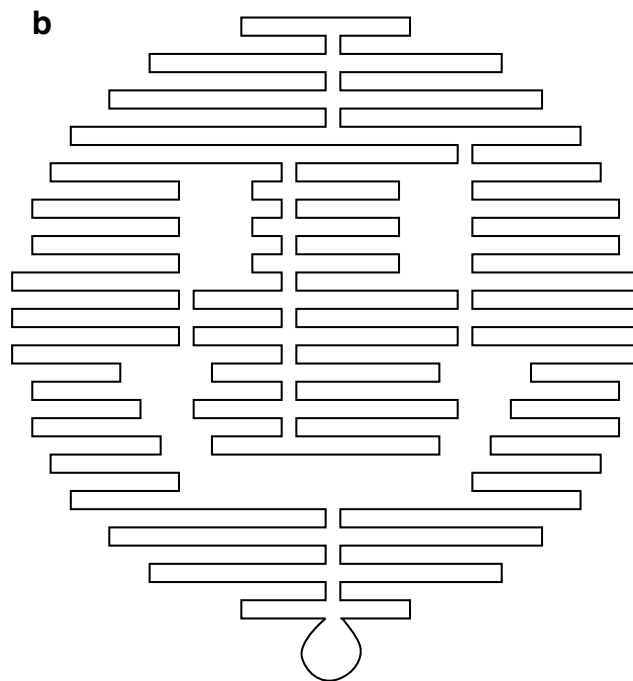
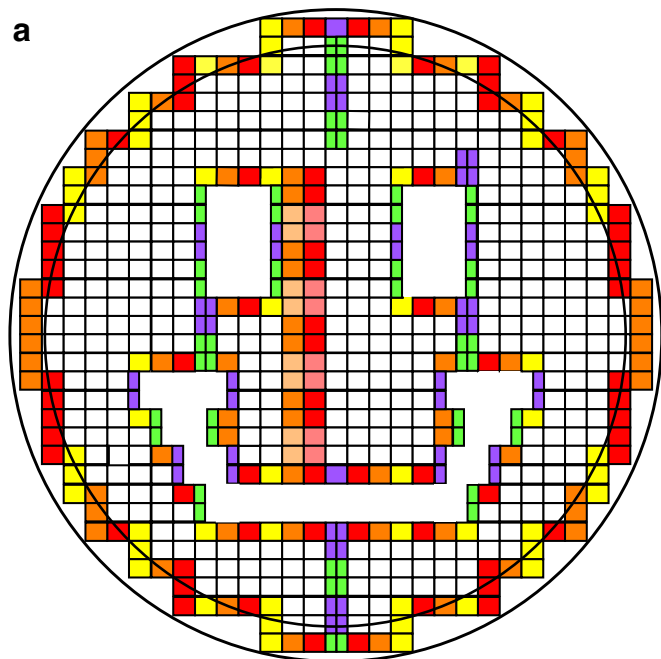
Supplementary Figure S20: Crossover diagram for the rectangle.



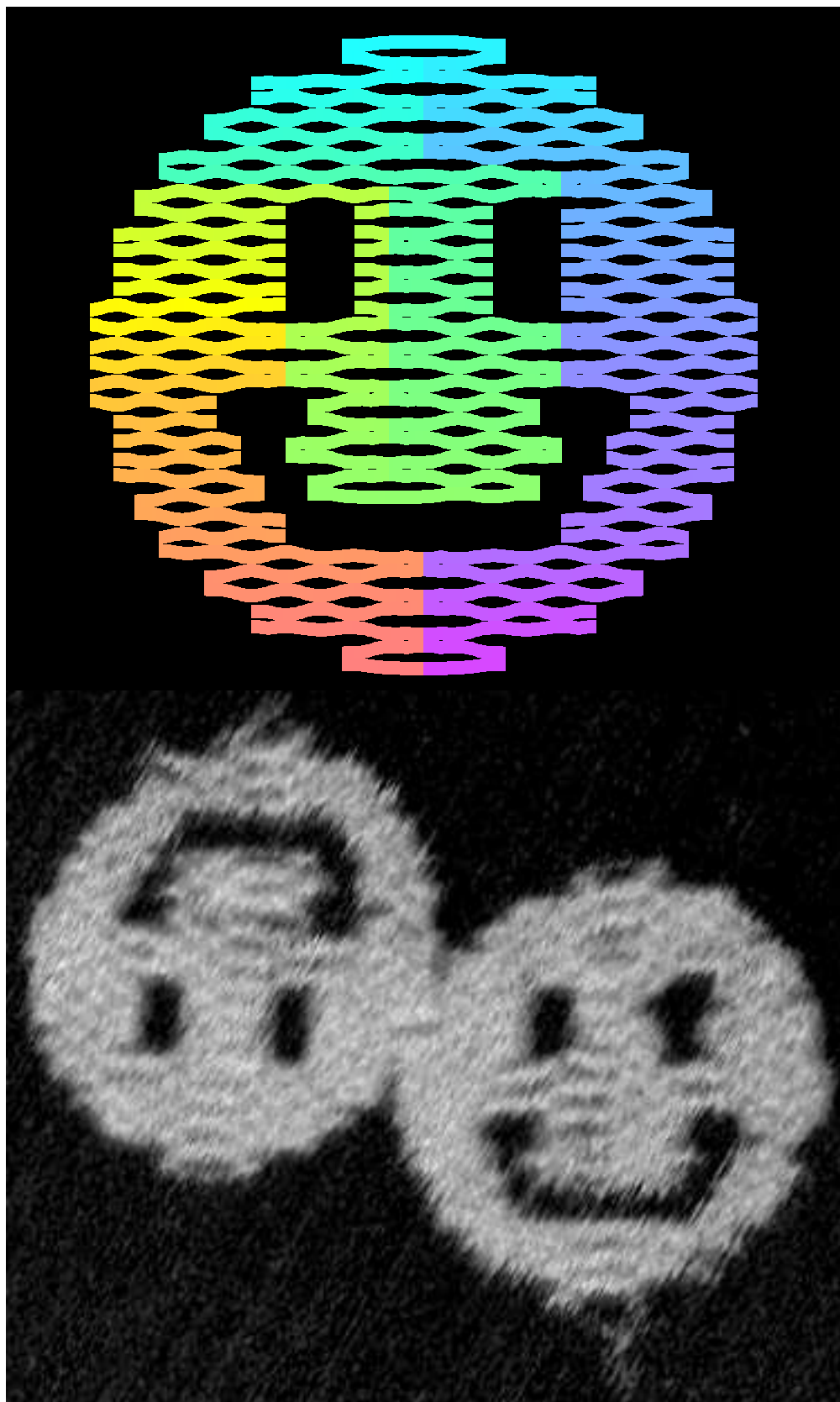
Supplementary Figure S22: More design details for the star **a**, Original block diagram assuming that each block (1 turn of DNA) would have an aspect ration of roughly 1:1 (3.5 nm per turn:3.5 nm per helix) based on the inter-helix gap for 2.5 turn spacing. In reality 1.5-turn spacing appears to have a ratio of roughly 1.2:1 (3.6 nm per turn:3 nm per helix) and so the stars were somewhat squat **b**. **c** reproduces the folding path for reference. In **a**, turns that occur between columns of red blocks and orange blocks have offset 0 with respect to the underlying crossover lattice. Other turns on the left and right outer edges have +1 or -1 offsets depending on which side of the star they occur. Purple and green half-blocks show that turns (in the scaffold) made on the seam or on the interior of the bottom left and right star arms are made an odd number of 1/2 turns (DNA half-turns) away from turns (in the scaffold) on the outer edges.



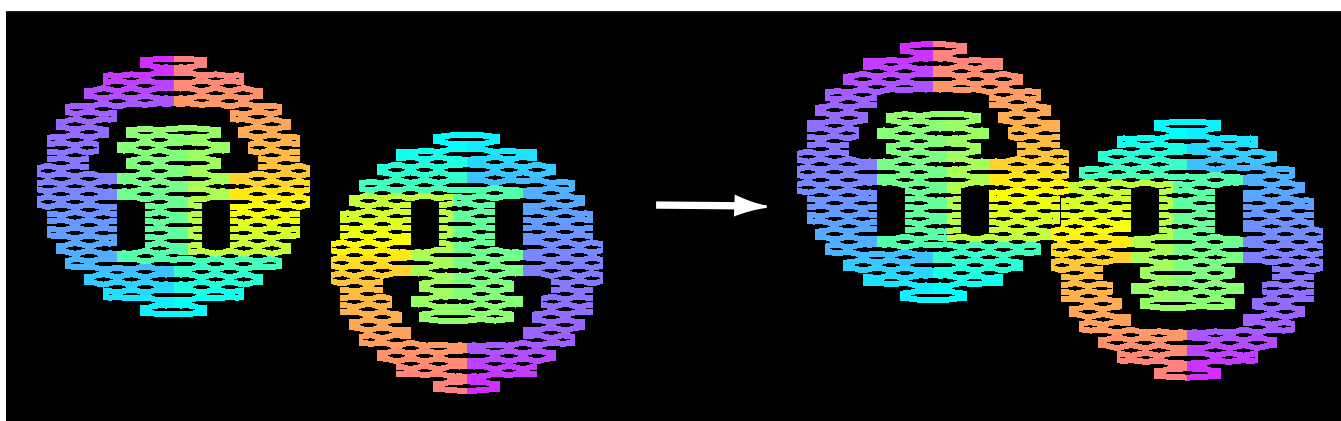
Supplementary Figure S23: Crossover diagram for the star (top) and high resolution AFM (bottom, taken by E. Winfree) which shows the crossover structure in great detail. Defects are probably tip damage. White arrow points to a section of helix that does not image well and appears to be a hole. On edges where helices can move unimpeded by neighbors helices often disappear at high tapping amplitude.



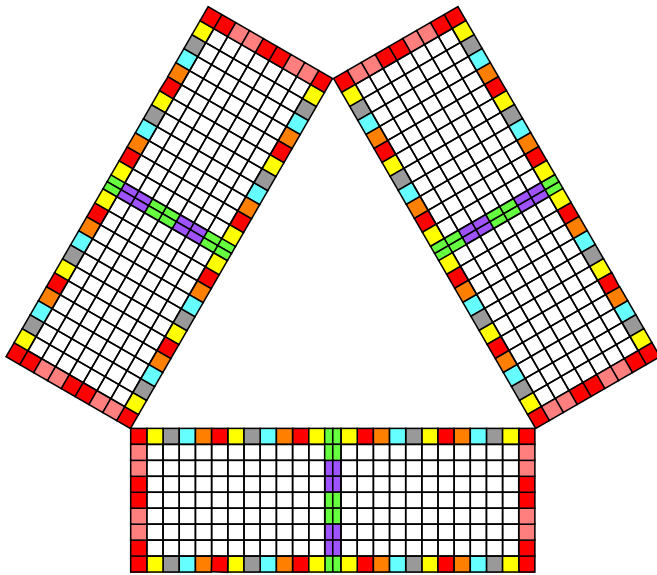
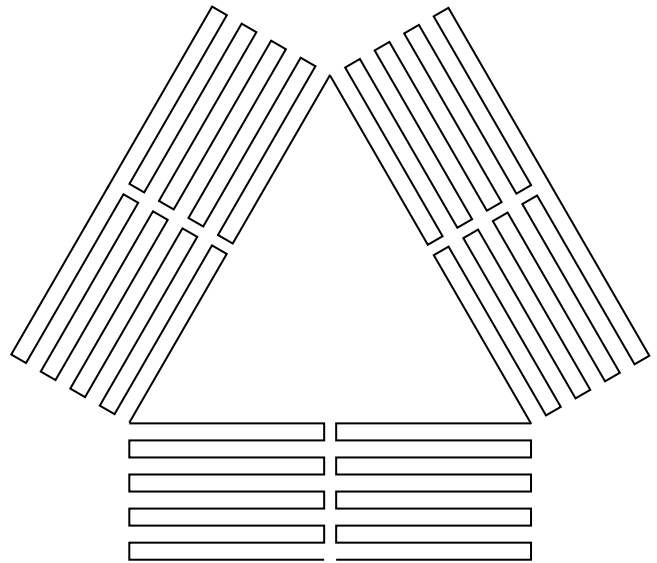
Supplementary Figure S25: More design details of the 3-hole disk (smiley). **a**, Block diagram. **b**, Reproduction of the folding path. **c**, Block diagram with all colors and notations removed. In **a**, turns that occur between columns of red blocks and orange blocks have offset 0 with respect to the underlying crossover lattice. Other turns on the left and right outer edges have +1 or -1 offsets depending on which side of the smiley they occur. Purple and green half-blocks show that scaffold turns made at most seams or on the interior of voids are an odd number of $1/2$ DNA turns away from scaffold turns on the outer edges. A pair of columns with alternating light and dark orange and red blocks marks a seam of 0 offset, placed 1.5 turns to the left of the central seam.



Supplementary Figure S26: Crossover diagram for the disk with holes (smiley) with a high resolution zoom out of Fig. 2: d_3 for comparison of fine structure. Some tip damage has occurred to the right eye of the righthand smiley.

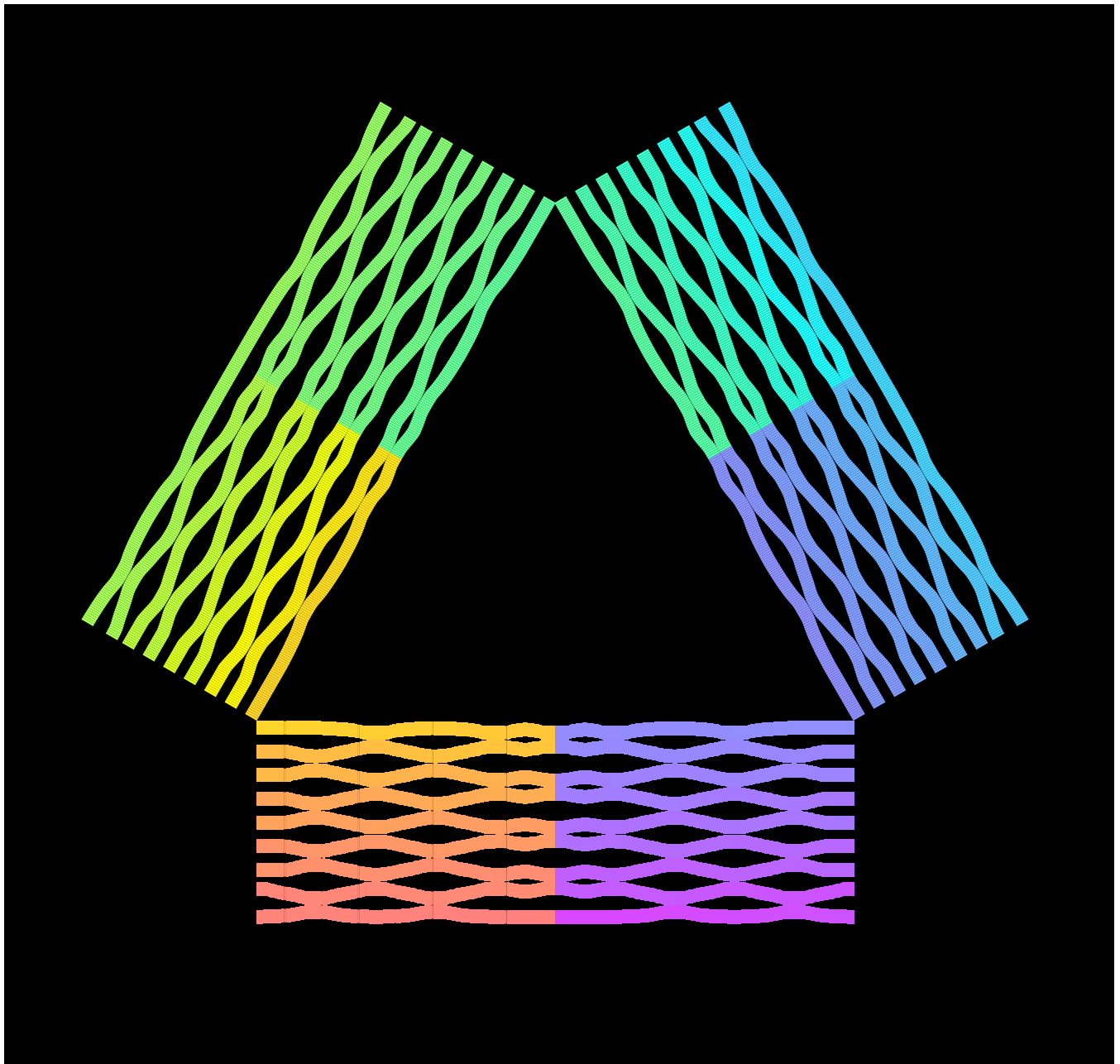


Supplementary Figure S27: Diagram showing how the smileys stick together to maximize the number of blunt end stacking interactions. Compare to previous Supplementary Fig. S26.

a**b**

25 turns wide at 10.4 bases/turn -> 260 bases
 9 helices / domain, 27 helices in all

Supplementary Figure S29: Schematics for the triangle Fig. 2e. **a** Block diagram. Designed for 2.5-turn spacing blocks have 5 different offsets with respect to the underlying lattice of crossovers, hence the 5 different hues of blocks in different columns. As in other block diagrams, orange block/red block boundaries have an offset of 0 turns with respect to the underlying lattice of crossovers. **b** Folding path.



Supplementary Figure S30: Crossover diagram for the equilateral composed of rectangular domains.

Plate number: 1

e0t11d, A1, CNTAGT... e0t13b, B1, GCGGACAA... e0t13d, C1, GAGCAAC... e0t15c, D1, ACTCCT... e0t15d, E1, AAAGCT... e0t17c, F1, AATCA... e0t17d, G1, GTCTG... e0t19c, H1, CTAAT... e0t19d, A2, TCCTT... e0t1d, B2, CAATG... e0t21d, C2, TAACA... e0t23c, D2, CCGAG... e0t23d, E2, TACCA... e0t25c, F2, AGCTA... e0t25d, G2, CAAA... e0t27c, H2, CGCA... e0t27d, A3, ATCA... e0t29c, B3, GAAAG... e0t29d, C3, ACAC... e0t3c, D3, GTATC... e0t3d, E3, ATTAG... e0t5c, F3, CATTC... e0t5d, G3, GATTG... e0t7c, H3, CTATT... e0t7d, A4, CAGTA... e0t9c, B4, AGAGA... e0t9d, C4, GACAC... e1t10e, D4, TAAG... e1t12a, E4, TAAT... e1t12b, F4, CTAT... e1t14a, G4, CGGG... e1t14b, H4, GCATA... e1t16a, A5, CAGT... e1t16b, B5, TGGT... e1t18a, C5, AGCA... e1t18b, D5, AGAA... e1t20e, E5, GAAT... e1t22a, F5, CGAAT... e1t22b, G5, TAAC... e1t24a, H5, TTAT... e1t24b, A6, TTGA... e1t26a, B6, AACCT... e1t26b, C6, CCAG... e1t28a, D6, CTGG... e1t28b, E6, TATTT... e1t2a, F6, CGCG... e1t2b, G6, TGAG... e1t30e, H6, CCAC... e1t4a, A7, TAAAT... e1t4b, B7, TGAC... e1t6a, C7, TTAG... e1t6b, D7, GAAAC... e1t8a, E7, CACAA... e1t8b, F7, GTGG... e2t11e, G7, TATG... e2t13a, H7, AGGA... e2t13b, A8, AGCT... e2t15a, B8, TGAG... e2t15b, C8, GCAA... e2t17a, D8, TAAG... e2t17b, E8, GCTG... e2t19a, F8, ACTA... e2t19b, G8, AAAT... e2t1e, H8, ATATA... e2t21e, A9, CAAA... e2t23a, B9, TGAT... e2t23b, C9, AGTA... e2t25a, D9, GCGA... e2t25b, E9, GCCC... e2t27a, F9, GACCT... e2t27b, G9, CGCT... e2t29a, H9, ACGC... e2t29b, A10, TTGA... e2t3a, B10, AAGC... e2t3b, C10, TCTG... e2t5a, D10, ATCG... e2t5b, E10, ACCA... e2t7a, F10, TTAC... e2t7b, G10, TTAG... e2t9a, H10, AATG... e2t9b, A11, CAAA... e3t10e, B11, GAAG... e3t12a, C11, AGCC... e3t12b, D11, GCTG... e3t14a, E11, ATAT... e3t14b, F11, AATC... e3t16a, G11, ATTT... e3t16b, H11, TTTT... e3t18a, A12, TATC... e3t18b, B12, TCAT... e3t20e, C12, GACG... e3t22a, D12, AAGA... e3t22b, E12, TTA... e3t24a, F12, GAT... e3t24b, G12, ATT... e3t26a, H12, AGA...

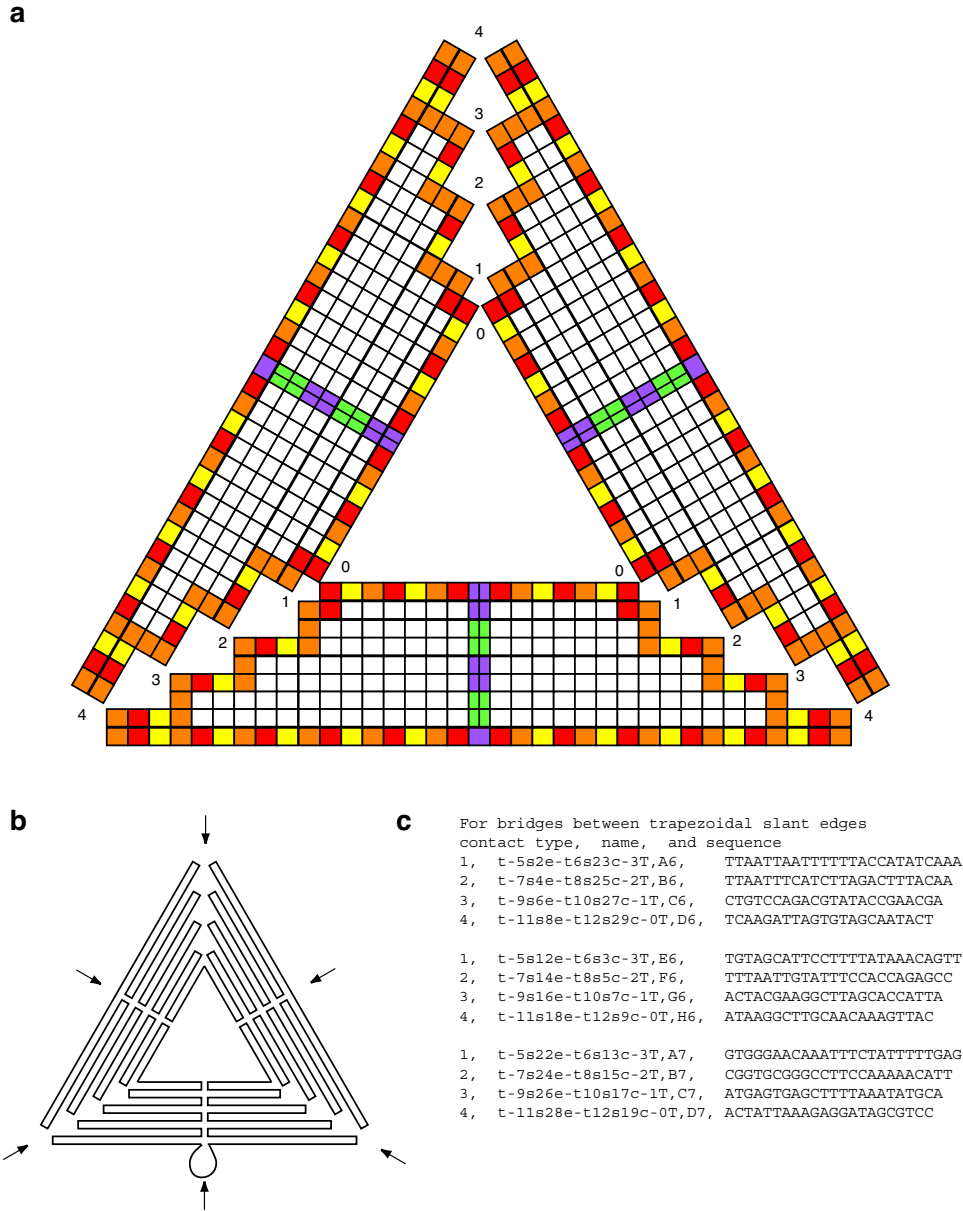
Plate number: 2

e3t26b, A1, AGAG... e3t28a, B1, ACAG... e3t28b, C1, AAAA... e3t2a, D1, ATCG... e3t2b, E1, CCTC... e3t4a, G1, CAGT... e3t4b, H1, CCAC... e3t6a, A2, TAT... e3t6b, B2, CAAA... e3t8a, C2, ACAT... e3t8b, D2, AGAC... e4t11e, E2, AGCA... e4t13a, F2, TGTG... e4t13b, G2, CATC... e4t15a, H2, TAGC... e4t15b, A3, AATG... e4t17a, B3, GCGA... e4t17b, C3, AATG... e4t19a, D3, GCTT... e4t19e, E3, GGAT... e4t1e, F3, CGCC... e4t21e, G3, CAAT... e4t23a, H3, ATGG... e4t23b, A4, TAAA... e4t25a, B4, GAGC... e4t25b, C4, TTTA... e4t27a, D4, AGTC... e4t27b, E4, AAG... e4t29a, F4, GCCT... e4t29e, G4, TATT... e4t3a, H4, TGAT... e4t3b, A5, ACAG... e4t5a, B5, TCAA... e4t5b, C5, CACC... e4t7a, D5, GTA... e4t7b, E5, TTGA... e4t9a, F5, GATG... e4t9e, G5, AATC... e5t12a, H5, ATAT... e5t14a, A6, AGA... e5t16a, B6, GCTG... e5t18a, C6, ACAG... e5t22a, D6, ATG... e5t24a, E6, AAA... e5t26a, F6, CCG... e5t28a, G6, CTA... e5t2a, H6, GAA... e5t4a, A7, TTT... e5t6a, B7, ACC... e5t8a, C7, AAA... e-1t10e, D7, TCA... e-1t12a, E7, CCG... e-1t12b, F7, TTG... e-1t14a, G7, TTA... e-1t14b, H7, AGC... e-1t16a, A8, AAG... e-1t16b, B8, ACC... e-1t18a, C8, GAC... e-1t18b, D8, AGT... e-1t20e, E8, TTG... e-1t22a, F8, TTT... e-1t22b, G8, AAC... e-1t24a, H8, TCG... e-1t24b, A9, CA... e-1t26a, B9, GTA... e-1t26b, C9, CTC... e-1t28a, D9, AT... e-1t28b, E9, AAT... e-1t2a, F9, GCT... e-1t2b, G9, GTC... e-1t30e, H9, ACG... e-1t4a, A10, CAT... e-1t4b, B10, ACC... e-1t6a, C10, AAG... e-1t6b, D10, ACC... e-1t8a, E10, TTA... e-1t8b, F10, TCC... e-2t11e, G10, GT... e-2t13a, H10, AT... e-2t13b, A11, TGA... e-2t15a, B11, CAC... e-2t15b, C11, GAG... e-2t17a, D11, GGC... e-2t17b, E11, AG... e-2t19a, F11, TTA... e-2t19b, G11, AAC... e-2t1e, H11, TTA... e-2t21e, A12, TCG... e-2t23a, B12, GGC... e-2t23b, C12, GAT... e-2t25a, D12, CA... e-2t25b, E12, GGG... e-2t27a, F12, ACG... e-2t27b, G12, AC... e-2t29a, H12, AAG...

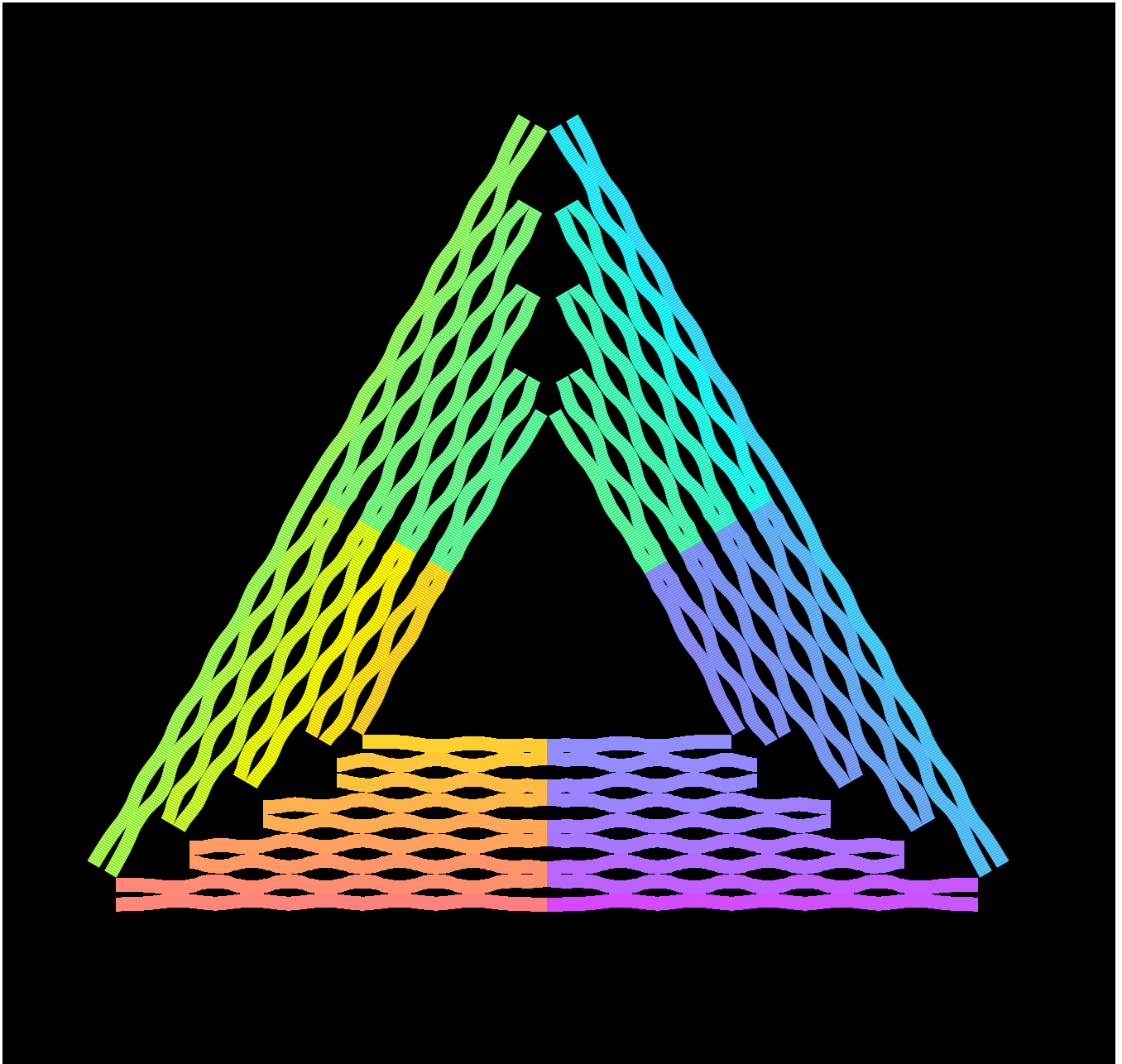
Plate number: 3

e-2t29b, A1, GTT... e-2t3a, B1, CGT... e-2t3b, C1, CGC... e-2t5a, D1, AAG... e-2t5b, E1, TAG... e-2t7a, F1, GCG... e-2t7b, G1, TTA... e-2t9a, H1, GAA... e-2t9b, A2, GCT... e-3t10e, B2, AAA... e-3t12a, C2, TAG... e-3t12b, D2, AAC... e-3t14a, E2, AA... e-3t14b, F2, TTT... e-3t16a, G2, CAT... e-3t16b, H2, GTT... e-3t18a, A3, CGG... e-3t18b, B3, CTT... e-3t20e, C3, AAT... e-3t22a, D3, CCA... e-3t22b, E3, CCG... e-3t24a, F3, CCG... e-3t24b, G3, AAC... e-3t26a, H3, AAT... e-3t26b, A4, AAT... e-3t28a, B4, CCG... e-3t28b, C4, CTT... e-3t2a, D4, AAT... e-3t2b, E4, GAT... e-3t30e, F4, GCG... e-3t4a, G4, AAT... e-3t4b, H4, TTA... e-3t6a, A5, CAG... e-3t6b, B5, CCA... e-3t8a, C5, GAT... e-3t8b, D5, TTA... e-4t11e, E5, TTC... e-4t13a, F5, TGA... e-4t13b, G5, TGA... e-4t15a, H5, TAA... e-4t15b, A6, GAA... e-4t17a, B6, ACC... e-4t17b, C6, TTA... e-4t19b, D6, ATC... e-4t1e, E6, TGT... e-4t21e, F6, TTT... e-4t23a, G6, TCG... e-4t23b, H6, TGG... e-4t25a, A7, CAG... e-4t25b, B7, CGC... e-4t27a, C7, TAA... e-4t27b, D7, TTT... e-4t29b, E7, AAG... e-4t3a, F7, TCT... e-4t3b, G7, CAG... e-4t5a, H7, AA... e-4t5b, A8, CAG... e-4t7a, B8, CAA... e-4t7b, C8, GCA... e-4t9b, D8, AT... e-5t10e, E8, AAA... e-5t12b, F8, AAT... e-5t14b, G8, GAA... e-5t16b, H8, CGC... e-5t18b, A9, TTA... e-5t20e, B9, CAT... e-5t22b, C9, CAG... e-5t24b, D9, CCG... e-5t28b, F9, GAT... e-5t30e, H9, GTA... e-5t4b, A10, GAA... e-5t6b, B10, GAA... e-5t8b, C10, TTT... et-rem1, D10, ACC... et-rem2, E10, TTA... et-rem3, F10, AAG... et-rem4, G10, TAA... et-rem5, H10, GTA... et-rem6, A11, GCCT...

Supplementary Figure S31: Sequences of the equilateral composed of rectangular composed of rectangular

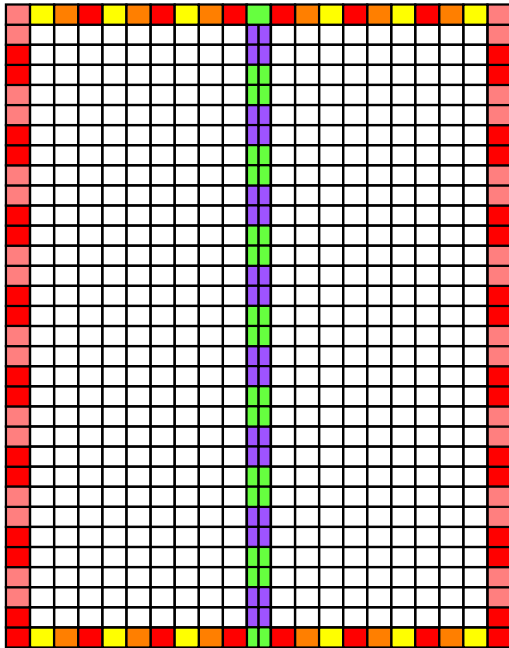


Supplementary Figure S32: More details of sharp triangle design. **a** Block design for the sharp triangle composed of trapezoidal domains. Contacts between trapezoids on their slant faces are of type 0, 1, 2, 3, and 4. Contacts of type 0 are bridged by the scaffold strand as shown in the folding path (**b**). Other contacts are bridged by special staples (**c**) that each replace two of the staple strands in the staple sequences (Supplementary Fig. S34), identified by the composite names of the bridging staples. Assuming a 1 nm inter-helix gap and 32 bases/3 turns, I calculated that the contacts would have gaps of width of 1.5696 nm, 1.0822 nm, 0.5944 nm, 0.1070 nm for contact types 1,2,3, and 4. (The gap widths drawn in the block diagram above are not accurate; contact type 4 has essentially no gap given an inter-helix gap of 1 nm.) Assuming that an unpaired thymine can bridge .43 nm (the length per base-pair of single stranded DNA³⁴), this would require adding 3.7, 2.5, 1.4, or 0.25 T's in the bridging staple for each contact point. In fact, 4T loops are often used to bridge 2 nm wide double helices to make them into hairpins assuming .5 nm per T. I used 3, 2, 1, and 0 T's for contacts of type 1, 2, 3, and 4 as can be seen inserted into the middle of the sequence in **c**. As in other block diagrams, in **a**, turns that occur between columns of red blocks and orange blocks have offset 0 with respect to the underlying crossover lattice. Other turns on the left and right outer edges have +1 or -1 offsets depending on which side of the trapezoid they occur. Purple and green half-blocks show that scaffold turns made at the central seams are an odd number of DNA 1/2 turns away from scaffold turns on the outer edges.

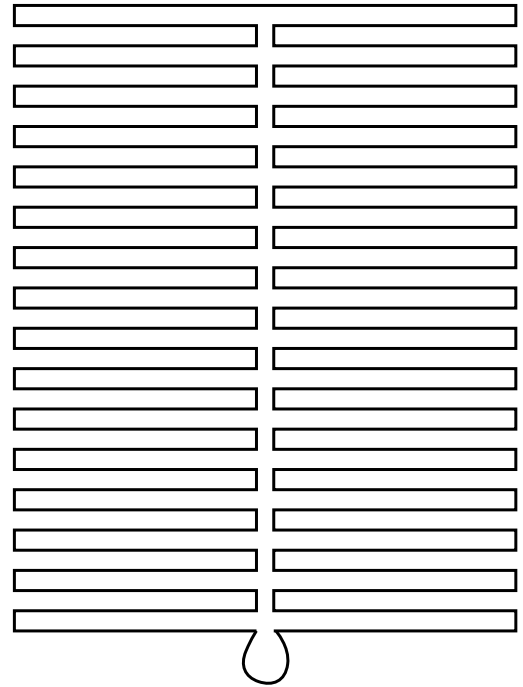


Supplementary Figure S33: Crossover diagram for the sharp triangle composed of trapezoidal domains.

a

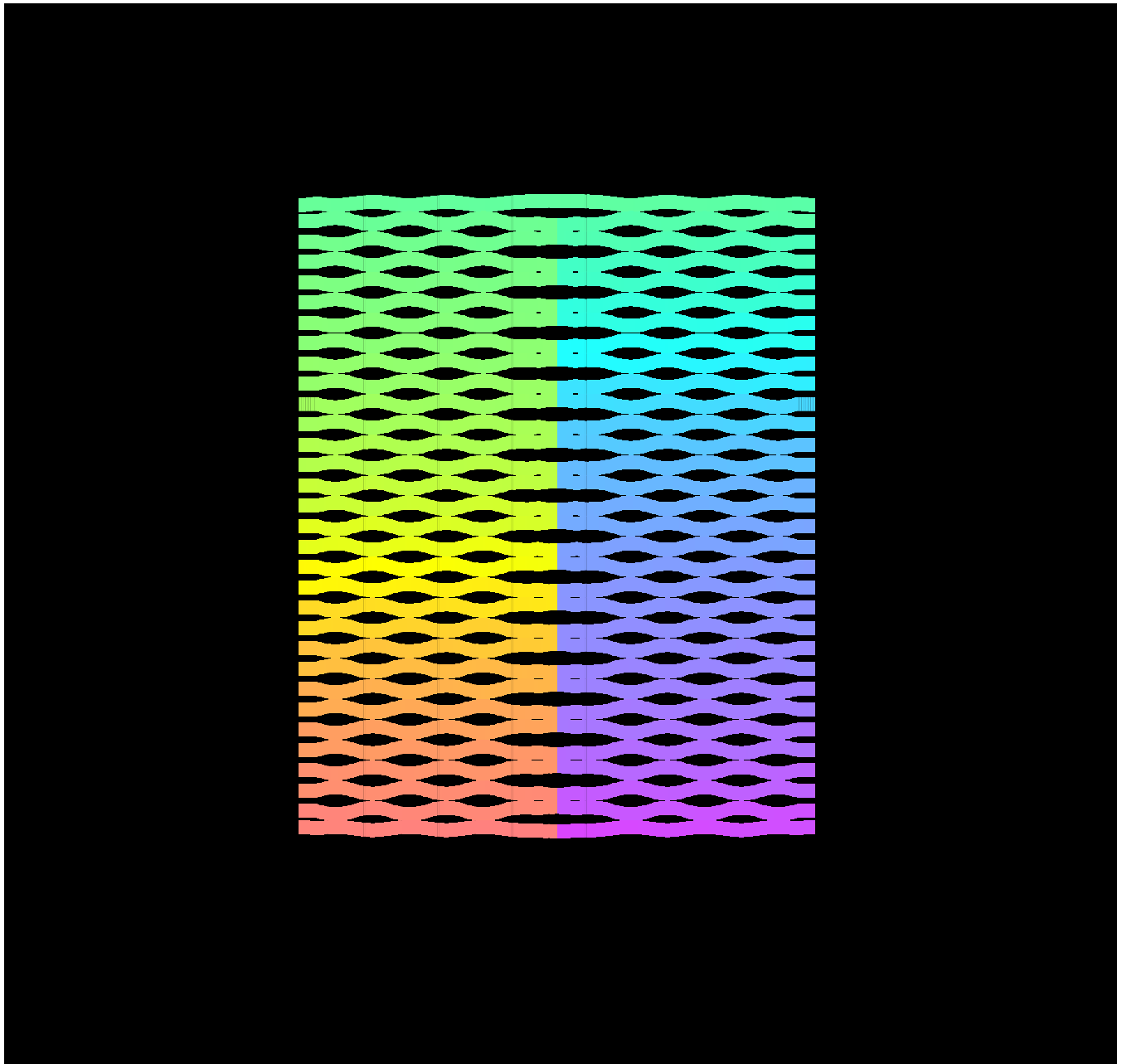


b

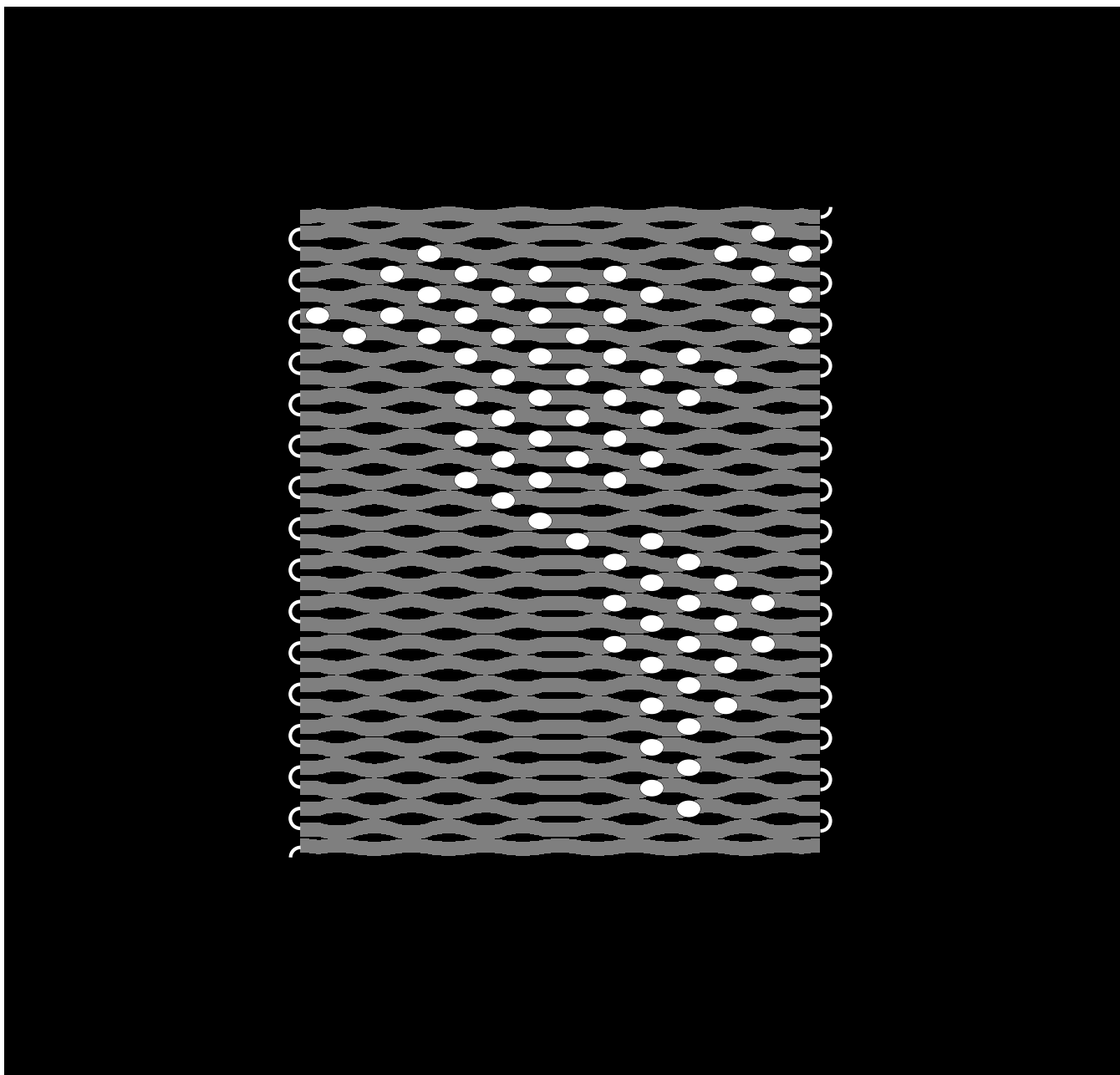


21 turns wide at 10.666 bases / turn -> 224 nt
32 helices tall

Supplementary Figure S35: Schematics for the “tall” rectangle used for the map pattern shown in Fig. 4e-i. **a** Block diagram. **b** Folding path.



Supplementary Figure S36: Basic crossover diagram for the “tall” rectangle used for the map pattern shown in Fig. 3e-i. Note, here I show the crossovers at the seam as bridged by staple strands. In the experiments shown in Fig. 3f and g, the seam was unbridged and only stacking interactions held it together, as diagrammed in Fig. 3e. For comparison, Fig. 3e is reproduced in the next figure, Supplementary Fig. S36



Supplementary Figure S37: Actual crossover diagram for the “tall” rectangle used for the map pattern shown in Fig. 3e-i. The seam is unbridged and staple strands with ‘TTTT’ loops have been added to the edges to discourage blunt-end stacking. At two corners 4-T tails have been added.

Supplementary Note S4: Experimental Methods

Supplementary Note S4.1: Design, synthesis, and sample preparation.

Single-stranded M13mp18 DNA (New England Biolabs), resequenced in 2002, was quantitated by UV absorbance at 260 nm. (Different clones of M13mp18 have small sequence differences, with the potential to affect folding; by AFM no qualitative difference was observed for a Bayou Biolabs clone—see Supplementary Note .) Staple and remainder strands were purchased unpurified (Integrated DNA Technologies; the manufacturer’s mass spectrophotometry indicated that strands had a few percent $n - 1$ truncation products.) in water at 100 μM or 150 μM and stored at -20°C . The desired set of up to 273 short strands was mixed with M13mp18 (typically 160 nM of each short strand, 1.6 nM M13mp18 circular or linear, a 100-fold excess of short strands) in a 100 μl volume of 1X Tris-Acetate-EDTA (TAE) buffer with 12.5 mM magnesium acetate (pH=8.3) and annealed from 95°C to 20°C in a PCR machine (Eppendorf) at a rate of $1^\circ\text{C}/\text{minute}$ in $.1^\circ\text{C}$ steps. When composing sharp triangles into hexagons or lattices the best results were obtained when staples that mediated the interaction, i.e. extended staples, were used in only 4-fold excess. To create linear DNA for the square and star, circular single-stranded M13mp18 DNA was incubated in restriction buffer with a short complementary strand at 37°C for 15 minutes, then linearized by digestion with BsrB I (New England Biolabs), phenol-chloroform extracted, and ethanol precipitated.

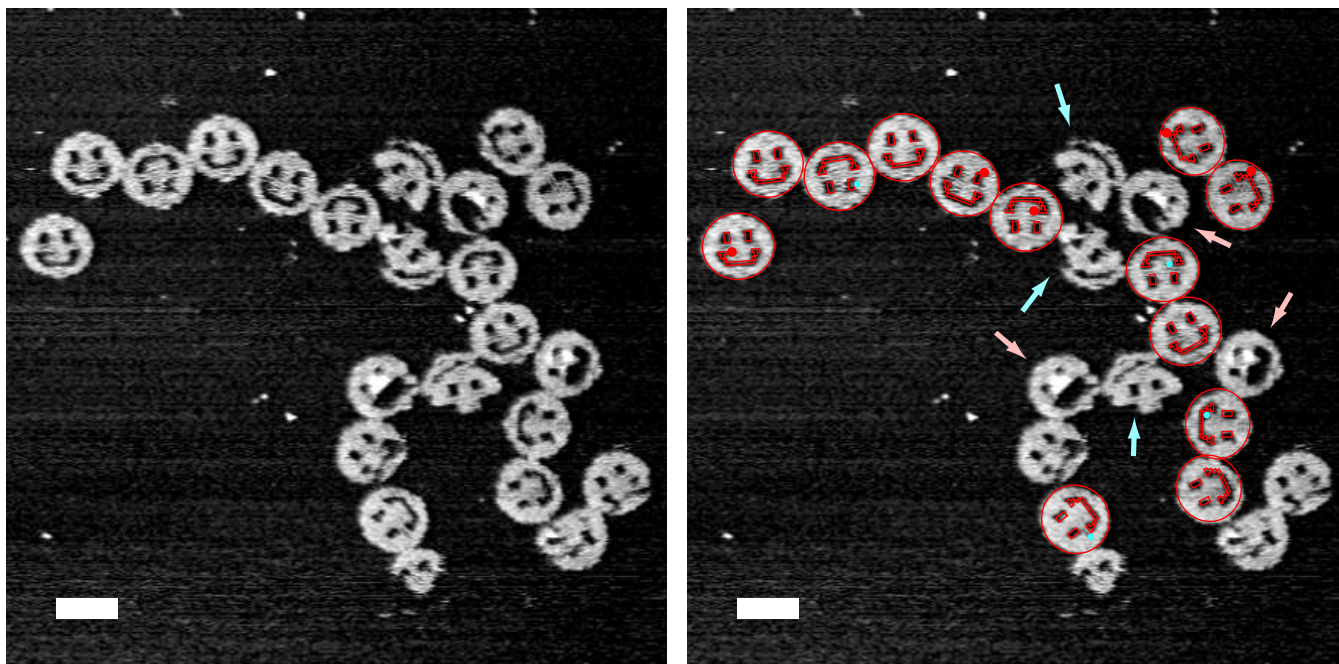
Supplementary Note S4.2 Atomic force microscopy.

Imaging was performed in Tapping Mode under TAE/Mg²⁺ buffer on a Digital Instruments Nanoscope III Multimode AFM (Veeco) with a nanoAnalytics Q-control III (Asylum Research) and a vertical engage J-scanner, using the ≈ 9.4 kHz resonance of the narrow 100 μm , 0.38 N/m force constant cantilever of an NP-S oxide-sharpened silicon nitride tip (Veeco). Samples were prepared by deposition of ≈ 5 μl onto freshly-cleaved mica (Ted Pella).

After self-assembly was complete, samples were prepared for AFM imaging by deposition of ≈ 5 μL onto a freshly-cleaved mica surface (Ted Pella) attached by hot melt glue to a 15 mm metal puck; an additional 30 μL of buffer was added to both sample and cantilever (mounted in the standard Tapping Mode fluid cell) before the sample and fluid cell were positioned in the AFM head. The tapping amplitude setpoint, after engage, was typically 0.2 - 0.4 volts, the drive amplitude was typically 100-150 millivolts, scan rates ranged from 2-5 Hz. Fine structure associated with crossovers was most clearly resolved for low amplitude setpoint and high drive amplitude values. However, under such conditions, the greatest damage is done to the sample and the hairpin labels are less distinct, sometimes disappearing entirely. Thus, to prevent damage to samples, drive amplitude was minimized subject to the constraint that fine structure was still visible; this often involved lowering the amplitude setpoint. After this procedure, the drive amplitude was typically 70-90 millivolts and the amplitude setpoint .15-.25 volts. Drive amplitude was often further reduced through use of the Q-control.

The single most important factor in acquiring high resolution images appears to be the quality of the AFM tip. In a single AFM session only 1 in 10 NP-S AFM tips might prove capable of revealing fine structure in origami or distinguishing individual hairpin labels. Practically the best approach seems to be to change tips as quickly as possible until the desired resolution is achieved.

Images were flattened by subtracting a low-order polynomial from each scan line, or by adjusting each scan line to match intensity histograms. In Fig. 2:a₃-f₃ the scale of AFM images was adjusted (by $< 5\%$) so that the width of experimental structures matched the theoretical widths of origami. Theoretical widths were calculated assuming .34 nm/base. The width change due to bending of helices by small angles between crossovers (~ 10 degrees) was ignored; simple geometry suggests it would change theoretical widths by $< 2\%$ (Supplementary Note 2).



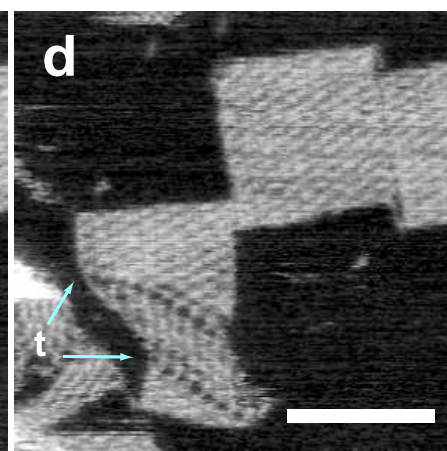
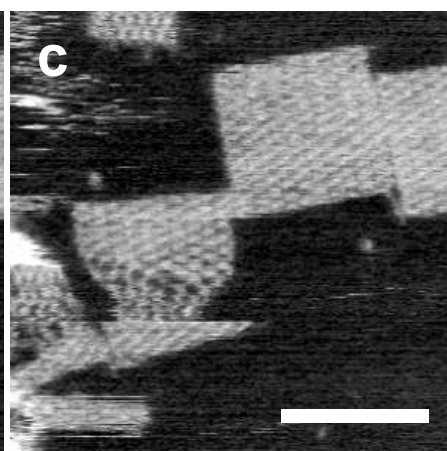
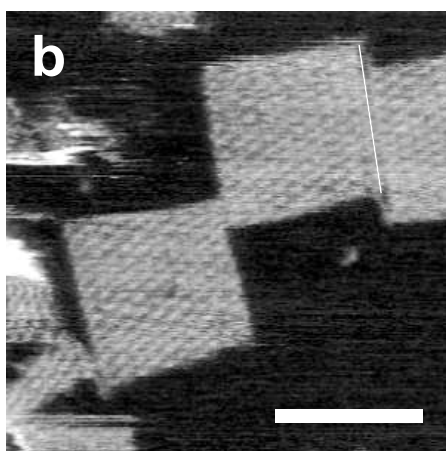
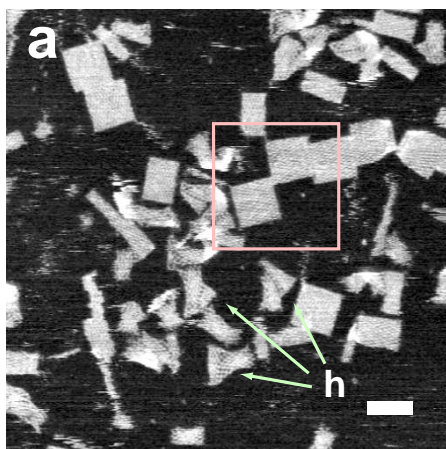
Supplementary Figure S40: Scale bar, 100 nm.

Supplementary Note S5: Experimental variations and controls

In this note I give a text or data for any experimental variation, control, or phenomena that was mentioned in the text but not shown.

Supplementary Note S5.1: Counting well-formed structures

Supplementary Fig. S40 shows one of the fields (reproduced from Fig. 2:d₄) used to obtain the frequency of well-formed structures smileys (here a smiley variant that has the seam above its right eye unbridged). Red dots are 15 nm in diameter, blue dots are 10 nm in diameter. These dots help determine the size of holes. Deciding which apparent holes are defects and which are correct high-resolution crossover structure (see Supplementary Fig. /refsmileyrainbow) is a matter of judgment. At right, templates of smileys are superimposed over experimental structures. To better fit the smileys some templates have been stretched up to 10%. In this field 13 structures have been judged well-formed, and 10 structures have been judged malformed. Two characteristic deformations of smileys are indicated: pink arrows indicate structures in which the ‘upper lip’ of the smiley has been flipped up onto the nose; light blue arrows indicate structures in which the ‘jaw’ has become dislocated, landing over the ‘forehead’ of the smiley.



Supplementary Figure S41: Scale bars, 100 nm.

Supplementary Note S5.2: Stretching of squares into hourglasses

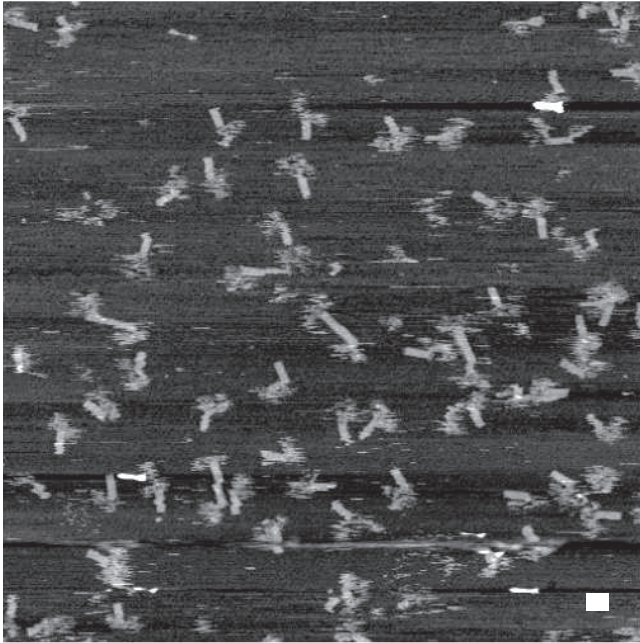
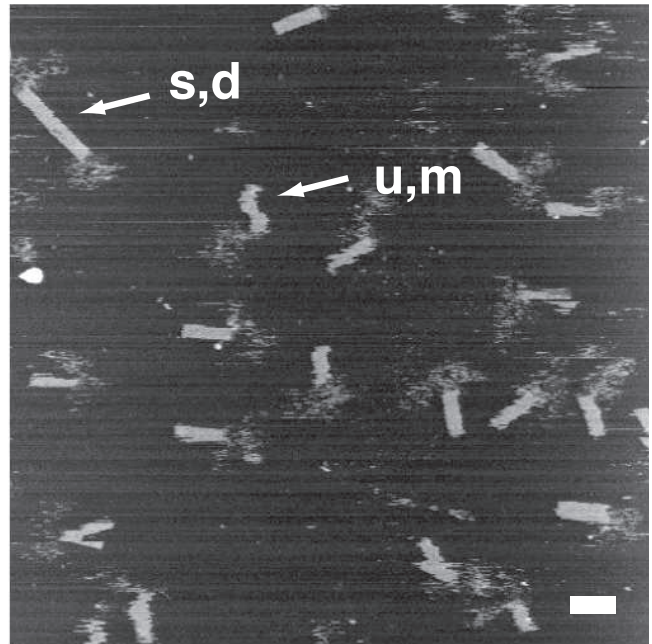
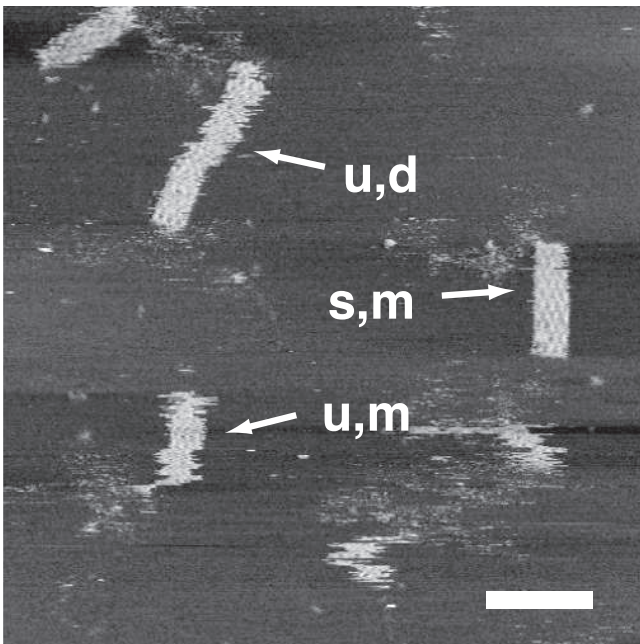
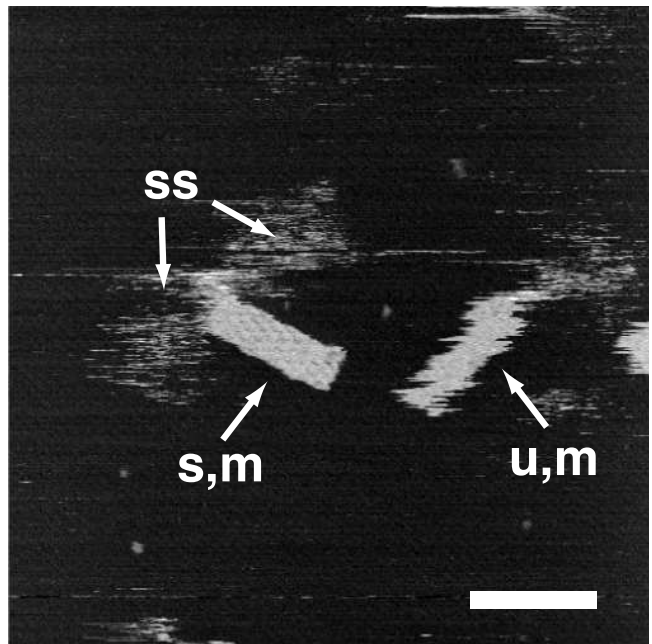
Supplementary Fig. S41a shows a typical field of 26-helix squares. A few structures are square, but many others are rectangular fragments or hourglass shapes (green arrows, marked 'h'). Supplementary Fig. S41b–d document the stretching of a square, over the course of three AFM scans, into an hourglass shape. The hourglass shape that results has what appear to be transitions between the normal folded lattice, and stretched lattice, along diagonals in the structure (blue arrows marked 't'). This is in contrast with the hourglass shown in the main text (Fig. 2:a₄) which appears to have a continuous deformation of the lattice.

Supplementary Note S5.3: One third of the square

The first test of the scaffolded DNA origami method, before the creation of the full square, was the creation of the bottom $\sim 1/3$ of the square (Supplementary Fig. S42). Also, a circular M13mp18 scaffold DNA was used rather than a linearized one, because the corners of the rectangle were close enough that the unfolded portion of the M13mp18 scaffold DNA could easily bridge the corners without deforming the rectangle. No remainder strands were used on the $\sim 2/3$ of M13mp18 DNA left unfolded. Apparently long, unfolded single-stranded sections of the scaffold do not adversely affect folding and remainder strands (where they are used for other designs) are probably unnecessary.

The $1/3$ squares were observed singly (Supplementary Fig. S42, structures marked ‘m’ for monomer) or as dimers (Supplementary Fig. S42, structures marked ‘d’ for dimer). Dimers always appeared to be the result of stacking of $1/3$ squares by vertical edges *opposite* from the unfolded single scaffold. Thus the unfolded scaffold appeared to prevent stacking at adjacent vertical edges. Single-stranded scaffold takes on a ‘cloud-like’ appearance that varies from AFM image to AFM image (Supplementary Fig. S42, marked ‘ss’).

Coplanar helices in DNA nanostructures appear to bind mica cooperatively; the larger a DNA nanostructure, the more tightly it appears to bind mica. This trend is apparent in the mobility of DNA nanostructures deposited on mica and imaged by tapping mode AFM under buffer. Most of the structures described in the main paper move infrequently during imaging, occasionally rotating by a few degrees or slipping by a few tens of nanometers (as judged by stationary structures around the mobile structure). The $1/3$ squares, however, were more difficult to image because they often slipped, as shown by structures marked ‘u’ (for “unstable”) in Supplementary Fig. S42. In the same field, other structures may stick well (and are thus labelled ‘s’ for “stable”); when structures are stable, their fine structure (the lattice of crossovers) can often be observed. Sometimes, a structure that appears stable in one image moves in the next (data not shown). Thus, as for DNA nanotubes¹⁵ and other DNA nanostructures, the interaction of scaffolded DNA origami with the mica surface (under buffer) is complex and dynamic and must be taken into account when interpreting AFM images.

a**b****c****d**

Supplementary Figure S42: The first experiment performed for this paper was to create $\sim 1/3$ of the 2.5-turn spacing square by adding $\sim 1/3$ of the staples for the square to circular M13mp18 DNA. Structures that appear to be moving under imaging are marked with a 'u' for "unstable"; structures that appear to be stable are marked with an 's'. Monomers of the $1/3$ square are marked with an 'm'; dimers are marked with a 'd'. Single-stranded scaffold, unfolded by staples is marked with an 'ss'. Scale bars, 100 nm.

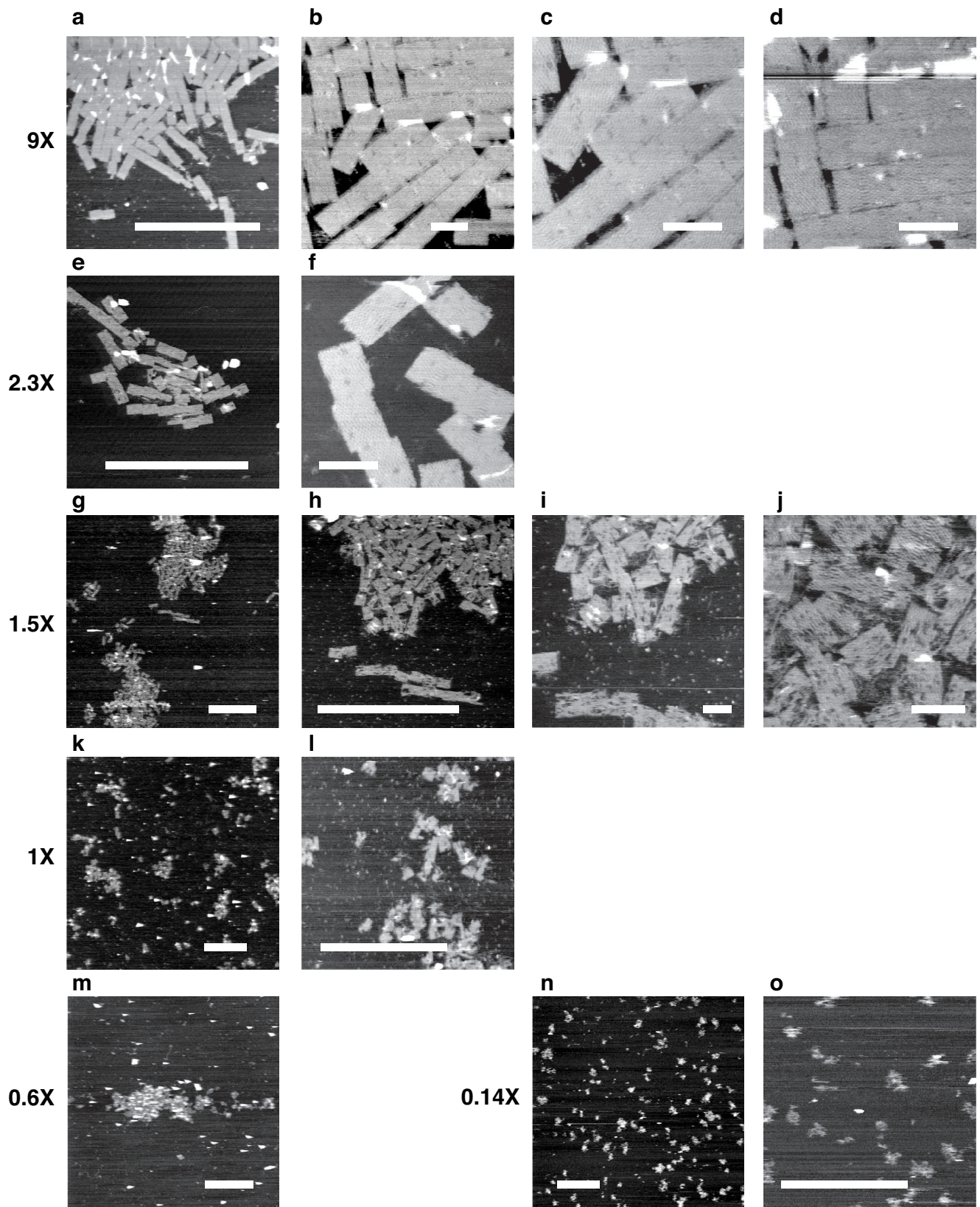
Supplementary Note S5.4: Stoichiometry

Oligos were received from the manufacturer (Integrated DNA technologies) at a nominal concentration of 100 or 150 μM as determined by UV absorbance at 260 nm. To estimate the error in stoichiometry, the concentration of 10 staple strands were remeasured by UV absorbance upon receipt by diluting 4 μl of stock solution with 196 μl of distilled water. This modelled the type of pipetting errors that occurred in the experiments since typically 3-7 μl of each staple stock solution was used when staples were mixed. (In a given experiment a fixed volume of each staple strand was used so no renormalization was performed.) Concentrations were calculated based on extinction coefficients calculated according to a nearest neighbor model³⁵. Assuming that the nearest neighbor model is correct, errors in absolute concentrations ranged from -5% to +13% and averaged +6% with a standard deviation of 6%. This may have reflected a systematic difference between the manufacturer's and the laboratory's spectrophotometers or measurement of volume. Nevertheless, this means that errors in relative concentration had a range of roughly 20%, and thus I estimate the error in concentration to be $\sim 10\%$. The M13mp18 scaffold strand was similarly quantitated but variable volumes of it were used to achieve a desired concentration in the final experiment. Pipetted in small 1-2 μl volumes, its stoichiometry relative to the staple strands is assumed to have, similarly, at least $\sim 10\%$ error.

In most experiments, a vast excess of staple strands (100 to 300-fold) over the scaffold were used. A question becomes, how small an excess can be effectively used to create DNA origami. Supplementary Fig. S43 shows AFM images of samples in which a smaller staple:scaffold ratio (from 9-fold down to .14-fold) was used. At a 9-fold excess (Supplementary Fig. S43a-d), rectangles are indistinguishable from those at higher molar excess of staple strands. Small 'hole' defects were sometimes observed but these defects are often observed upon repeated high resolution scanning even at high (100 to 300-fold) molar excess of staple strands. Rectangles created with just a 2.3-fold excess (Supplementary Fig. S43e-f) were difficult to distinguish from rectangles created with higher staple strand excess – that is, I am not sure they are distinguishable. It appeared that fewer long stacked chains formed, and that there were more malformed rectangles, but I made no attempt to quantify this.

In contrast, at a 1.5-fold excess of staple strands (Supplementary Fig. S43g-j), clear differences from normal rectangles were observed. Rectangles take on a "moth-eaten" appearance and have holes that often cover over 10% of their area. Linear stacks of rectangles may still be observed, however (bottom of Supplementary Fig. S43h). At a 1:1 staple:scaffold ratio (Supplementary Fig. S43k,l) no clear stacking is observed and it requires imagination to make out rectangular structures. At a 0.5 staple:scaffold ratio (Supplementary Fig. S43m) aggregates of partially folded scaffold strands still form but at a 0.14 ratio (Supplementary Fig. S43n,o) no large aggregates are formed; Instead, structures that appear to contain 1-3 scaffold strands are observed and they have a "streaky" appearance characteristic of structures that are mobile on the mica surface.

Because of the sloppiness with which strands were quantitated, no precise conclusions should be drawn from these experiments. However, I conclude that a 10-fold excess of staple strands is a "safe" concentration to work with for DNA origami containing 32-mer staple strands and that, because of the structures observed at a 2.3-fold excess, the use of a *vast* excess of staple strands should not be seen as a fundamental requirement of scaffolded DNA origami. Better control of concentrations may allow a 2-fold excess to be used for the construction of well-formed origami.



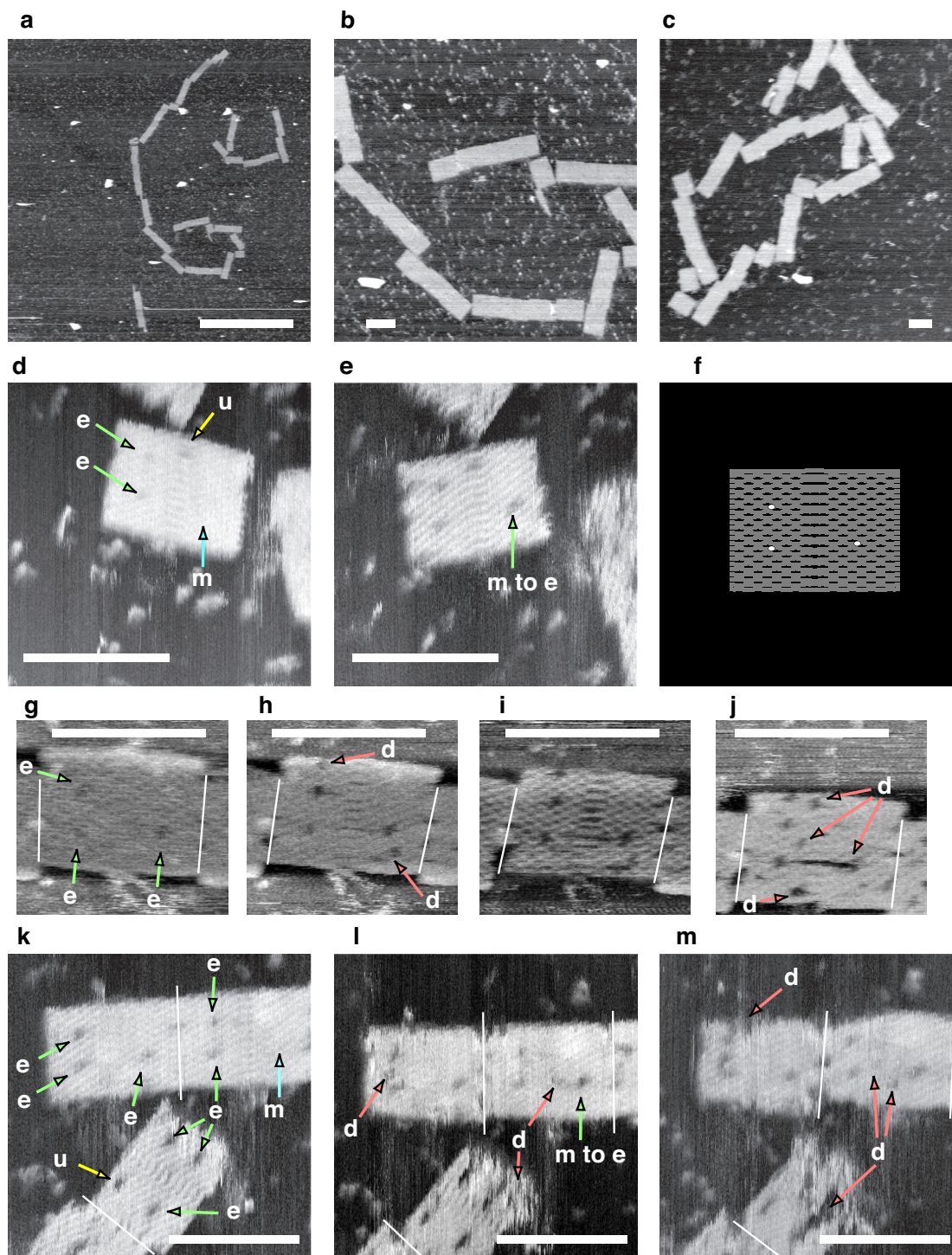
Supplementary Figure S43: Changing the concentration of staple strands relative to the scaffold. Scale bars in **a,e,g,h,k-o** are 1 micron. Scale bars in **b-d, f, i, j** are 100 nm

Supplementary Note S5.5: Removal of a strand

To test the ability of atomic force microscopy to detect defects in origami, rectangles were prepared with three staple strands intentionally omitted (**r-5t8e**, **r-5t16e** and **r5t14f**). The positions of the omitted strands in the rectangle are diagrammed in Supplementary Fig. S44f as white dots. At low magnification, no defects could be observed (Supplementary Fig. S44a–c). Even at high magnification, in images of typical resolution, no defects were observed; the majority of AFM tips did not provide resolution that allowed imaging of the defects. Roughly 1 in 5 tips were sufficiently sharp to allow ‘holes’ at the position of the omitted strands to be observed (features marked ‘e’ for ‘expected’ in Supplementary Fig. S44d–e, and g–m), although not all rectangles showed all three holes immediately upon imaging (features marked ‘m’ for ‘missing’). It sometimes took repeated imaging for holes to appear (features marked ‘m to e’), as if repeated scanning of the AFM tip was enlarging the defect.

A difficulty is that unexpected defects (features marked ‘u’) were sometimes observed during initial scans and further, repeated scanning often created holes and tears in structures (features marked ‘d’). Two examples, in which (upon an initial scan) holes appear in the expected positions without other holes elsewhere, convinced me that the observed defects were associated with the omission of strands. These examples were not culled from hundreds of images, only about a half-dozen high-resolution examples of the sample were obtained. Thus these examples appear to be statistically significant (although I have made no attempt to calculate their significance based on the rate of appearance of holes in high-resolution images of pristine rectangles).

I conclude that, while omitted strands are difficult to observe, any strands systematically missing from structures (say because of bad secondary structure in a staple strand or the scaffold) should be detectable in multiple high-resolution images.



Supplementary Figure S44: Visualization of the positions of omitted strands in rectangles. **a–c** show that at low magnification and resolution, defects due to omitted strands cannot be observed. **f** diagrams the position of the three omitted strands. **d–e** and **g–m** show high resolution images of rectangles with omitted strands. ‘e’ marks expected defects, ‘u’ marks unexpected defects, ‘m’ marks a missing defect, and ‘d’ marks AFM damage. Defects on the vertical edges of rectangles (ragged edges) are so common that I do not mark them. Such defects seem to be created or enhanced easily by AFM imaging. White lines mark boundaries between rectangles. Rectangles do not always land in the ‘canonical’ orientation and under imaging roughly 50% appear flipped. Thus **d–e** and **k–m** have been flipped left to right so that the rectangles they contain may be more easily compared with **f**. In **k–m** the diagonally oriented rectangle at bottom is flipped with respect to **f**. Inspect **f** and note that the singleton omission on the right hand side is slightly raised with respect to the pair of omissions on the left; AFM defects show a similar pattern. Scale bar in **a**, 1 micron. Scale bars in **b–e** and **g–m** are 100 nm.

Supplementary Note S5.6: Unbridged seams

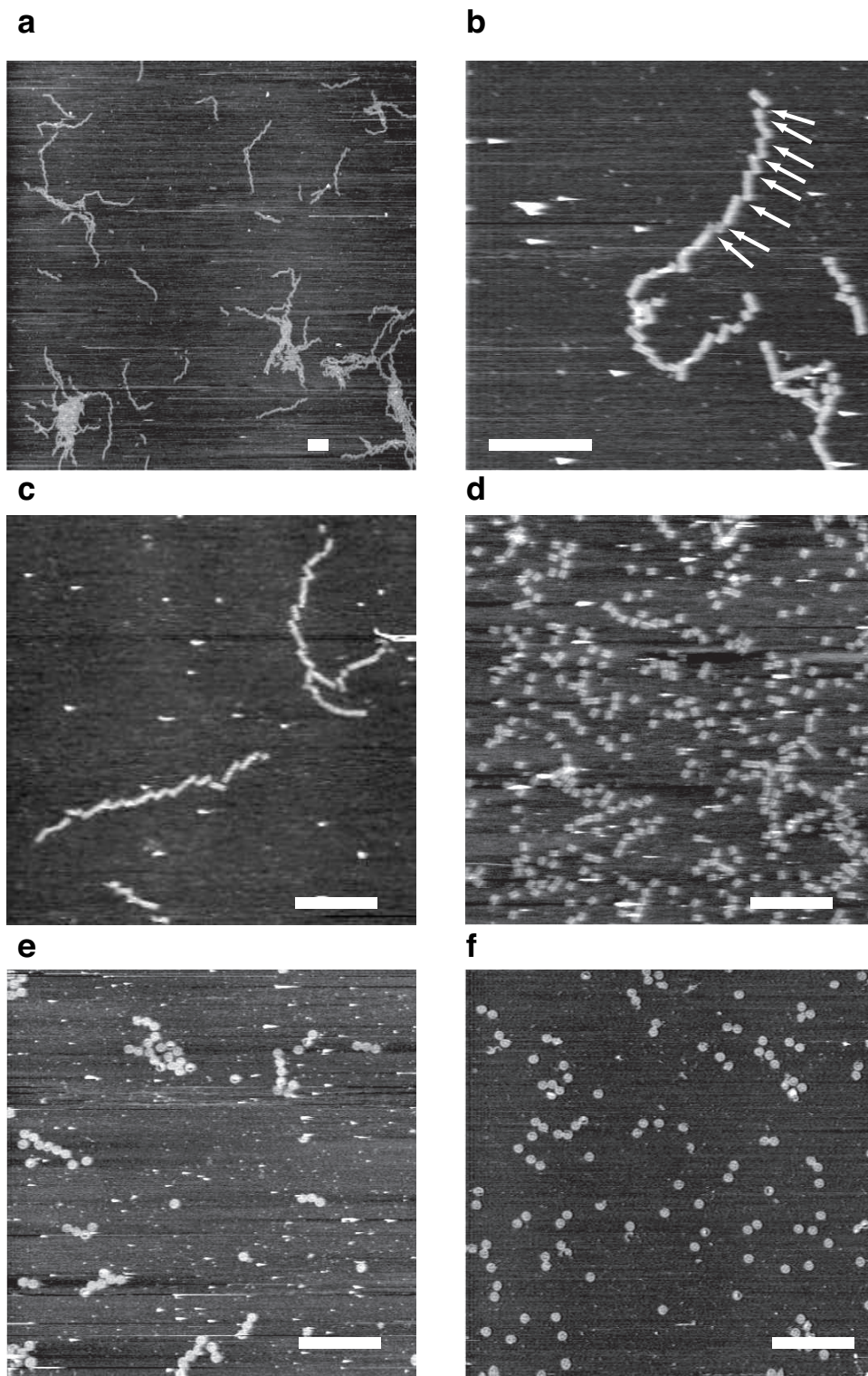
Unbridged seams in scaffolded origamis are those held together only by stacking interactions. Sometimes such seams dislocate; this is best observed in patterned rectangles because the two distinct halves of a rectangle can be unambiguously identified, as snowflake patterns in Supplementary Note S6 show. Supplementary Fig. S53d shows a small dislocations along an unbridged seam. Large dislocations at unbridged seams are also common. Supplementary Fig. S53c has white arrows that point to dislocations in which the two halves of the origami are completely separated.

Supplementary Note S5.7: Prevention of stacking

Stacking interactions based on blunt-ended helices can be quite strong; rectangles which have many parallel blunt-ends along their left and right edges stack so strongly that they may form long chains over 5 microns in length (Supplementary Fig. S45a–c). As deposited on mica, such chains exhibit frequent ~ 75 nm dislocations, every few rectangles along the chain (arrows, Supplementary Fig. S45b). I hypothesize that in solution rectangles in such chains are completely stacked and and no such offsets occur.

To avoid aggregation based on stacking interactions, several methods can be employed. First, the staple strands along the edges of a shape may be simply left out, and the scaffold left unstructured along these edges. Supplementary Fig. S45d shows rectangles that have been disaggregated in this way. Simply omitting staple strands out leaves unstructured scaffold at the edges of the rectangle and decreases the size of the potential pixel array by two columns. Thus a second, more aesthetically pleasing, method is that employed in Fig. 3e: the addition of 4T hairpin loops to staple strands on the edges of a shape. (The use of 4T hairpin loops to disaggregate DNA nanostructures was first demonstrated by Rebecca Schulman for her “zig-zag boundaries”.) A third very similar method is to add 4T tails to staple strands that have ends on the edge of the shape. Supplementary Fig. S45e shows the normal amount of aggregation for 3-hole disks. Supplementary Fig. S45f shows that the addition of just a small number (12) of 4T tails to the 3-hole disks causes almost complete disaggregation.

These experiments show that, when it is desirable to do so, stacking and the aggregation it induces can be almost entirely suppressed.



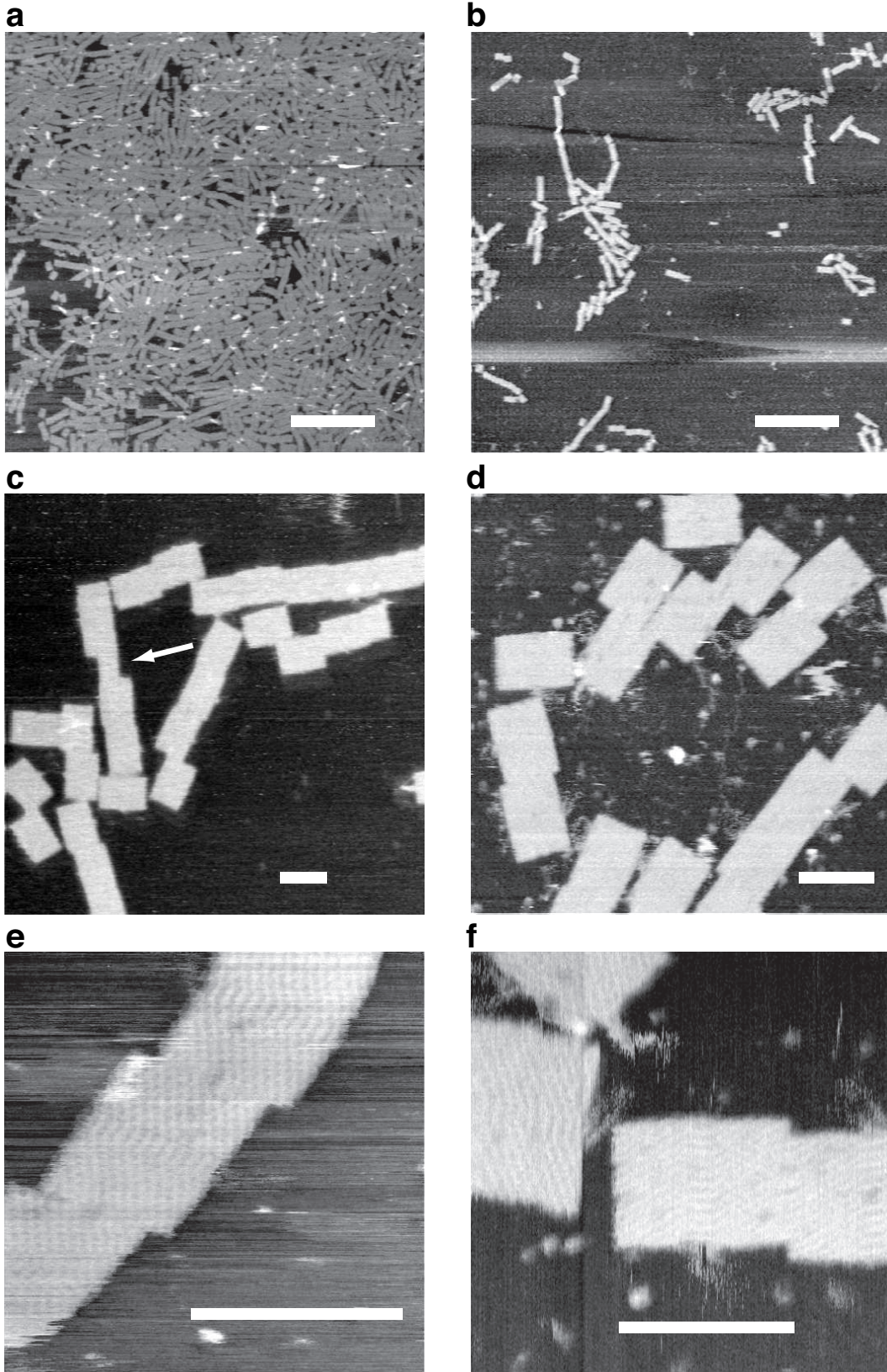
Supplementary Figure S45: Methods to discourage stacking of DNA origami. **a–c** In addition to large aggregates, rectangles often form very long stacked chains. Arrows indicate dislocations of rectangles by a single rectangle width (roughly 75 nm). **d** Stacking (and aggregation) are almost completely inhibited by omitting staples on the left and right edges of the rectangle. **e** Normal 3-hole disks aggregate strongly; almost no 3-hole disks occur as singletons. **f** The simple addition of 4T-tails to the 6 blunt-end helices its left and right edges of the 3-hole disks almost completely abolishes stacking and aggregation. Scale bars, 1 micron.

Supplementary Note S5.8: A different M13mp18 clone

While all viruses labelled M13mp18 are supposed to have identical DNA sequences, in practice this does not appear to be the case. The originally deposited sequence for M13mp18 in Genbank (accession X02513, 7249 bases long,³⁶) appears to have an error that was corrected by adding a ‘T’ at position 900 (accession M77815, 7250 bases long). Amersham Biosciences gives the sequence of M13mp18 (evidently their clone) as a 7249 sequence that differs from X02513 by a pair of compensatory frame shifts (bounding the region from 977 to 1556) and 3 point mutations outside of the frameshift. New England Biolabs gives a 7249 sequence (Supplementary Fig. 39) for their clone (resequenced in 2002) that differs from the Amersham sequence by a pair of compensatory frameshifts (bounding the region 900-977) and 23 point mutations outside of the frameshift.

The staple strands given in this paper were created using the New England Biolab’s sequence and all experiments save those described here were performed with New England Biolab’s M13mp18 single-stranded DNA (Catalog number: N4040S). To test whether small differences in sequence could be detected by AFM, staples for the rectangle were used to fold a sample of M13mp18 DNA from Bayou Biolabs (which reports that their sequence is the same as that of Amersham, although it has not been recently resequenced). Thus the staple strands should have had mismatches with the scaffold at 23 positions and a 78 base section should have been shifted by 1 base with respect to the scaffold. Qualitatively, no differences were observed between rectangles created with Bayou Biolabs M13mp18 DNA and New England Biolabs M13mp18 DNA (Supplementary Fig. S46).

While this seems to suggest that small sequence differences do not matter, I am uncomfortable suggesting that the staple sequences described in this paper be used for M13mp18 DNA with a sequence that is known to be different. Thus I suggest either generating new staple strand sequences, or using New England Biolabs M13mp18. Given that the difference (in point mutations) between the New England Biolabs sequence and Amersham sequence is 0.32% of the M13mp18 genome, and that the sequencing error rate in both these sequences could easily be 1%, this suggestion is probably based in irrational fear.

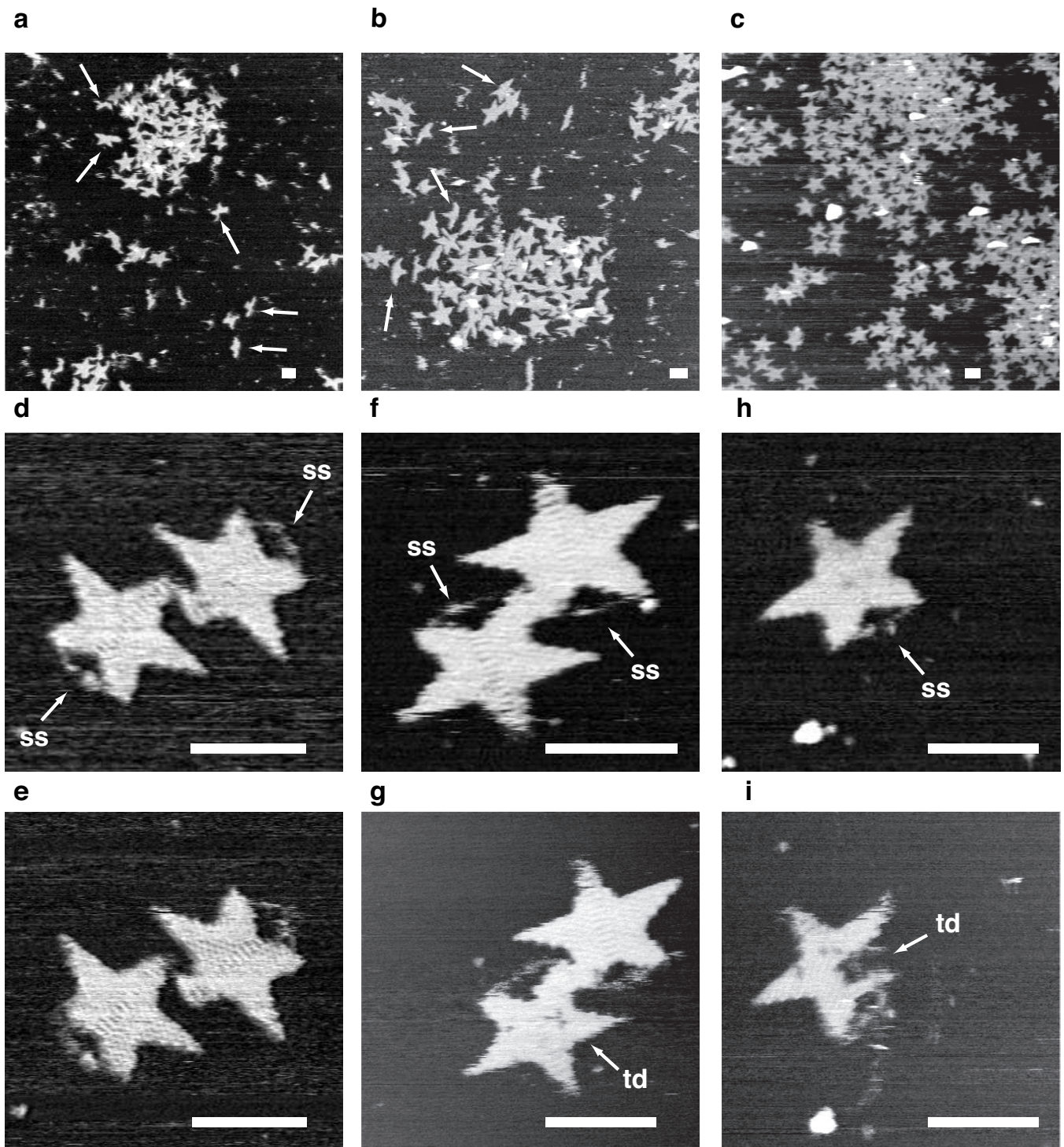


Supplementary Figure S46: Rectangles created using Bayou Biolabs M13mp18 DNA.

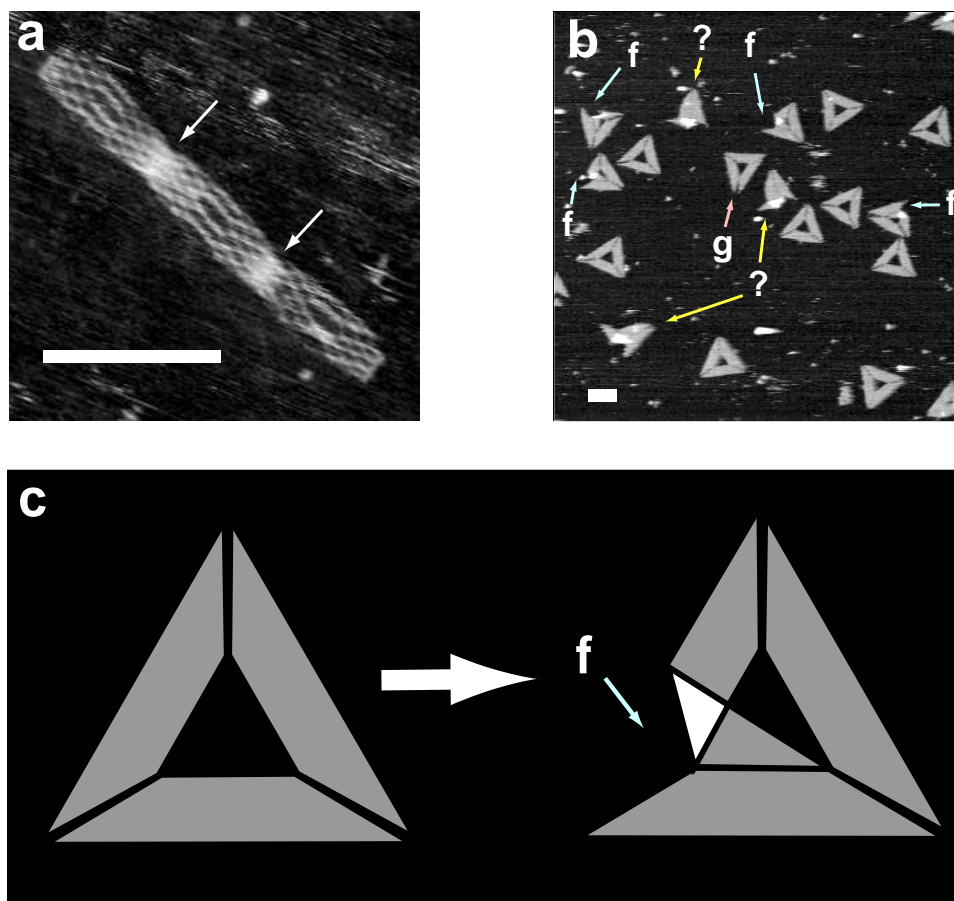
Supplementary Note S5.9: Use of circular scaffold for Stars

Use of circular scaffold with stars (Supplementary Fig. S47c–i) appears to give better results than with linear scaffold (Supplementary Fig. S47a,b). Fewer structures appear to be fragments of stars (arrows in Supplementary Fig. S47a,b). However, it is difficult to tell whether the lower two points of the star, which the circular scaffold bridges and often image poorly, are well-formed. The circular scaffold that bridges the two lower points is easily visualized, however, as a single, somewhat diffuse, arc (labelled as ‘ss’ in Supplementary Fig. S47d,f, and h). The fact that circular scaffold appeared to give better results may be attributed to the high purity of the circular scaffolds. After linearization, the quality of linear scaffold, in terms of the percentage of strands that were full length, was not assessed and a large percentage of the strands may have not been full length.

Of incidental interest, Supplementary Fig. S47d–i show the range of outcomes that is observed when a structure is imaged more than once in an attempt to get higher resolution images. (In an attempt to get higher resolution, the tip-sample interaction is increased by increasing the tapping amplitude or decreasing the amplitude setpoint.) Sometimes a structure (Supplementary Fig. S47d) is imaged with higher resolution (Supplementary Fig. S47e.) Sometimes a structure (Supplementary Fig. S47f) sustains a small amount of damage from the tip (labelled ‘td’ for “tip-damage” in Supplementary Fig. S47g). Sometimes a structure (Supplementary Fig. S47h) sustains severe damage (Supplementary Fig. S47i).



Supplementary Figure S47: The difference between stars created using a circular scaffold and those created using a linear scaffold. **a,b** Stars created using a linear scaffold. Arrows indicate example fragments; not all fragments are labelled. **c–i** Stars created using a circular scaffold strand.



Supplementary Figure S48: Deformation of triangles. **a** Triangles made from rectangle domains sometimes break and form 3-domain rectangles based on stacking interactions (white arrows). **b** Sharp triangles made from trapezoidal domains but without bridges. ‘g’ and a pink arrow mark a gap between trapezoids in a non-equilateral triangle. ‘f’ and green arrows mark places where tips of trapezoids have folded into the interior of sharp triangles. ‘?’ and yellow arrows mark structures for which no sensible interpretation has been made. **c** Interpretation of the sharp triangles with folded trapezoids from **b**. Gray indicates a single thickness of DNA structure, white a region of double thickness. Scale bars, 100 nm.

Supplementary Note S5.10: Deformation of triangles and unbridged sharp triangles

In experiments designed to create triangles from three rectangular domains, 88% of structures (of 199 structures observed) had roughly triangular shapes but < 1% (a single structure) were equilateral. The remaining 12% of structures took a variety of forms but, strikingly, 3% of structures took the form of three-domain rectangles held together by stacking interactions (Supplementary Fig. S48a). This suggests that the scaffold may break preferentially at the vertices of the triangle.

A large percentage (55%) of sharp triangles (created from trapezoidal domains) remain well-formed when bridges are not used along the seams between trapezoidal domains (Supplementary Fig. S48b). Typical defects take the form of trapezoids that fold back away from seams (‘f’ labels) into the interior of the triangle. Some structures cannot easily be interpreted (‘?’ labels).

Supplementary Note S6: Hairpins for creating patterns

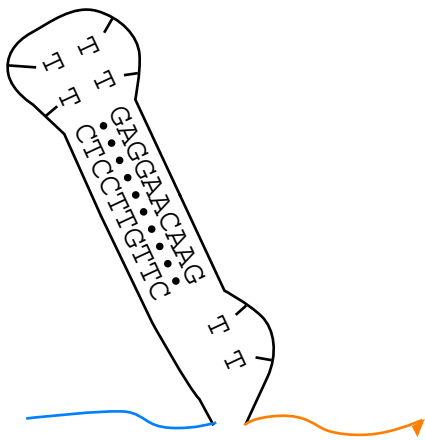
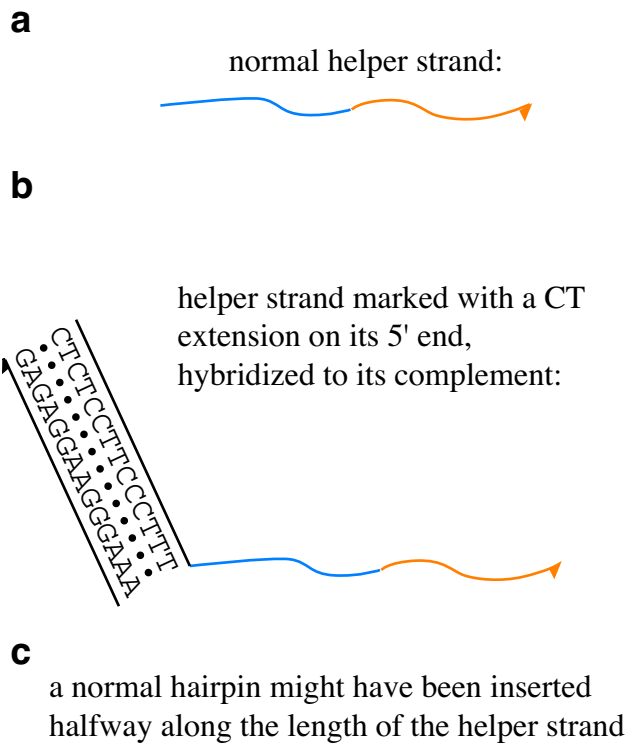
To label a DNA nanostructure, DNA hairpins are often added to increase the height of the nanostructure at a desired location. DNA hairpins have a tendency to dimerize, and, at the high concentrations at which they occur (up to 40 μM if all positions were labelled by the same hairpin) might inhibit formation of the shapes. Thus a new type of hairpin, a *dumbbell* hairpin was designed (Supplementary Fig. S49d) that, in order to dimerize, must form a presumably strained pseudoknotted structure (Supplementary Fig. S49i). Dumbbell hairpins were inserted between nt. 16 and 17, for all 32-mers in the rectangle design *except* strands **r9t0f** and **r-9t24e** which had the hairpins inserted between nt. 8 and 9. Note that (1) no normal hairpins were tested, they might have worked without difficulty and (2) the idea that dumbbell hairpins to form fewer dimers has not yet been tested (by say gel electrophoresis comparing normal and dumbbell hairpins at high concentration).

In an attempt to allow post-labelling of the shapes after formation a second type of marker was explored (Supplementary Fig. S49b): a 14 base mixed C and T tail was added to the 5' end of each staple strand. The idea was that this polypyrimidine addition would not hybridize with any staple strands or to itself. After formation of a shape, the corresponding 14 base polypurine strand was added to create duplex at desired positions, which it was assumed would yield good AFM height contrast. Instead the duplex markers imaged very poorly in a manner that was highly scan angle dependent. Multiple scans from multiple angles suggest that the poly-CT tails do in fact get labelled by poly-AG complements but imaging was very difficult (data not shown). The duplex markers, because they are attached to the origami by only one covalent bond, appear to be flexible. Thus such a method may be useful for attaching gold balls or other materials to the shapes but serves as a warning that verification of the correct structure by AFM may be difficult.

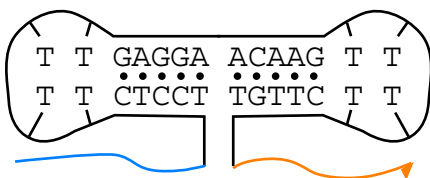
Despite the apparent complexity of the patterns, physically selecting and mixing strands was relatively simple. Because the set of '0' strands and set of '1' strands (bearing dumbbell hairpins) are complementary, and '0' and '1' strands are stored in characteristic positions of matched 96 well plates, two complementary pipette tip boxes are easily constructed, one for selecting the '0' strands and the other for selecting '1' strands. This is accomplished by taking a full tip box, and, for each position of a desired '1', moving that tip to the same position in an empty tip box. The originally full tip box becomes a box for selecting the '0' strands, and the originally empty tip box a box for selecting the '1' strands. A multichannel pipettor or robotic workstation can then be used to apply the tip boxes to the 96 well plates. The pipettor gets a tip if and only if the corresponding position in the tip box has a tip, and thus performs only the desired pipetting operations. This idea is diagrammed in Supplementary Fig. S50 and a worksheet for creating the snowflake design is given in Supplementary Fig. S51.

To give a better feeling for the range of structures that were observed in the pattern experiments, I give a page of images for each structure that was observed and include some zoom-outs of the images used in the paper (Supplementary Fig. S52, 53, and 54). Note the presence of flipped structures with hairpins down that image poorly. Note also that the "DNA" and "snowflake" patterns were rendered on a rectangle with 18×12 pixels and that the "Map" was rendered on a completely different rectangle with 14×16 pixels.

The resolution of patterns was measured directly from staggered patterns. Distances measured between pairs of '1' pixels in alternating columns (two pixel widths: $11.5 \pm .9$ nm s.d., $n = 26$) and adjacent rows (one pixel height: $6.6 \pm .5$ nm s.d., $n = 24$) are consistent with an expected pixel size of $5.4 \text{ nm} \times 6 \text{ nm}$. I note that the measured pixel width is exactly that expected given the measured width of the rectangle. The measured width was 104.14 nm and the theoretical width 97.92 nm. Assuming that the scale is off (by 6.36%) and that the latter value is correct, then the width of two columns of pixels is $10.8 \pm .85$ nm, spot on. The same holds true for the measured pixel height. The measured height was 77.08 nm and from our estimation of the gap (based on many experiments we would expect a height of 71 nm. Assuming the latter was actually correct the scale is off (by 8.56%) then one pixel height is $6.1 \pm .46$, very close to the expected value.



d instead each helper strands was marked with a dumbbell hairpin halfway along its length :



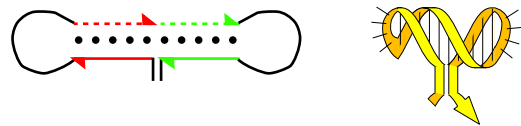
e a normal hairpin (**c** redrawn) that forms 10 base pairs intramolecularly:



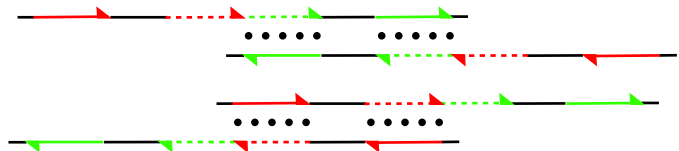
f can dimerize easily via 20 base pairs intermolecularly



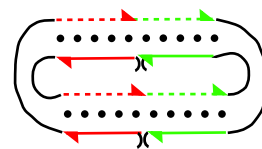
g a single dumbbell hairpin (**d** redrawn) forms 10 base pairs intramolecularly



h intermolecular dimers of a dumbbell hairpin can form 10 base pairs without becoming pseudoknotted



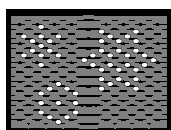
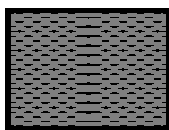
i a dumbbell hairpin must form a tight pseudoknot to make all possible (20) base pairs.



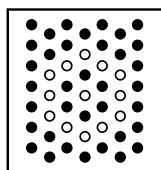
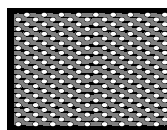
Supplementary Figure S49: Markers for AFM contrast, possible unintended interactions.

Creating arbitrary patterns

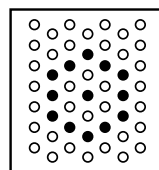
original shape strands



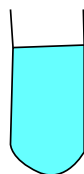
new strands with hairpin labels



From a full box (left) the desired pattern of tips (black dots) to an empty box (right) so that the boxes hold complementary patterns of tips.



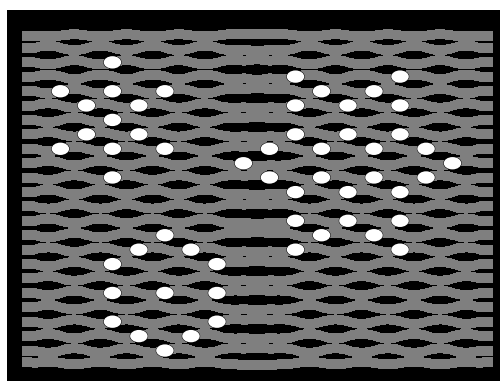
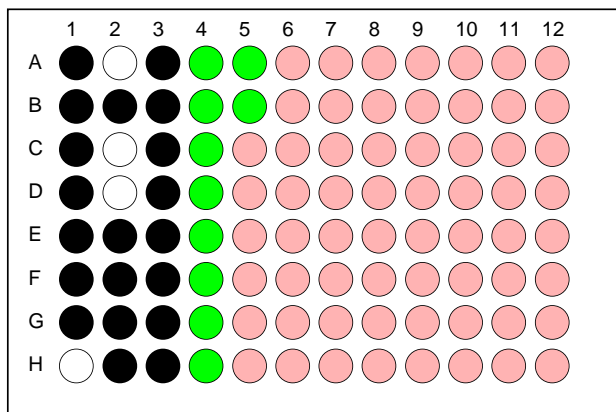
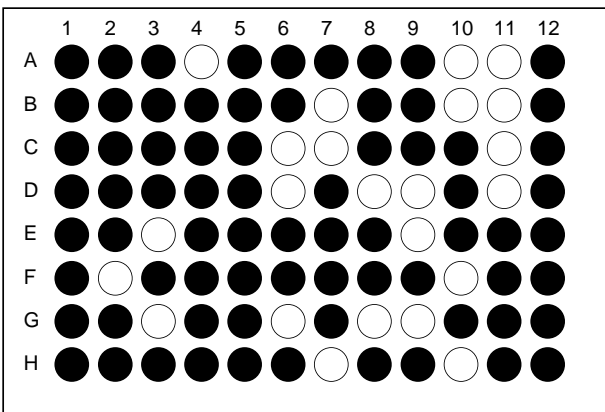
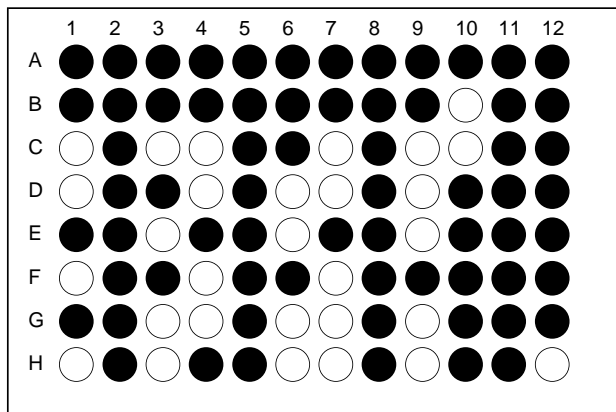
The formerly full box is used to draw from plates holding the original strands.



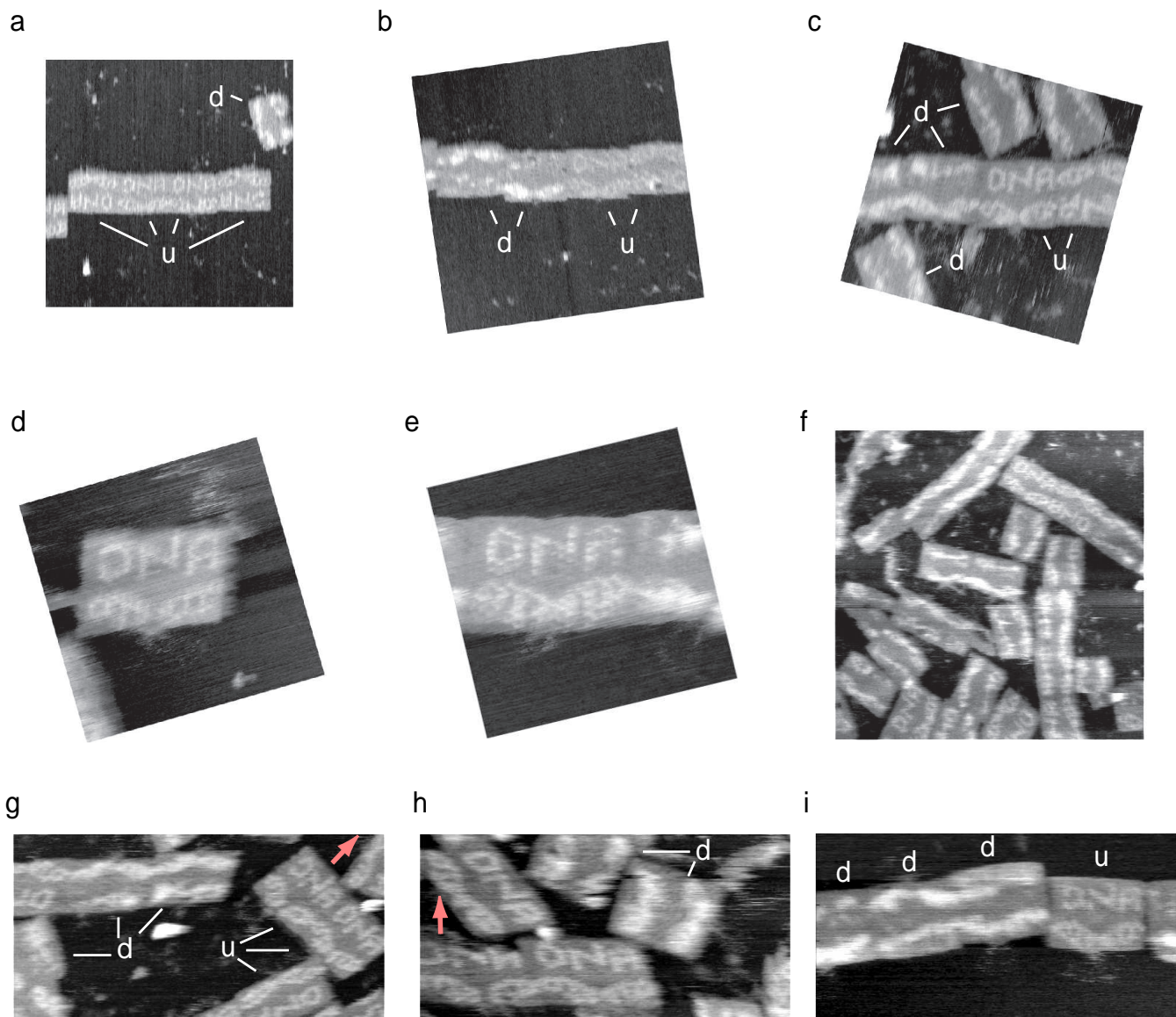
The formerly empty box is used to draw from plates holding the new strands with hairpins.

Supplementary Figure S50: Making a pattern on DNA origami.

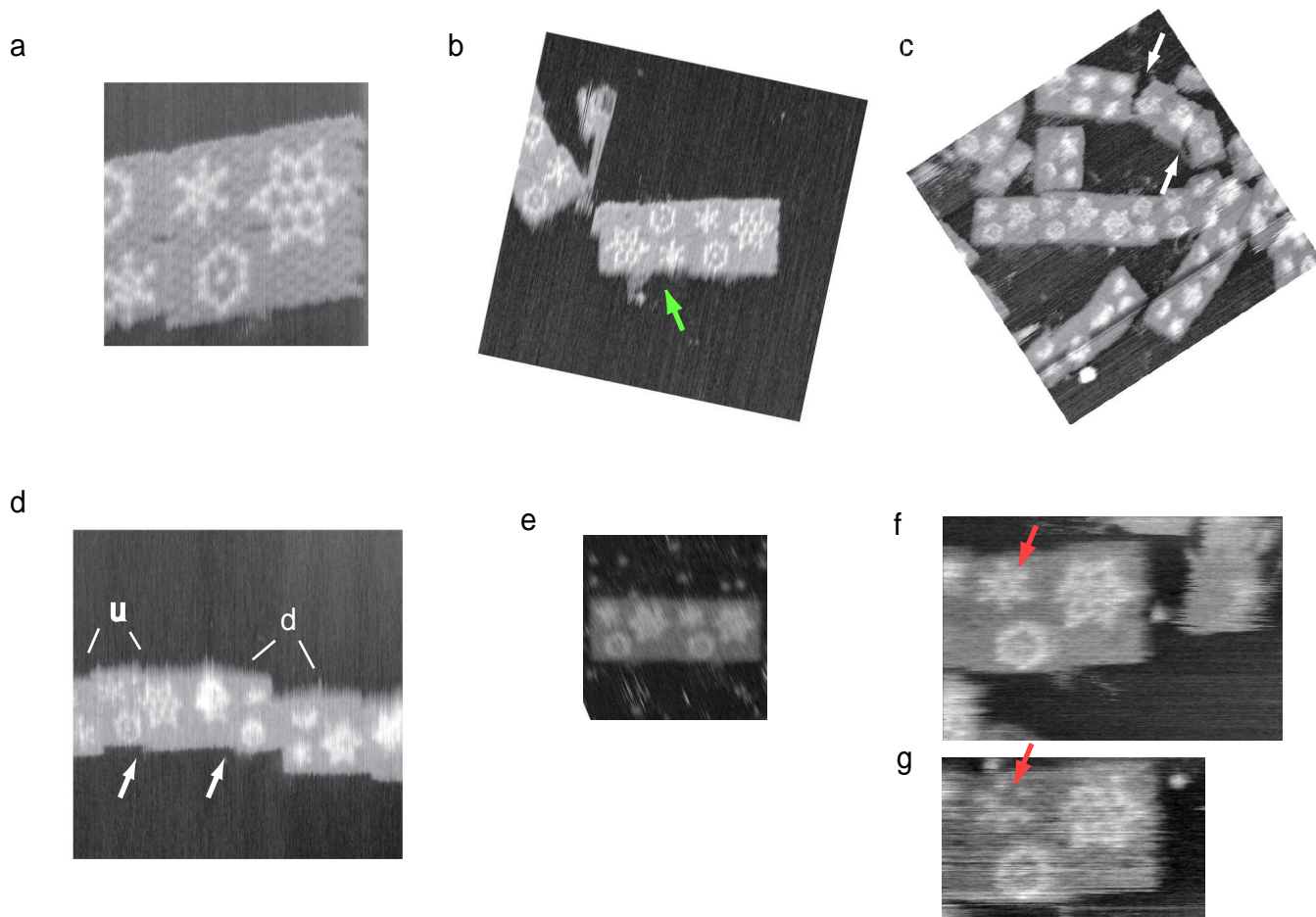
rectangle.1.5tn.16nt.18utX24hx.CG.gry.blk.bnd.PIX.SNOW_FLAKE.ps



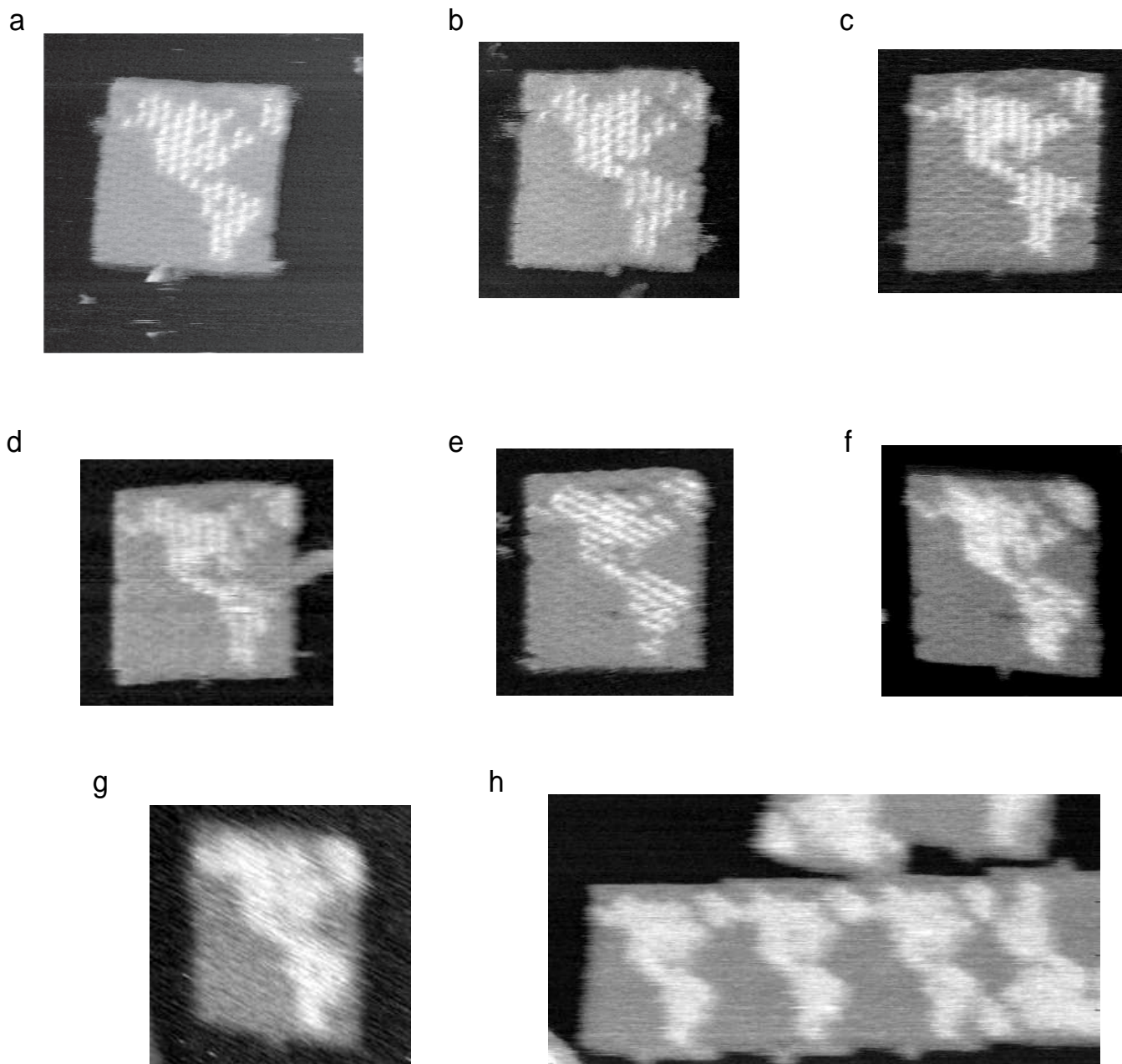
Supplementary Figure S51: A worksheet that allows easy preparation of a DNA pattern. Three 96 well plates are represented. Black circles mark wells that should be sampled from a set of 3 plates with unlabelled staple strands. White circles mark wells that should be sampled from a set of 3 homologous plates with dumbbell hairpin labels. Green circles represent the remainder strands that should be drawn independent of what pattern is being created. The pattern created using this mix of strands is diagrammed in the fourth quadrant.



Supplementary Figure S52: Extra images of 'DNA' pattern. **a** Enlarged view of Fig. 3b. **b-i** Other relatively high resolution images. 'u' indicates a rectangle with hairpins facing up; 'd' a rectangle with hairpins facing down. 42% ($S = 55$) of rectangles with the 'DNA' pattern were face-up. Pink arrow indicates the position and orientation of the same position in two images (**g** and **h**).



Supplementary Figure S53: Extra images of 'snowflake' pattern. **a** An uncorrected version (unsheared and unstretched) of Fig. 3d; this original was heavily distorted by AFM drift. **b** An uncorrected zoom out (none was required) of the structures from Fig. 3d showing surrounds. Green arrow indicates an area of damage in a neighboring structure, probably caused by the tip. **c–g** Extra relatively high resolution images. 'u' indicates hairpins are facing up; 'd' that hairpins are facing down. Rectangles in all these images have unbridged seams that occasionally dislocate slightly (white arrows, **d**) or grossly (white arrows, **c**). Sometimes a hairpin irreversibly disappears, see pink arrows in **f, g**.



Supplementary Figure S54: Extra images of the 'Map' pattern. **a** An uncorrected version (unsheared and unstretched) version of Fig. 3f; this original was distorted by AFM drift. **b-f** Other high resolution maps for comparison. Observe that there is no correlation between missing pixels. Depending on the batch of AFM tips used (Veeco NP-S, oxide sharpened), only 1 tip in 5 to 1 tip in 30 provides such resolution. **g,h** More typical (but still good) resolution.

Supplementary Note S7: Composition of shapes

To give sharp triangles specific binding interactions, staple strands along their edges were cut and pasted to yield two new types of staple strands: (1) extended staple strands that project 8 bases from the edge of the triangle which served as ‘donors’ and (2) truncated staple strands that left an 8 base section of the scaffold single-stranded available as an ‘acceptor site’. Given a sharp triangle as drawn in the design (with a particular face of the triangle facing up out of the page), extended staple strands were always positioned on the righthand half of the sharp triangle’s edge and truncated staple strands were always positioned on the lefthand half the sharp triangles edge. In this way, whenever the edges of two triangles met (with the faces of the triangle pointing in the same direction) the position of extended staple strands on one edge matched up with the position of the truncated staple strands on the other edge (and vice versa). If the sequences of the 8-base donor sections of the extended staple strands complemented the single-stranded acceptor portions of the scaffold, then the two edges could bind. Sequences are given in Supplementary Fig. S55.

The composition of sharp triangles into hexagons and lattices was only of limited success. While the interactions between sharp triangles were specific and as designed, the formation of hexagons and lattices were not quantitative. Several factors are likely to influence yields: (1) the stoichiometry of extended staple strands (2) the formation temperature of sharp triangles relative to the formation of inter-triangle bonds (3) the flexibility of inter-triangle bonds. There is much room for the optimization of these factors and quantitative composition of origami shapes into larger structures remains an open problem.

Because extended staple strands are not like normal staple strands in that they do not bind exclusively to a single scaffold strand, the stoichiometry of the extended staple strands immediately becomes important. For example, if a full 100-fold excess of extended staple strands were used, then excess staple strands could fill up all of the available single-stranded vacancies left by truncated staple strands. Ideally, there would be exactly 1 copy of each extended staple strand for each scaffold strand. Practically, because the stoichiometries of staple strands were uncertain, I used a range of extended staple:scaffold ratios (approximately 100, 20, 4 and 1) and retained the normal 100-fold excess for the rest of the staple strands. As expected, at a high relative excess of extended staple strands (100-fold) few triangles associated into hexagons. At a somewhat lower excess (20-fold) some hexagons formed. No matter what the ratio of extended staples to scaffold the yield of hexagons was low (Supplementary Fig. S56); the best results were obtained with a ratio of 4.

The formation temperature of sharp triangles relative to the formation of inter-triangle bonds is probably very important to the correct composition of triangles. Ideally, over the course of annealing, sharp triangles would form completely at a high temperature, and then only at a much lower temperature would weak inter-triangle bonds be strong enough to bring triangles together. If the bonds between triangles are too strong, then they will form at a temperature near that at which the sharp triangles themselves form and the sharp triangles may still be partially melted, disordered and floppy. This would seem to result in poorly formed structures.

The strength of inter-triangle interactions can be tuned by the number of extended staple strands that are used. I tried variations in which 2, 4, 8, and 16 staple strand bridges should have formed between sharp triangle edges (using subsets of the sequences in Supplementary Fig. S55). Hexagons and lattices formed with 4 and 8 staple strand bridges between edges but not for 2 and 16 staple strands. The experiments suggest that 2 bridges are too weak, and 16 bridges are too strong, for proper composition of triangles. These experiments are preliminary, however. Given the poor stoichiometry in the experiments, it is possible that on average 2 acceptor sites per edge were filled with excess extended staple strands. If this were true then it would explain why in 2-bridge experiments, few triangles bound each other. Further, the 16-bridge experiments are not really comparable with the others. In the 16-bridge experiments, the acceptor (left side) of a sharp triangle is left almost completely single-stranded and floppy because 8 truncated staple strands occur in a single row. This is in sharp contrast to the 4 and 8 bridge experiments in which truncated staple strands alternate with normal staple strands on the acceptor side of the edge; the normal staple strands potentially make the edge more rigid.

Finally, I note that the hexagon of triangles may, at 30 megadaltons, hold the record for the largest man-made molecular complex. It has $6 \times (7249 + 7156 + 980) = 92310$ nt (counting scaffold, staples and 35 hairpins/triangle at 28 bases each, not counting remainder strands) for a total molecular weight of 30.46 megadaltons (counting 330 daltons per nt). Individual unpatterned origami are all ~ 4.7 megadaltons. For comparison, the molecular weight of the eukaryotic ribosome is 4.2 megadaltons.

Truncated versions of the right hand side bottom row strands. To make lattices of sharp triangles, or hexagons these strands are used to create acceptor sites. Potentially all of them might be used for a lattice (since acceptors must be placed on 3 sides) but only 2/3 of them might be used for hexagons (since acceptors must be placed on 2 sides). The actual number depends on the number of donor/acceptor pairs desired. Here, the name of the strand indicates the position in the sharp triangle plates that it is meant to replace.

t1s10g-TR-P1-B2, A5, AATTAACCTCGAATAAGTTTATTCCAGCGCC
t1s20g-TR-P1-G2, B5, CATTCAACTTAAGGGAAGCCCGATCAAAGCG
t1s30g-TR-P1-E3, C5, CACGTATACTGAAATGGATTATTAATAAAG
t3s10g-TR-P1-E5, D5, GTAATTGATGGCAACATATAAAGCGGATTGAG
t3s18g-TR-P1-H5, E5, AACTCCAAGATTGCATCAAAAAGATAATGCAG
t3s20g-TR-P1-A6, F5, GGAATTACAGTCAGAAGCAAAGCGCAGGTCAG
t3s28g-TR-P1-D6, G5, AGAGATAGTTGACGCTCAATCGTACGTGCTT
t3s30g-TR-P1-E6, H5, AGCGGGAGATGAAAATACCTACATAACCCCTC
t3s8g-TR-P1-H6, A6, CATTCAACAAACGAAAGACCCAGAACACCC
t5s10g-TR-P1-E8, B6, ACAAGAATGTAGCAAACGTAGAAAATTTATC
t5s18g-TR-P1-H8, C6, TAATTGCTTTACCTGACTATTATGAGGCGATA
t5s20g-TR-P1-A9, D6, CATAACCCATCAAAAATCAGGTCCTCTTTGA
t5s28g-TR-P1-D9, E6, GAATACGTAACAGGAAAACGCTCCTAAACAG
t5s30g-TR-P1-E9, F6, ATTTTGTAGTACCCGCGCCATGCGGCACAGA
t5s8g-TR-P1-H9, G6, TTGACGAAAATACATACATAAAGGGCGCTAAT
t7s10g-TR-P1-B11, H6, AAGAAACATGGCATGATTAAGACTCCGACTTG
t7s20g-TR-P1-F11, A7, CCAAAATATAAAGCAGTTAGAAATTTAGAGCT
t7s18g-TR-P1-E11, B7, CGGATGGCAGGAGATGACCAATATCGTTTAC
t7s28g-TR-P1-A12, C7, CTATTAGTATATCCAGAACATATCAGGAACG
t7s30g-TR-P1-B12, D7, AGAAGTGTATCGGCTTGGTGTACTTTAATG
t7s8g-TR-P1-E12, E7, CACCGTCACCTTATACGAGTATTGAGTTAA
t9s10h-TR-P2-D1, F7, CGAAGCCAAACGCAATAATAACGAAAATCACCG
t9s18g-TR-P2-F1, G7, TGCTTAGATCCCCCTCAAAATGCTCGGAGAG
t9s20h-TR-P2-G1, H7, TTTGCCAGCATAAATATTCATTGACTCAACATGTT
t9s28g-TR-P2-A2, A8, TAAACATAGAAGAACTCAAACCTTTTATAA
t9s30h-TR-P2-B2, B8, GTAAAGAACATCACTTGCTGAGCGCCATTAAAA
t9s8g-TR-P2-D2, C8, GAGCCAGGAAATACCCAAAAGAACATGAAATA

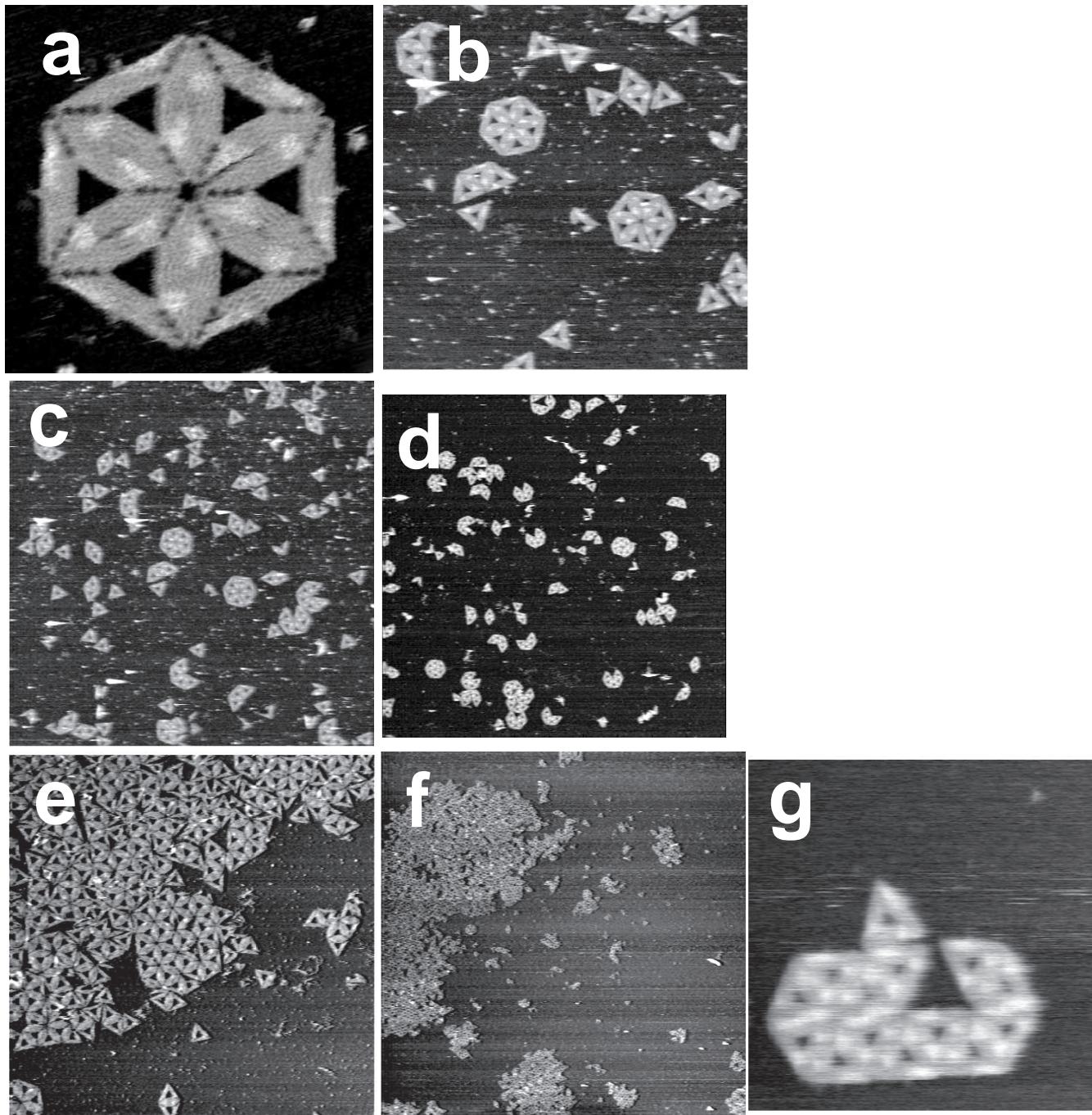
These strands have been extended to provide donors that make triangular lattice.
Here again the name of the strand gives its provenance.

t-10s17h-LT-P2-E2, A1, ACCAACCTAAAAATCAACGTAACAAATAAATGGGCTTGAGAAAAAGAT
t-10s27h-LT-P2-F2, B1, AACTCACATTTAGTGGTTTCCAGAAACCGCTATCAGGGCCACCGCA
t-10s7h-LT-P2-G2, C1, ACGACAATAAATCCCGACTTGGGGAGATCCTGAATCTTACCATATCTTAC
t-1s18g-LT-P2-D4, D1, CGACCTGCGGTCAATCATAAGGGAACGGAAACAACATTATTGAATACCA
t-1s28g-LT-P2-D5, E1, TTTCCACGAGCTGGCCCTGAGAGAAAGCCGCGAAGCTGGTTGACGAG
t-1s8g-LT-P2-D6, F1, TTTCCCTAGCACATCAGAGAACAATAGCAGCCTTTACAGGACGGGAG
* t-3s10g-LT-P2-B8, G1, TGAACAAAACGTCAAAATGAAAGCAAGCCGTTTTATGAAACCAA
t-3s18g-LT-P2-E8, H1, TATCATCGTTGAAAGAGGACAGATGGAAGAAAATCTACGCGCCAAA
* t-3s20g-LT-P2-F8, A2, ATACATAATTAATAAAGCAACTAACCGAACTGACCAACTCCTGATA
t-3s28g-LT-P2-A9, B2, GTTTGCGTCACGCTGGTTTGGCCAAAGGAGCCCGGATTAGAAATCAG
* t-3s30g-LT-P2-B9, C2, TCCTCGTTAGAGCTTGACGGGAGTTGACGAAAGCGGTTGTTGGCG
t-3s8g-LT-P2-E9, D2, AGCATGTATTTCATCGTAGGAATCAAACGATTTTTGTTGTCAGAGG
* t-5s10g-LT-P2-B11, E2, ATCAGAGTCCCAATCCAAATAAGATTACCGCGCCCAATAAATAAT
t-5s18g-LT-P2-E11, F2, CCAAGCGCAGCGCATAGGCTGGCAGAACTGGCTCATATAACACTAT
* t-5s20g-LT-P2-F11, G2, GTAAGCAGCAGTCAAGGAGTTGGAACGGTTACAGACCGAAACAAA
t-5s28g-LT-P2-A12, H2, TTAATGAAGTTGATGGTTCGCGAGTGGCTTAAAGCATAAAGGG
* t-5s30g-LT-P2-C12, A3, GAGGCGGACTAAATCGGAACCCTAAGCAGGCGAAAATCCTCGGCCAA
t-5s8g-LT-P2-E12, B3, ACAAGAAAGCAAGCAAAATCAGATAACAGCCATATTTTATGATAACCC
* t-7s10g-LT-P3-G1, C3, GCCCAATAGCCAGTTACAAAATAATAGAAGGCTTATCCGGTTATCAAC
t-7s18g-LT-P3-A2, D3, AAAACACTTAATCTTGACAAGAACTTATCATTGTGAATGATAAAAA
* t-7s20g-LT-P3-B2, E3, CAGACGACCTTATGCGATTTTATGACCTTATCAAGAGACTCTTTTG
t-7s28g-LT-P3-D2, F3, TTCCAGCTTATAAATCAAAAAGAGAACCATACCCAAATGAATCCTG
* t-7s30g-LT-P3-E2, G3, GTACGCCACAAGTTTTTTGGGGTCGAAATCGGCAAAATCCGGGAAAC
t-7s8g-LT-P3-G2, H3, GCGCTGTTATTCTAAGAACCGGATCCAGAGCCTAATTTATAAGAGC
* t-9s10g-LT-P3-F3, A4, GCAATAGCAGCCTAACGAGCGTCTGGCGTTTTAGCGCAACCAACATGT
* t-9s20g-LT-P3-H3, B4, CTTTGTGATGGTTTAAATTCACCTCGGATATTCATTACCCAGCAAGA
* t-9s30g-LT-P3-B4, C4, TCAGTAGGAGTGGCCACTACGTATAGCCGAGATAGGATGCGTT

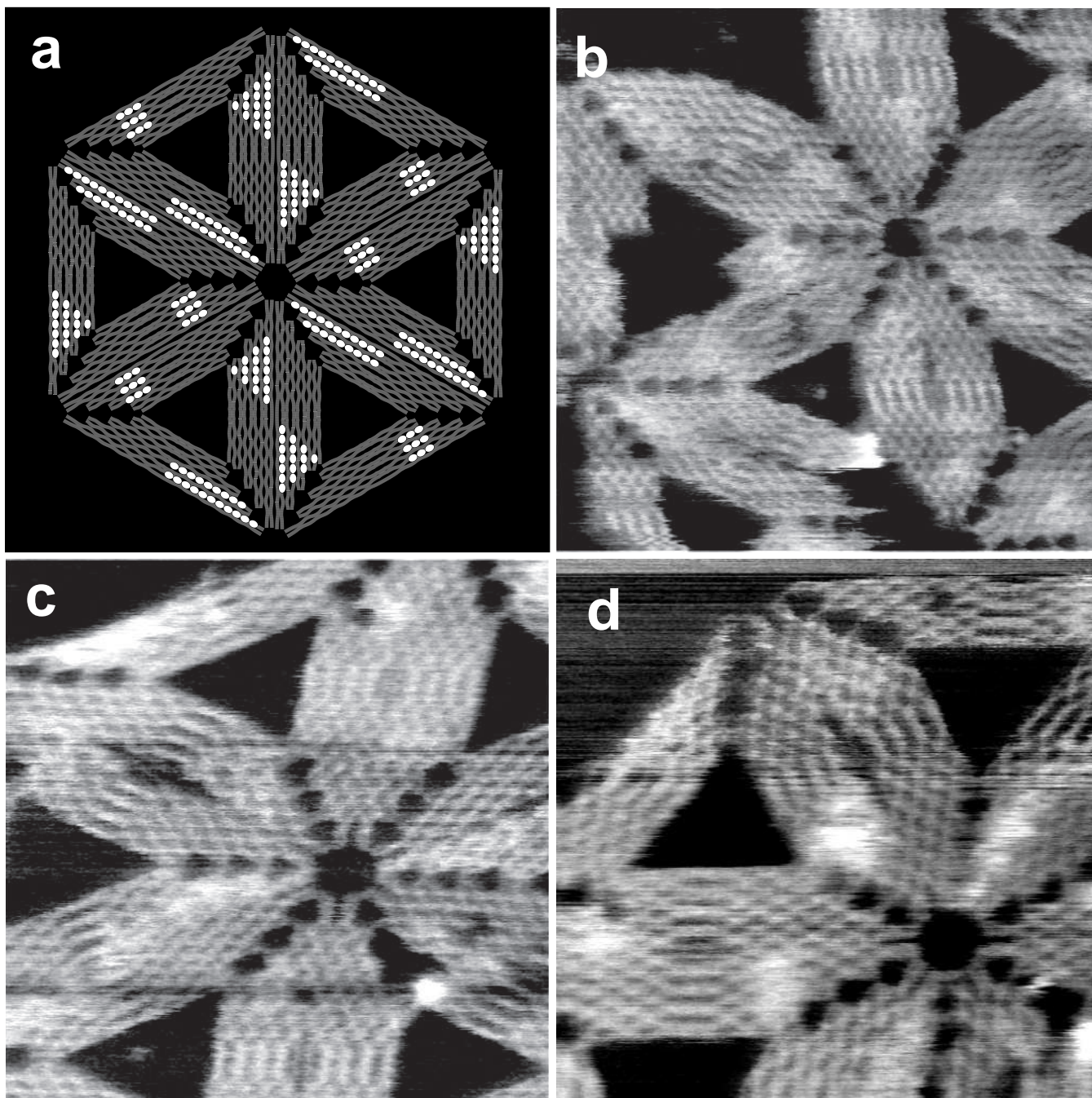
t-10s17h-HX-P2-E2, A6, ACCAACCTAAAAATCAACGTAACAAATAAATGGGCTTGAGATATCTTAC
t-10s7h-HX-P2-G2, B6, ACGACAATAAATCCCGACTTGGGGAGATCCTGAATCTTACAAAAGAAAGT
t-1s18g-HX-P2-D4, C6, CGACCTGCGGTCAATCATAAGGGAACGGAAACAACATTATTGACGGGAG
t-1s8g-HX-P2-D6, D6, TTTCCCTAGCACTCATCGAAGCAATAGCAGCCTTTACAGGAATACCA
* t-3s10g-HX-P2-B8, E6, ATACATAAAGCGTCAAAAATGAAAGCAAGCCGTTTTATGAAACCAA
t-3s18g-HX-P2-E8, F6, TATCATCGTTGAAAGAGGACAGATGGAAGAAAATCTACGGTCAGAG
* t-3s20g-HX-P2-F8, G6, TGAACAAATTAATAAAGCAACTAACCGAACTGACCAACTCCTGATA
t-3s8g-HX-P2-E9, H6, AGCATGATTTTCATCGTAGGAATCAACGATTTTTGTTGCGCCAAA
* t-5s10g-HX-P2-B11, A7, GTAAGAGCTCCCAATCCAAATAAGATTACCGCGCCCAATAAATAAT
t-5s18g-HX-P2-E11, B7, CCAAGCGCAGCGCATAGGCTGGCAGAACTGGCTCATATGATAACCC
* t-5s20g-HX-P2-F11, C7, ATCAGAGAACCGTCAAGCAGTGGAAAGCTGTAAGCAACCCAAACAA
t-5s8g-HX-P2-E12, D7, ACAAGAAAGCAAGCAAAATCAGATAACAGCCATATTTTAAACACTAT
* t-7s10g-HX-P3-G1, E7, CAGACGCGCAGTTACAAAATAATAGAAGGCTTATCCGGTTATCAAC
t-7s18g-HX-P3-A2, F7, AAAACACTTAATCTTGACAAGAACTTATCATTGTGAATATAAGAGC
* t-7s20g-HX-P3-B2, G7, GCCCAATACCTTATGCGATTTTATGACCTTATCAAGAGCACTCTTTG
t-7s8g-HX-P3-G2, A8, GCGCTGTTATTCTAAGAACCGGATTCAGAGCCTAATTTGATAAAAA
* t-9s10g-HX-P3-F3, B8, CTTTGTGACGCTAACGAGGCTCTGGGTTTTAGCGCAACCAACATGT
* t-9s20g-HX-P3-H3, C8, GCAATAGCTGGTTTTAATTTCACTCGGATATTCATTACCCAGCAAGA

These strands have been extended to provide donors that make hexagons.

Supplementary Figure S55: Staple strand variants for creating hexagons and lattices from triangles. Truncations provide acceptor sites, extended versions, donor sites. Stars (*) indicate extended staples that were used for the 8-bridge hexagons (8 starred strands) and 8-bridge lattices (12 starred strands) described in this paper. Four extended staples per side were used. Corresponding truncated strands were also used, and may be derived from the design.



Supplementary Figure S56: Extra images of the composition of triangles into hexagons and lattices. All structures shown here use 4 donor and 4 acceptor sites per edge (as depicted in Fig. 3n and o), for a total of 8 staple strand bridges between each pair of edges; all structures also use a 100-fold excess of normal staple strands. **a** Higher resolution image of hexagon from Fig. 3q. The tip-sample interaction force has been increased and hairpins marking the hexagon are less visible (but finer details appear.) **b** and **c**, Zoom-outs of Fig. 3q show that the fraction of hexagons formed is quite low $< 2\%$; the excess of extended staples is about 20-fold. **d** Another sample with a lower concentration of extended staples (about 4-fold excess) has fewer free triangles but no greater a number complete hexagons. **e** and **f**, Zoom-out of Fig. 3t shows large aggregates of triangles with only small well-ordered domains; the extended staple:scaffold ratio was roughly 1:1. **g** A well-formed 13-triangle aggregate at low resolution; the resolution is barely sufficient to show that the matching rules are correct in this structure. The extended staple excess was about 4-fold.



Supplementary Figure S57: High resolution images of the composition of triangles into lattices. Compare the fine structure of the model to AFM images. **a** Six triangles arranged in the bonding pattern used for the lattice. **NOTE:** this is **not** the hexagon, it is the inner segment of Fig. 3r rotated by 30 degrees. **b** a reproduction of Fig. 3u, only larger. **c** and **d** two more high resolution views. While damaged and suffering from AFM scan artifacts, these images show fine structure associated with crossovers well.

Supplementary Note S8: M13mp18 scaffold and staple strand secondary structure

Repetition of sequences (and their complements) in the scaffold and staple strands may cause them to have undesired binding to each other or to themselves (secondary structure). How much repetition can be tolerated is an interesting question. Clearly a poly-A scaffold cannot work, but could scaffolds limited to an AT alphabet fold robustly? Understanding such limits will require solving difficult combinatorial and thermodynamic problems. Here, I give examples of secondary structure and other undesired binding interactions in the M13mp18 scaffold and the staple strands, structure that was not too difficult to overcome. I argue that, for its length and base composition, M13mp18's sequence is not special in this regard—it is not a particularly “lucky” sequence with little secondary structure.

To get a feeling for M13mp18 secondary structure, I used Michael Zuker's DNA Mfold³⁷

<http://www.bioinfo.rpi.edu/applications/mfold/old/>

to obtain predicted foldings for 6000 base sections of M13mp18 sequence, as well as predicted foldings of 6000 base random sequences of similar base composition. All folds were computed at 20°C, 40 mM Na⁺ and 12 mM Mg²⁺. Rather than use the M13mp18 sequence reported in Genbank, I used the sequence found by New England Biolabs (NEB) the last time their M13mp18 clone was resequenced, (F.J. Stewart, NEB, 5/28/02).

Lowest energy folds for seven 6000 base segments of the M13mp18 sequence (using a sliding window, starting at $n = 1, 1001, 2001, 3001, 4001, 5001, 6001$ and 7001) were obtained. (I would have folded all 7249 bases at once, but 6000 is the Mfold server's limit). The strongest structure ($n=4001, -1003$ kcal/mole) and weakest structure ($n = 6001, -904$ kcal/mole) are shown in Supp. Fig. S58 and Supp. Fig. S59. I noticed strong secondary structure around base 5500. This structure, a series of several strong hairpins, is well-known structure of biological significance and occurs in the intergenic region (5500-6000) of M13³⁸. Of particular interest is a strong 20 base hairpin, [A], that has been enlarged in the inset of Supp. Fig. S58.

To get a quantitative measure of the predicted secondary structure I averaged free energies of folding (for the lowest energy structures). For the seven sections examined the average is -965 ± 37 kcal/mole. The large variation in energy is due to the fact that these 6000 base segments can be classed into two types. (1) Those that span the intergenic region ($n = 1001, 2001, 3001, 4001, 5001$) with its strong, biologically relevant secondary structure; they have an average energy of -990 ± 12 kcal/mole. (2) Those that don't span the intergenic region completely ($n = 1, n = 6001, n = 7001$) which have an average energy of -924 ± 24 .

To evaluate whether M13mp18's sequence has unusually strong or weak secondary structure, ten random 6000 base sequences were generated to have a base composition similar to the M13mp18 sequence (24.4% A 21.1% C 21.2% G 33.4% T, fixed at 1462 A's, 1266 C's, 1270 G's, 2002 T's). Supp. Fig. S60 shows the lowest energy fold for one of these sequences; visually it appears that the M13mp18 sequence (Supp. Fig. S58 and 59) has secondary structure similar to that of a random sequence of similar length. However, the average calculated energy for random sequences is significantly less than that for M13mp18's sequence, -867 ± 13 kcal/mol. Thus it seems that M13mp18's sequence has somewhat stronger secondary structure than would be expected.

The secondary structure of M13mp18 DNA does appear to be less strong than that predicted for sequences of even base composition. For comparison, ten 6000 base sequences of composition A=G=C=T=1500 have an average calculated free energy of -1080 ± 21 . To explore the strong effect that base composition has on secondary structure, I looked at two more examples. For A=G=T=2000 and C=0 the predicted average energy is -157 ± 13 . And for A=C=T=2000 and G=0 the predicted average energy is -93 ± 6 . In the event that secondary structure becomes a limiting factor in the creation of DNA origami, such skewed base compositions might be used but at the cost of specificity in staple-scaffold binding.

Of all the potential secondary structure that the M13mp18 sequence has, only the [A] loop was deemed worrisome enough to be avoided. Mfold predicts the structure of loop [A] as a hairpin, (20 nt stem, 4 G-T mismatches, $\Delta G = -14.4$ kcal/mole) at positions 5515-5557. The sequence at these positions is:

```
GGCGGGTGTGGTGGTTACGCGCAGCGTGACCGCTACACTTGCC
```

In designing DNA origami, I decided to avoid the entire 73 base section (5515-5587).

```
GGCGGGTGTGGTGGTTACGCGCAGCGTGACCGCTACACTTGCCAGCGCCCTAGCGCCCGCTCCTTTTCGCTTTC
```

This allowed me to linearize M13mp18 DNA by incubating with the complement of bases (5558-5587)

```
GAAAGCGAAAGGAGCGGGCGCTAGGGCGCT
```

and cutting with BsrB I between positions 5573 and 5574. (BsrB I has recognition sequence, CCGCTC at 5571-5576; it leaves a blunt end between bases 3 and 4.) Because I did not purify the linearized DNA away from the complement used to linearize it, in all designs I avoided the entire 73 base section. I don't know if this is necessary.

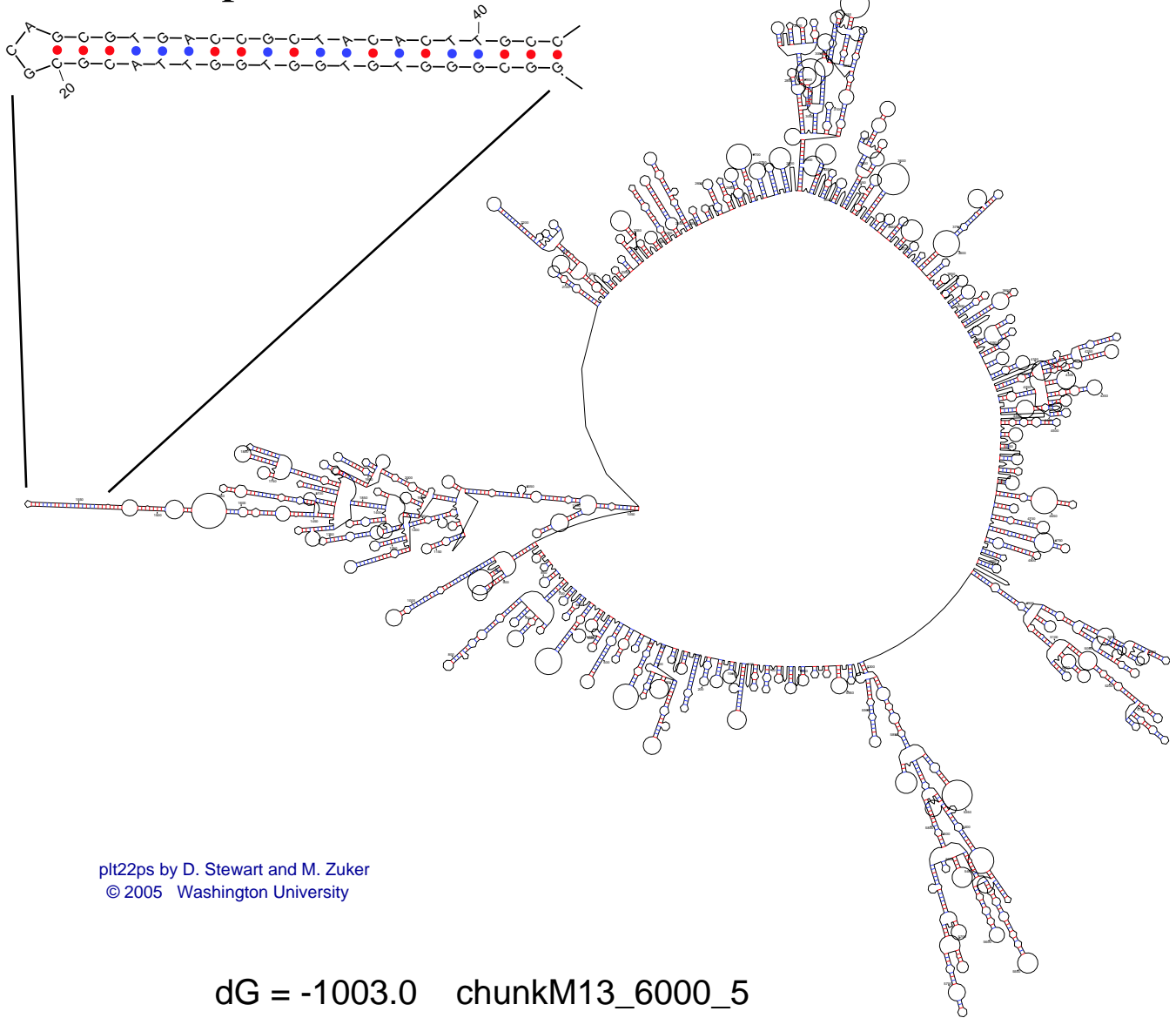
Other less strong but well known secondary structure in the scaffold did not seem to cause problems. For example, the hairpin [C] GGGTGATGGTTCACGTAGTGGGCCATCGCCC has a 14 base-pair stem. Occurring at bases 5704-5734, this sequence is 116 nucleotides into the origami structures. It occurs, for example in the rectangle on the bottom edge of the lower left corner, a position that suffers no apparent defects.

Finally, I note that staple strands themselves may have unintended secondary structure or binding interactions. By concatenating the sequences of staple strands with 'NNNN' linkers between them and folding the resulting sequence with Mfold, I was able to find a couple potential bindings between different staple strands (with lengths of 10 and 11 nucleotides and having single G-T mispairs) as well as some secondary structure within single staple strands. For example, the rectangle staple strand r7t22e, GCCAACAGTCACCTTGCTGAACCTGTTGGCAA can form an 8 base hairpin:

```
GCCAACAGTCACCTT\
| | | | | | | |
AACGTTGTCCAAGTCG/
```

Such secondary structure would normally be considered unacceptable in the design a DNA nanostructure. The next section explores reasons for why scaffold and staple secondary structure might not cause problems for the formation of scaffolded DNA origami.

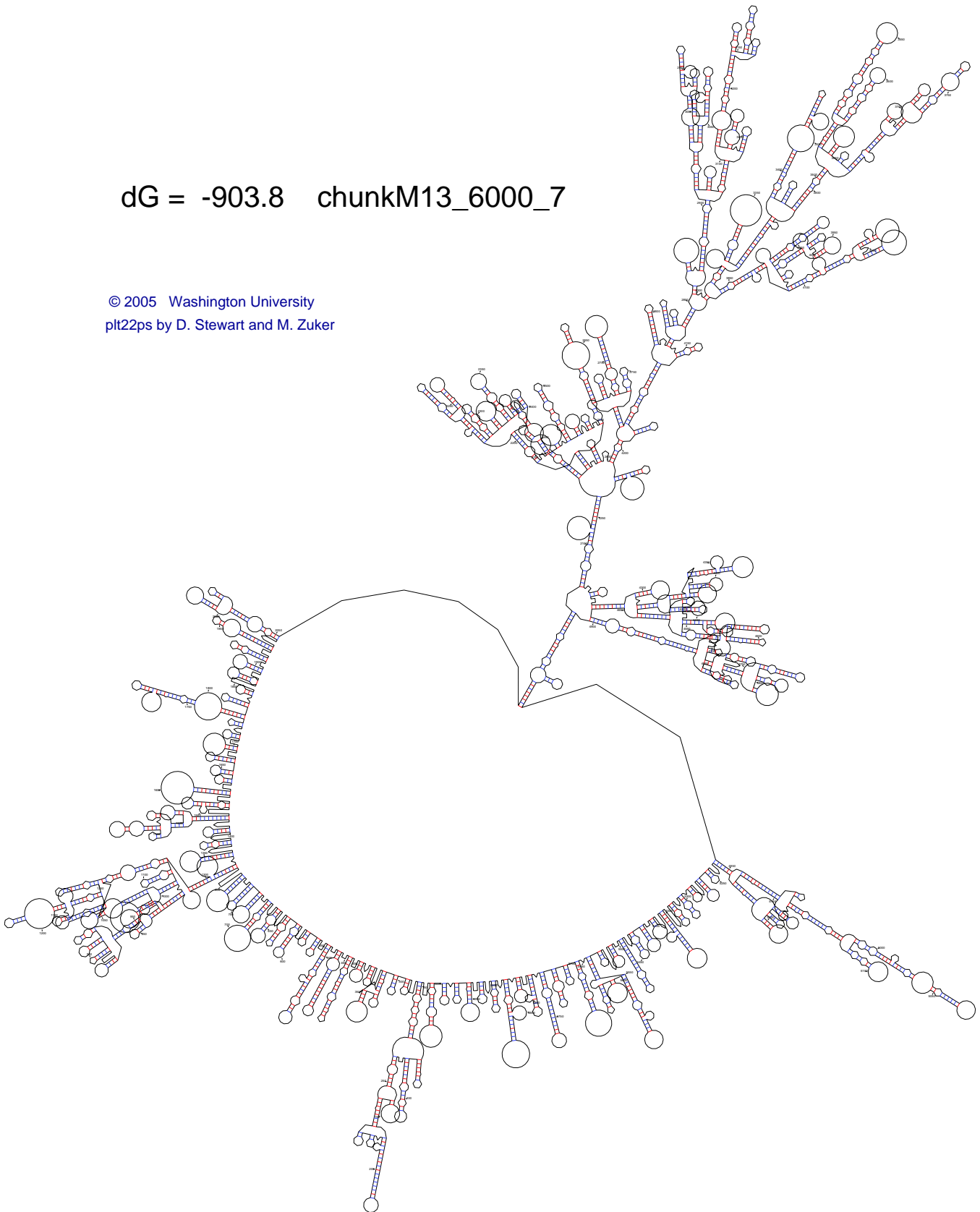
Hairpin [A]



Supplementary Figure S58: A 6000 base chunk of M13mp18 sequence spanning the intergenic region.

dG = -903.8 chunkM13_6000_7

© 2005 Washington University
plt22ps by D. Stewart and M. Zuker



Supplementary Figure S59: A 6000 base chunk of M13mp18 sequence that skips the intergenic region.

dG = -858.4
rand_M13A_6000_2

plt22ps by D. Stewart and M. Zuker
© 2005 Washington University



Supplementary Figure S60: A 6000 base random sequence with the same base composition as M13mp18's sequence.

Supplementary Note S9: Why does scaffolded DNA origami work?

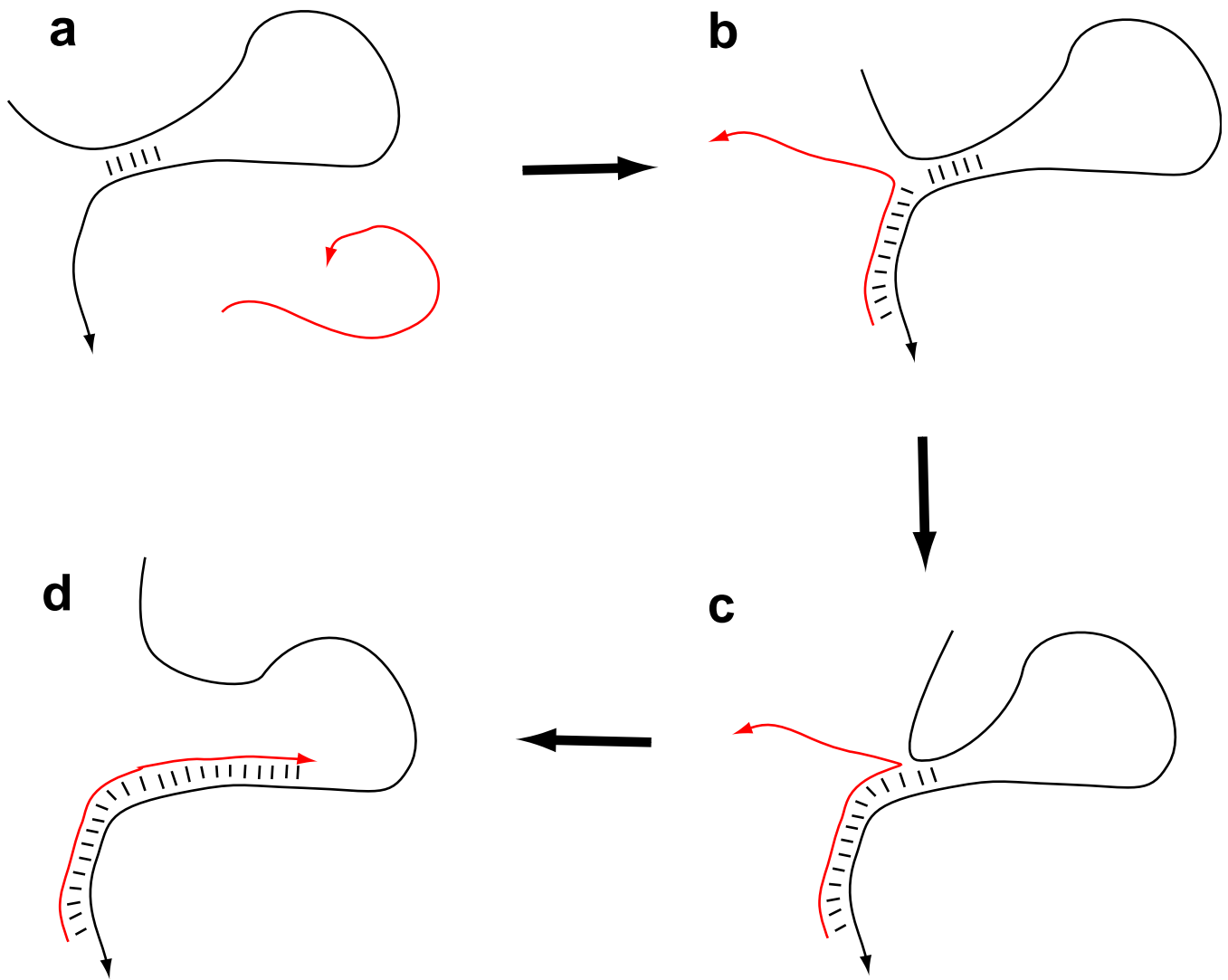
Consider any secondary structure that the scaffold might assume. It is unlikely that this secondary structure perfectly blocks the binding sites for all the staple strands that should bind its sequence. Thus staple strands may bind by partial matches at first (to gain a ‘toehold’), and then participate in a branch migration that displaces the secondary structure (Supplementary Fig. S61). A longer region of complementarity between the staple and the scaffold stabilizes the staple-scaffold interaction over the scaffold secondary structure. The excess of staple strands may help drive this process. Explicit use of strand displacement to actuate nanomachines appears in^{39, 40, 41, 42}. (It was Bernie Yurke’s work on DNA motors that convinced me that strand invasion might make scaffolded DNA origami possible.)

Another factor that may work against scaffold secondary structure is the role of staple strands as intramolecular bridges. Each successful addition of a staple strand organizes the scaffold for subsequent binding of adjacent staple strands and constrains the scaffold in a way that precludes a large set of undesired secondary structures. Thus one might expect the binding of staple strands to be highly cooperative. To see why intramolecular interactions may be important, consider cutting a scaffolded shape into a multi-stranded structure based on unique tiles (for which the minimum free energy state should be the scaffolded shape, just with more backbone nicks). For such a system the addition of a tile at any one position does not significantly constrain the global structure.

Next consider the interactions of staple strands with themselves. Many strong complexes exist between them; none is a perfect match, however. The scaffold can displace such structure and gain a required staple strand.

Now consider purity. A truncated staple strand might bind to the scaffold. However, because of the excess of staple strands, there exist many full length length staple strands that can bind and displace the truncated strand. This means that only the purity of the scaffold matters; because the scaffold is derived from a biological source, it is very pure.

In a similar way, because *staple strands do not bind to each other*, the relative stoichiometry between the staple strands does not matter. With staple strands in excess over the scaffold, the remaining relevant concentration is the effective local concentration of scaffold in intramolecular events. Here the intramolecular nature of scaffold folding enforces a kind of equimolarity—any two sections of the scaffold that are brought together by a staple strand are by definition, equimolar. Again, such could not be said for the same sections if the scaffolded structure were cut into multi-stranded unique tiles. This highlights a crucial difference between the scaffolded method shown here and that previously proposed^{17,18}. In the latter scheme the scaffold runs through *every other* helix; the structure is held together by interactions between multi-stranded tiles and so the *staple strands must bind to each other*. For such schemes precise equimolarity is likely important.



Supplementary Figure S61: Opening of scaffold secondary structure by strand displacement. **a** Five bases of undesired secondary structure in the scaffold occur in the middle of the binding site for the red staple. **b** The red staple strand can still bind by 10 bases adjacent to the hairpin stem and gain a 'toehold'. **c** A random walk at the junction between the staple and hairpin allows the staple strand to gain three more basepairs. **d** Eventually the random walk results in the hairpin opening, which allows the rest of the staple to bind.

Supplementary Note S10: Cost

The going rate for oligonucleotides synthesized unpurified, in plates, at the 100 nmole scale is between \$.18 and \$.25 per nucleotide (USD). Thus a 32-mer oligonucleotide costs about \$7 for about 80 nmol of material. (Additional PAGE purification costs \$40-80 per oligonucleotide and yields, on average, 10 nmol of material. Thus per nmol, purified oligonucleotides are about 50× as expensive as unpurified ones.) The total cost then, for about 80 nmol of each staple strand to complement the 7249 base pair M13mp18 scaffold is \$1500; staples thus cost about \$19/nmol. Four picomoles (10 micrograms) of scaffold was purchased from New England Biolabs for \$30; scaffold thus cost \$7500/nmol. Using a 100-fold excess of staple strands, the cost of DNA origami (of the current size) would be $\$7500 + \$1900 = \$9400$ per nmol of which the scaffold strand is 80% of the cost.

Recent controls have shown two things: 1) results using only a 10-fold excess of staple strands are indistinguishable from those with a 100-fold excess and 2) results using a 10-fold cheaper source of M13mp18 DNA (Bayou Biolabs) yield results indistinguishable from those with New England Biolabs. The net result of these observations is that, if these two modifications to the protocol were implemented, the cost of DNA origami would be closer to \$1000 per nmol but that the scaffold strand would still be 80% of the cost of the origami.

In sum, the price of synthetic oligonucleotides does not, as one might expect, dominate the cost of DNA origami. In principle excess staple strands might be recycled—removed from the reaction after folding of the scaffold is complete—further decreasing their contribution to the cost of origami.

Supplementary Note S11: Additional references

- [24] LaBean, T., Yan, H., Kopatsch, J., Liu, F., Winfree, E., Reif, J., and Seeman, N. Construction, analysis, ligation, and self-assembly of DNA triple crossover complexes. *J. Am. Chem. Soc.* **122**, 1848–1860 (2000).
- [25] Winfree, E., Liu, F., Wenzler, L., and Seeman, N. Design and self-assembly of two-dimensional DNA crystals. *Nature* **394**, 539–544 (1998).
- [26] Wang, J. C. Helical repeat of DNA in solution. *Proc. Nat. Acad. Sci. USA* **76**, 200–203 (1979).
- [27] Rhodes, D. and Klug, A. Helical periodicity of DNA determined by enzyme digestion. *Nature* **286**, 573–578 (1980).
- [28] Kallenbach, N., Ma, R.-I., and Seeman, N. An immobile nucleic-acid junction constructed from oligonucleotides. *Nature* **305**, 829–831 (1983).
- [29] Murchie, A., Clegg, R., von Kitzing, E., Duckett, D., Diekmann, S., and Lilley, D. Fluorescence energy transfer shows that the four-way DNA junction is a right-handed cross of antiparallel molecules. *Nature* **341**, 763–766 (1989).
- [30] Duckett, D., Murchie, A., Diekmann, S., von Kitzing, E., Kemper, B., and Lilley, D. The structure of the Holliday junction, and its resolution. *Cell* **55**, 79–89 (1988).
- [31] Sha, R., Liu, F., and Seeman, N. Direct evidence for spontaneous branch migration in antiparallel DNA Holliday junctions. *Biochemistry* **39**, 11514–11522 (2000).
- [32] von Kitzing, E., Lilley, D., , and Diekmann, S. The stereochemistry of a four-way dna junction: a theoretical study. *Nucleic Acids Research* **18**(9), 2671–2683 (1990).
- [33] Eis, P. and Millar, D. Conformational distributions of a four-way junction revealed by time-resolved fluorescence resonance energy transfer. *Biochemistry* **32**(50), 13852–13860 (1993).
- [34] Jr., M. R., Anderson, C., and Lohman, T. Thermodynamic analysis of ion effects on the binding and conformational equilibria of protein and nucleic acids: the roles of ion association or release, screening, and ion effects on water activity. *Quarterly Reviews of Biophysics* **11**, 103–178 (1978).
- [35] Puglisi, J. and I. Tinoco, J. Absorbance melting curves of RNA. In *Methods in Enzymology: RNA Processing*, Dahlberg, J. and Abelson, J., editors, volume 180, 304–325 (Academic Press, New York, 1989).
- [36] Yanisch-Perron, C., Vieira, J., and Messing, J. Improved M13 phage cloning vectors and host strains: nucleotide sequences of the M13mp18 and pUC19 vectors. *Gene* **33**(1), 103–119 (1985).
- [37] Zuker, M. Mfold web server for nucleic acid folding and hybridization prediction. *Nucleic Acids Research* **31**(13), 3406–3415 (2003).
- [38] Zinder, N. and Horiuchi, K. Multiregulatory element of filamentous bacteriophages. *Microbiological Reviews* **49**(2), 101–106 (1985).
- [39] Yurke, B., Turberfield, A., Mills, Jr., A., Simmel, F., and Neumann, J. A DNA-fuelled molecular machine made of DNA. *Nature* **406**, 605–608 (2000).
- [40] Simmel, F. and Yurke, B. Using DNA to construct and power a nanoactuator. *Physical Review E* **63**, 041913–1–5 (2001).
- [41] Yan, H., Zhang, X., Shen, Z., and Seeman, N. A robust DNA mechanical device controlled by hybridization topology. *Nature* **415**, 62–65 (2002).
- [42] Turberfield, A., Mitchell, J., Yurke, B., Mills, Jr., A., Blakey, M., and Simmel, F. C. DNA fuel for free-running nanomachines. *Physical Review Letters* **90**(11), 118102–1–4 (2003).